An experimental investigation of camshaft dynamics.

ANDERSON, S.W.

1996

AN EXPERIMENTAL INVESTIGATION OF CAMSHAFT DYNAMICS

STEFAN W ANDERSON BEng (Hons)

A thesis submitted in partial fulfilment of the requirements of The Robert Gordon University for the degree of Master of Philosophy

September 1996

Summary

The construction of the internal combustion engine, since its first use in vehicles in 1865, has steadily increased in complexity. It is because of this increase of complexity that has lead to increase in vibration levels throughout the engine. Unwanted vibrations in the camshaft area can lead to accelerated wear of the valvetrain mechanism, causing the engine to lose power.

To try and gain a better understanding of the vibration levels in the camshaft area it was decided to focus this research project on one particular aspect of valvetrain dynamics. It tried to determine whether there was a simple direct relationship between the rotational vibration measured from the camshaft and the vibrations transmitted through the camshaft bearings.

Using the influence coefficients theory for a static linear system equations were developed for use in a dynamic system. A test rig was designed and built around a Ford 2.0L DOHC engine so that experimental vibration information, in the form of frequency response tests, could be determined and used in the developed equations to determine the values of the influence coefficients.

The values determined for the influence coefficients found that there would appear to be no direct relationship between the two sets of vibration information. After further analysis to try and determine whether there were any particular similarities between the values for the influence coefficients, using experimental data measured at the same position in the engine but at different speeds, no apparent similarities could be determined.

This could be due to two possible reasons. Firstly, the vibration measured by the accelerometers attached to the camshaft bearings is not solely due to the vibration of the camshaft but due to all the vibration levels transmitted throughout the engine. Thus, invalidating the initial premise that there is a simple direct relationship between the two

sets of vibration data and thus also the working equations used. One possible next step of this research project would be to try and overcome these problems by taking the other vibrations into account in the initial equations. Secondly, using the influence coefficient theory for a static loading case could be developed for a dynamic case. In that case a more realistic set of equations would have to be developed and used.

Acknowledgments

I would like to acknowledge the following people, without whose assistance this research project would not have been able to be completed.

I would like to especially thank my director of studies, Dr Allan Adam, for his continual support and constructive criticism, and also Mr Bob Taylor for similar reasons. All the technical staff for their cooperation and comments on the design and construction of my test rig. The engineering applications personnel, especially Mr Bob Phillips and Mr Brian Craig who were always willing to give me advice and a helping hand when required. The computer technical staff for helping and forgiving me on my many mistakes. The secretarial staff for helping me in many little ways. I would also like to acknowledge the contribution of Ford, who supplied the engine. I would also like to thank AE Goetze in Bradford and Sunderland, especially the Marketing Department, for allowing me to use their computer facilities to finalise my thesis for submission and corrections.

I would also like to mention my family and friends, especially Andrew Irvine, Sean Austin, Lisa Morris and Joan Black for enduring my moods and making me laugh during the low points of the last three years.

Contents

Chapter 1

Introduction

1.0. Introduction.

Since the internal combustion engine was first successfully transferred into a vehicle in 1865 by Gottlieb Daimler there has been significant advances in this particular field of engineering. Most of these advances took place around the turn of the century where a great period of experimentation on the basic design occurred. It was about this time that the public first started to become interested in racing. This led to car manufacturers to improve on the basic design of the engine to achieve more powerful engines than their competitors, and thus achieve a certain level of prestige. Since the 1930's, however, the design of the internal combustion engine has not significantly changed, with only improvements on the various subsystems taking place. Since this time though the main principle of the power created within the engine has basically remained the same.

The power obtained within the internal combustion engine is derived from the movement of the pistons during the expansion stroke of the operating cycle. Fuel is injected into the cylinder, using the inlet valve and ignited by the sparkplugs. The expansion of the gases produced by the burning fuel forces the pistons downward, thus turning the crankshaft. The exhaust gases are then forcibly removed from the cylinder, through the exhaust valve, when the pistons move back up the cylinder (through both inertia and additional pistons moving down thus turning the crankshaft back to its original position).

The valve mechanism basically consists of a camshaft, a tappet, springs and the valves. As the camshaft rotates, the rotation of which is directly related to the crankshaft by timing chains, the cams push against the tappets which in turn moves the valves in a certain order and at a specific time. The valve springs help control the opening and closing movement of the valves to reduce the problems associated with the valvetrain.

If the pressure of the fuel gases is lost during the operating cycle then the power produced by the engine will decrease. It is therefore important to determine whether there is any significant vibrations caused by the running of the camshaft, within its normal working speed range. These vibrations, if any, would cause the valvetrain mechanism to function improperly, thus causing accelerated wear on the individual valvetrain components.

1.1. Literature Revue.

To try and understand the problems associated with this research project it is necessary to take a closer look at a few of the basic principles about the valvetrain mechanism.

1.1.1. Rotating Shafts.

In many different kinds of modern machinery there are many parts that rotate. These rotating parts are basically one form of a shaft or another. It is therefore important that they work perfectly, with no deformities of any kind that would cause them to turn in any way other than the ideal direction. It is, however, inevitable that inaccuracies are incurred during the manufacturing stage of the machines construction. These inaccuracies will cause an imbalance, no matter how small, in the rotating part. The forces produced by unbalance can lead to excessive wear on the surrounding components, usually the bearings, and will eventually lead to failure of the component. The presence of any unbalanced force can also lead to vibration in the machine, which can be monitored to determine what affect it is having on the machine. This vibration measurement can also be used, if measured regularly, to determine whether the unbalance is worsening and thus the mechanism needs re-balanced

A serious problem that can occur from unbalanced rotation is when the rotational speed reaches any certain critical speed. This speed excites the natural frequency of the system causing the rotational path of the primary unbalance to vastly increase in amplitude. The shaft is then said to 'whirl' [1 - 5]. Whirling causes the shaft to rotate in a bow shape, for the first critical speed. This problem will even occur in perfectly balanced machines, but because the vibration levels are so low then the rotational speed would have to be very close to the natural frequency of the system before the whirl would be noticeable. Any rotational deviation is a serious problem in camshafts because the valves have to be precisely controlled for optimum opening and closing.

1.1.2. Cams.

Among the first pieces of experimental work undertaken to study the vibratory performance of the valve spring was done by Jehle and Spiller [6] and Donkin and Clark [7], in the late 1920's. They determined experimentally the speeds at which the exhaust valve bounced and the speeds at which spring surge occurred in four different valve springs respectively. They were also one of the first to relate the surge phenomenon to the harmonics of the cam.

In 1948 Dudley [8] devised a mathematical model for the design of cams. This involved specifying a suitable cam contour and then determining the sum of the forces at any point in time. The summation of the forces was overcome by a driving force created by compressing the valve linkage. Thoren, Hengemann and Stoddart [9] expanded on this principle, deriving a polynomial equation to describe the motion of the valve, and designing a cam profile based on that equation. This method of cam design became known as the polydyne method, (derived from "polynomial" and "dynamics").

A few months later Hrones [10] published a paper that analysed the dynamics of the cam-follower linkage by reducing, and simplifying it into a single mass model. This enabled him to determine expressions of motion (displacement, velocity, acceleration) and force acting on the cam for the system. He was then able to insert into these expressions the equations for the profiles of three popular cams; constant acceleration (or gravity), harmonic and cycloidal cams and compare the findings. He showed that the cycloidal profile gave the lowest peak and transient forces. These findings were then confirmed by Mitchell [11] two years later when he performed tests on the three profiles.

Neklutin [12], in an attempt to get better dynamic characteristics of the follower system, proposed combining aspects from the cycloidal and constant acceleration profiles. He developed the modified trapezoidal cam which gave a gradual change of inertia force, thus a low initial acceleration, and lower peak acceleration values than the cycloidal profile. He was also the first to introduce the idea of residual vibration of the follower, looking at, as he put it, the "dynamic stresses for a certain number of free vibrations of the driven mechanism which occur during the stroke". This principle was extended further by Kwakernaak and Smit [13] in 1968 when they used an optimisation technique to design cam profiles that had minimum residual vibrations.

Up until 1973 all the models developed for the simulation of a cam-follower system were linear single or two mass models. Chen [14] developed a multi degree of freedom model with a hardening (non-linear) spring, as shown in Figure 1.1.

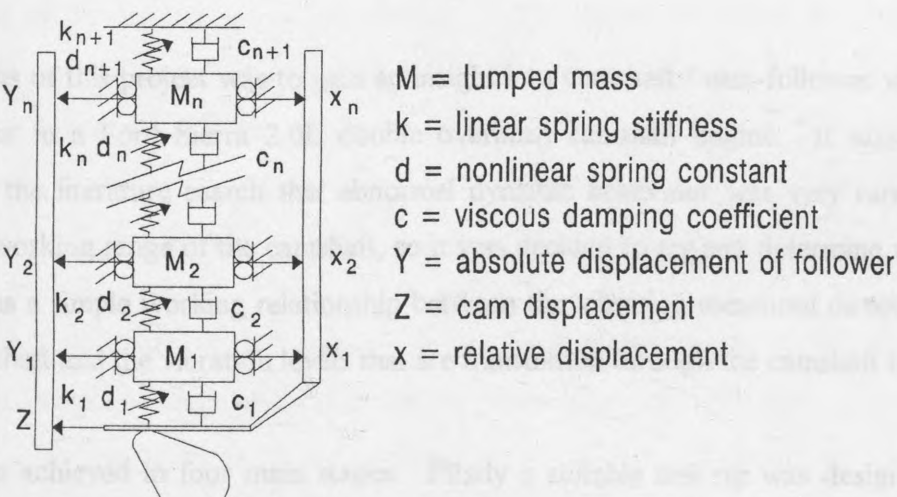

Figure 1.1: Multi degree of freedom model of cam-follower system.

Akiba, Shimizu and Sakai [15] adapted a single mass model into a two mass lumped model (one mass for the tappet and the other mass for the other components) with an additional distributed mass simulation for the valve spring. They concentrated their analysis on very high speeds, well above that at which abnormal behaviour occurs.

A reasonable 6 Degree-of-Freedom (DOF) model for a finger follower type overhead cam valve system was developed by Chan and Pisano [16]. They also introduced a simple model for a hydraulic tappet.

Phlips, Schamel and Meyer [17] developed an accurate multi-DOF model for the simulation of valvetrains with an overhead cam. This model incorporates a distributed spring, a variable tappet stiffness (by considering the variable contact point between cam and tappet) and a hydraulic lash adjuster. After verifying the accuracy of the model, by comparing the calculated and experimental valve accelerations, they used the model to determine various characteristics after changing some of the system parameters.

1.2. Project Focus and Scope of Work.

The focus of this project was to gain an insight into camshaft / cam-follower vibration behaviour in a Ford Sierra 2.0L double overhead camshaft engine. It was found, through the literature search that abnormal dynamic behaviour was very rare in the normal working range of the camshaft, so it was decided to try and determine whether there was a simple working relationship between the vibration measured directly from the camshaft and the vibration levels that are transmitted through the camshaft bearings or not.

This was achieved in four main stages. Firstly a suitable test rig was designed and constructed. A suitable theory was derived and the test rig's design finalised to suit the information required by the theory. A complete set of vibration data to be captured and processed, the third phase of the project, from the area of the engine that under investigation. When all the appropriate data has been processed it will be used in conjunction with the developed theory to determine whether there is a straight forward working relationship between the two sets of vibration.

1.3. Thesis Outline.

The project objectives as outlined in Section 1.2. are addressed in subsequent chapters of the thesis. These are :

Chapter 2 describes the design, construction and the commissioning of the test rig. This will include a detailed description of all the individual components, that had to be manufactured, and their use. There will be a description of the proximity transducers and the accelerometers chosen, as well as what tasks they will have to perform. The FFT analyser will also be described in detail to provide an insight into its function during the experimental work. The chapter will end by providing details of the engine, a Ford 2.0 litre double overhead cam engine, and the individual components of the valvetrain.

Chapter 3 details all the experimental work undertaken. This was be separated into all the tests performed and in a set pattern. Each section describes the theory (or reasoning) behind each test, and also a list of all the equipment used. A detailed procedure is set out to allow the test to be duplicate at a later date. The results are then shown, which will be followed by a brief discussion of the test as well as a short summing up. Each test will be discussed more fully later in Chapter 5.

Chapter 4 deals with the relationship between the camshaft vibration and the bearing vibration. The reasoning behind the research premise will be explained and equations derived. The frequency response information, in the form of amplitude and phase graphs, will be used in the equations to determine the values for one of the influence coefficients. This will be done for all the frequencies within the range under investigation, and for all the speeds as well. These values will be calculated for several different combinations of the frequency response data to determine the validity of the original premise.

Chapter 5 is basically an extended discussion chapter dealing with the most important parts of the thesis. Most of the points made during this chapter will already have been mentioned previously in the main text of the thesis, but this chapter will try to expand upon these points. This includes; some of the main problems associated with the construction of the test rig, the most important aspects of the experimental work and will finish off discussing the influence coefficients.

Chapter 6 will help to round the thesis off by making suggestions of future work that could be undertaken to try and tie up any loose ends associated with the work done up to present time.

The Conclusion completes the project by summing up the thesis as a whole, this will include all the aspects of what has gone before in the main text and what was gained by completing the project.

CHAPTER 2.

The Experimental Test Rig.

2.1. Introduction.

This chapter describes in detail the test rig. The test rig basically consists of a Ford Sierra 2.0 litre DOHC engine, the test rig components required to hold the engine in place and the motor required to run it. The overall rig also incorporates suitable instrumentation required to complete all the experimental work. This chapter will begin by describing in detail all the individual components that had to be especially manufactured and their function. All the transducers incorporated in the rig will also be outlined in relation to their specific application, these being the proximity transducers, accelerometers and the FFT analyser needed to capture and process the data. The chapter will finish with a description of the engine and the individual components of interest in the valvetrain.

2.2. The Test Rig.

The experimental test rig can be separated into four parts, the supporting structure required for the engine, the motor, the instrumentation required for gathering the data, and the engine itself. The layout of these parts can be seen in Figures 2.1 and 2.2.

The main function of the test rig is to support, and turn the engine whilst all the vibration information is collected. This information has to be gathered around the camshaft area of the engine and so the design of the test rig has to take this into consideration.

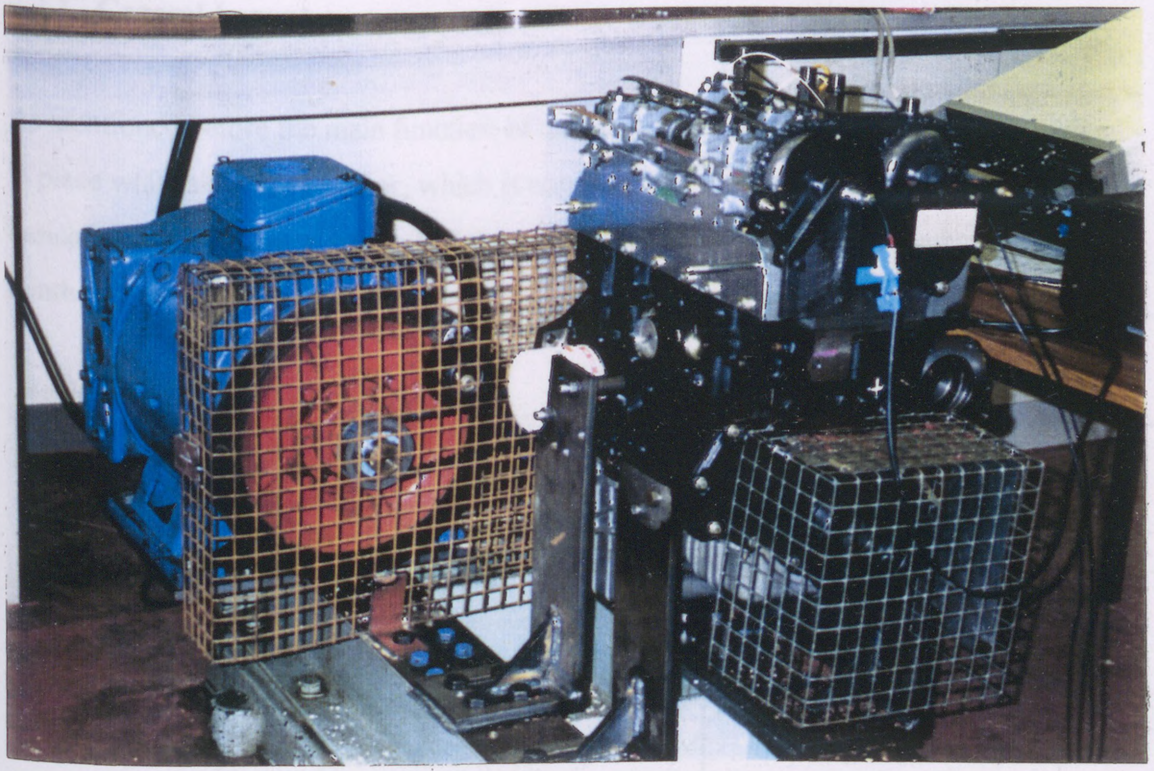

Figure 2.1.: The test rig layout.

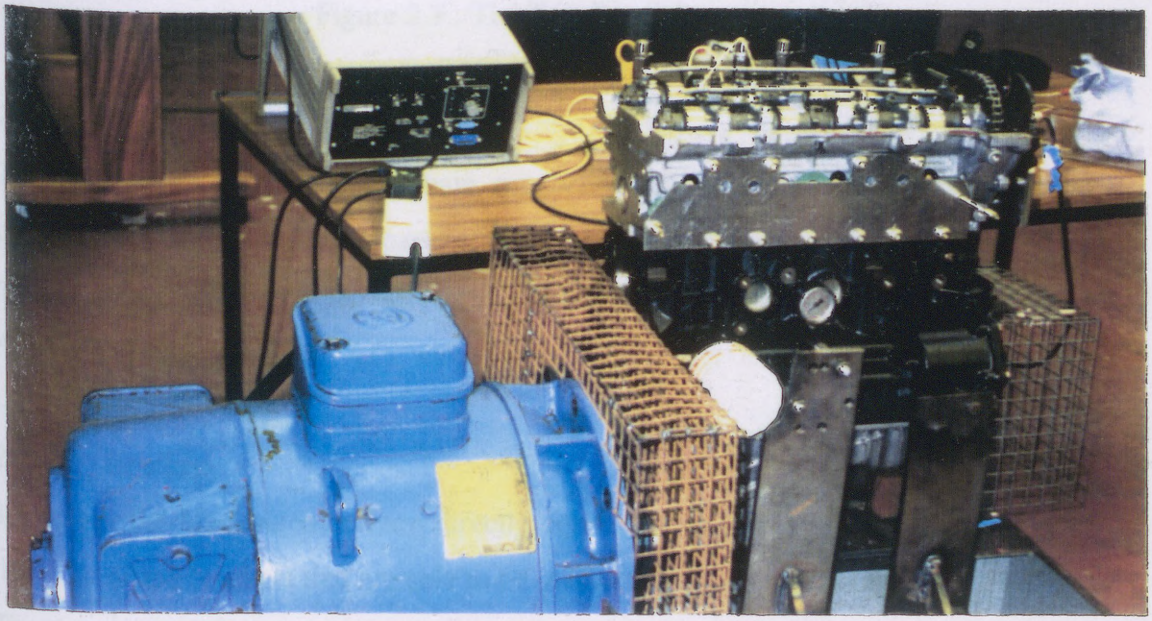

Figure 2.2.: The test rig layout.

2.2.1. General Layout.

As mentioned before the main function of the supporting structure is to hold the engine in place while allowing a motor, which is connected to the engine, to turn it. The rig is basically formed from a base platform and all the other parts are connected to this plinth. These can be seen in the schematic layout as shown in Figure 2.3.

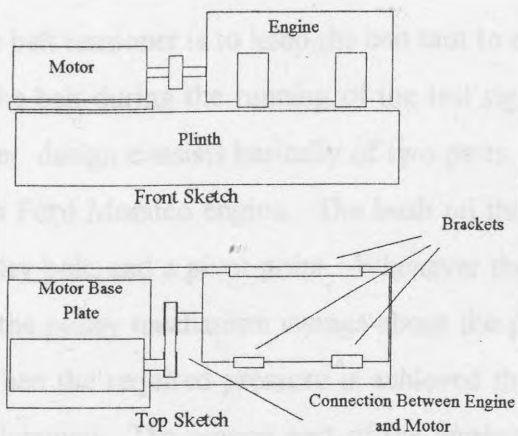

Figure 2.3.: The Test Rig Schematic

2.2.1.1. Plinth.

The base plinth is used as the main supporting structure for the test rig. It was previously available in the department and so did not have to be manufactured or bought in especially for the project. The drawing of the Plinth can be seen in Appendix 1.

2.2.1.2. Brackets.

These are the brackets which are directly connected to the engine. They consist of three 'L' shape brackets that are able to be connected to both the plinth and the engine. The drawings of the brackets can be seen in Appendix 1.

2.2.1.3. Motor Base Plate.

The motor base plate basically holds the motor in the appropriate place in relation to the engine. The drawing of the motor base plate can be seen in Appendix 1.

2.2.1.4. Connection Between The Motor and The Engine.

The motor cannot be directly attached to the crankshaft, so a small connecting part had to designed that would be able to easily connect the motor and the engine. A rubber toothed belt connects the two pulleys. The drawing of the connection can be seen in Appendix 1.

2.2.1.5. Belt Tensioner.

The main function of the belt tensioner is to keep the belt taut to ensure that there is no excessive vibrations in the belt during the running of the test rig, this is not shown in Figure 2.3. The tensioner design consists basically of two parts. The main part is the timing belt pulley from a Ford Mondeo engine. The bush on this pulley has a slotted hole, suitable for the pulley bolt, and a pivot point. Whenever the pressure on the belt needs to be varied then the pulley mechanism swings about the pivot point and in the direction of the slot. When the required pressure is achieved the bolt is tightened to ensure the tension is maintained. The second part of the tensioner consists of a mild steel rectangular plate, the drawing of which can be seen in Appendix 1.

2.2.1.6. Safety Cages.

There are two safety cages attached to the rig to ensure that the exposed rotating parts of the test rig are covered for maximum safety, these are not shown in the schematic in Figure 2.3. One safety cage is at the front of the engine to cover the rotating pulley attached to the crankshaft and the second, larger safety cage is at the back of the engine to cover the connection between the motor and the engine.

2.2.2. D.C. Motor.

In choosing the motor needed to power the engine it was necessary to consider the following requirements for the motor: The starting torque developed by the motor has to be able to overcome the initial high torque needed to turn the engine. The torque of the engine was crudely measured using a torque wrench, which was adjusted until it could just turn the engine over. The value determined in this method was 22.5 Nm.

The speed of the motor must be able to be accurately varied within the specified working range of the engine. Once set at a specific speed, the motor must not be prone to large fluctuations in speed, allowing a complete set of tests to be undertaken. The size and shape of the motor must not be so unreasonable that it could not be incorporated into a test rig, it must also be easily powered from the existing power supply in the laboratory. The motor chosen must either be currently available or bought at a reasonable cost.

2.2.2.1. The Motor Chosen

The motor chosen was a D.C. compound motor, mainly because of its ability to provide the initial high starting torque required and yet still provide a reasonable speed control range.

There was a compound motor available within the university that suited the requirements. This was a Laurence, Scott and Electromotors Ltd motor, with nameplate details as follows:

Serial Number	193413
Volts	330 / 44 / 18
HP	3 / 0.3 / 0.049
Wind	Comp Int
Rating	Comp / Int
Year	1966
Frame	TD18CF
RPM	2000 / 200 / 33
Amp	8.7
Excit Volts	220
Insuln	Class E
BSS 2613/57	

The motor can be clearly seen in Figures 2.1.- 2.3.

However due to the age of the motor it was not possible to obtain a speed-torque characteristic curve for that specific motor but it was connected to the engine and tested and it was found to provide an adequate starting torque.

2.2.2.2. The Speed Controller.

The speed controller used was a RS Components 512/16 DC Speed and Torque Control Module; stock number 320-758. The controller operates from a single phase mains supply using a simple transformer arrangement to allow the controller to be adjusted to suit the applied voltage. The speed can be set using a dial connected to the front of the unit. As a safety feature the controller will automatically switch the current from the motor, after 15 seconds, should the motor stall. It is also protected by an instantaneous over-current trip should excessive armature current overloads occur.

The wall box is a stainless steel to IP65 type 2 box; stock number 220-119. It has a lockable door that can open to 120° and has an internal mounting plate used to fix the speed controller in place. It is also mentioned, as in its name, environmentally sealed to IP65.

2.3. Engine Description.

The experimental test rig is based on a Ford Sierra 2.0 litre engine. The engine has four in line cylinders and eight valves working from two overhead camshafts, one for the inlet valves and the other for the exhaust valves. They are both driven by a timing belt connected to the crankshaft on a 2:1 step down ratio. The details of which are:

Engine type	Four-cylinder, in-line, double overhead camshaft.
Firing order	1-3-4-2
Bore	86.00 mm

Stroke	86.00 mm
Cubic Capacity	1998 cc
Compression Ratio	10.3:1
Maximum continuous engine speed	6050 rpm
Maximum engine power	80 kW at 5600 rpm
Valve timing:	
Inlet opens	13 ° BTDC
Inlet closes	39 ° ABDC
Exhaust opens	43 ° BBDC
Exhaust closes	13 ° ATDC

2.3.1. Engine Modifications.

The engine as a whole was kept intact. The crankshaft was the easiest method of turning the camshafts by the use of the existing timing chain. The engine was intended to be 'turned over' in the normal working speed range so the lubrication system was also needed intact. The oil pump used to power the lubrication system is an integral part of the engine and was also powered by the crankshaft by the use of a double sprocket at the front of the crankshaft, one for the pump and the other for the camshafts. The camshaft rotates at half the speed of the crankshaft, and the oil pump at twice the speed of the crankshaft. The oil pressure warning switch was replaced with an oil pressure gauge for a more accurate lubrication pressure reading.

As mentioned earlier there is no combustion occurring in the cylinders, however the pistons were left in the engine in an attempt to leave the overall balance of the engine unaffected. With no combustion occurring in the cylinders the movement of the pistons would still cause the compression part of the stroke cycle to occur. The sparkplugs were removed to allow air to circulate, thus removing the compression in the cylinders. The inlet and the exhaust manifolds were also removed for ease of mounting the engine. The flywheel was also removed from the engine because of motor restrictions.

The original cover was replaced with a larger perspex cover for two reasons. Firstly, to allow visual checking of the instrumentation and to ensure that the lubrication system was working properly. Secondly, the original cover did not allow enough space for the instrumentation to be attached to the cylinder head.

2.4. Test Rig Instrumentation.

The instrumentation used during the experimental work consists of three main parts; proximity probes (used to measure the camshaft vibration and the key phasor), the accelerometers and the FFT analyser. Each having its appropriate function within the test rig set up.

2.4.1. Proximity Probes

2.4.1.1 Introduction.

Proximity probes are a non-contact transducer that measure the distance between the transducer and the test subject.

The most common type of transducer, the eddy current transducer, uses the principle of impedance variation. This is when an electromagnetic field, created by the transducer, comes in contact with the target material. Eddy currents are induced in the target, and the amount that this disrupts the field is monitored by a sensor, as shown in Figure 2.4. Thus a direct relationship between the output signal and the distance between the probe and target can be found.

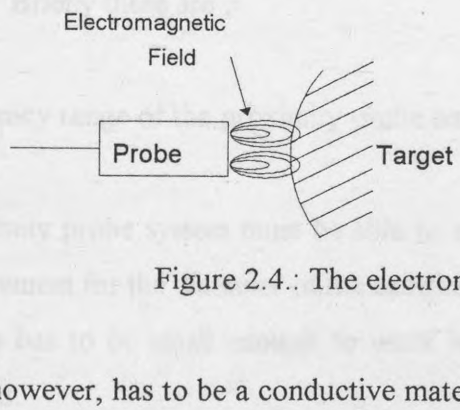

Figure 2.4.: The electromagnetic field.

The target however, has to be a conductive material for the electromagnetic field to be affected. The field is not affected by lubrication oil and most gases.

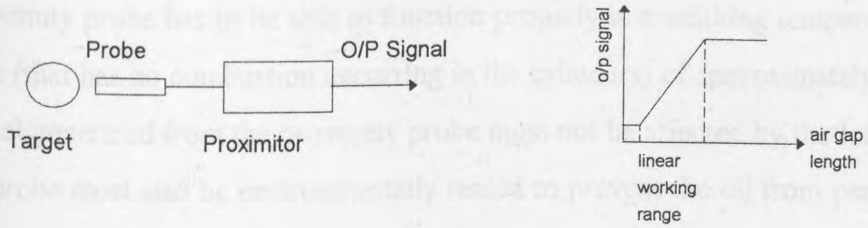

Figure 2.5.: System arrangement.

The probe cannot work by itself, it requires a proximitor to produce a radio frequency signal, as can be seen in Figure 2.5. above. When this signal is transmitted from the probe coil the radio frequency (RF) field is created. The signal is then returned to the proximitor and a demodulator circuit interprets the signal to produce an output voltage. If the target is moving within the field then the amplitude of the output voltage changes. The transducer requires that the target has a high quality surface finish. Any defects, such as scratches, flakes of rust etc., will affect the RF field and thus give inaccurate data. The proximity transducer is a non contact type of transducer and will therefore not affect the vibration characteristic of the target. The holder used for the transducers has to be seismically isolated from the target, ensuring that no background vibrations will affect the background signal. Because of the time and effort required for the installation of a proximity transducer system they are best installed on a permanent basis.

2.4.1.3. Specification.

When choosing the proximity transducer system the following requirements had to be considered. Briefly these are ;

- The frequency range of the proximity probe has to be the same as the accelerometer, 1000 Hz.
- The proximity probe system must be able to effectively measure the deviation from normal movement for the diameter of the camshaft.
- The probe has to be small enough to work in the restricted space available in the cylinder head.

- The proximity probe has to be able to function properly in a working temperature for the engine (that has no combustion occurring in the cylinders) of approximately 60° C

- The signal generated from the proximity probe must not be affected by the lubrication oil. The probe must also be environmentally sealed to prevent the oil from penetrating the probe.

- The proximity transducer system would be compatible with existing laboratory equipment.

- The proximity probe must be able to meet all the above requirements at a minimum cost.

2.4.1.4. Proximity Transducer System Chosen.

For the measurement of the camshaft vibration it was decided to purchase the Bentley Nevada 7200 proximity transducer system, an eddy current principle transducer. The 7200 proximity transducer system has a 5 mm proximity probe that has a frequency response of 0 to 10 kHz with only 5 % deviation at the upper limit of the working range. This more than adequately provides for the frequency range required. The minimum is a shaft of 15 mm diameter and will operate in temperatures up to 177° C. The casing of the probe has a 1/4" - 28 UNF thread for a 0.8 inch length. The total length of the probe, including the cable is 1 m ending with a miniature male coaxial connection. The probe is connected to a proximitor which provides an output signal that is compatible with existing laboratory equipment. The proximitor, when considering the signal from the probe, takes into consideration the total resistance of the cable. So to complete the system a 4 m extension cable was also bought.

The overall cost of the system, which includes the probe, the proximitor and an extension cable is £461 (£541.68 including V.A.T) which, though more expensive than the accelerometer is still reasonably priced.

The manual calibration of the proximity transducer system can be seen in Chapter 3.2.

The proximity transducer system was purchased from Bentley Nevada.

Part	Part Number	Serial Number
Probe	21500-00-08-10-02	JULU440763
Probe	21500-00-08-10-02	JULU440765
Extension Cable	21747-040-00	-
Extension Cable	21747-040-00	-
Proximitor	18745-03	JUNU118860
Proximitor	18745-03	JUNU118865

Table 2.1.: Part numbers and serial numbers for the proximity transducer system.

2.4.1.5. Proximity Probe Positioner Design.

The design of the proximity probe positioner ensured that both proximity probes were 90° to each other, and at 45° to the vertical of the camshaft. The distance between the tips of the probes and the camshaft was adjustable and positioned about 1 mm away from the shaft.

A schematic of this can be seen in Figure 2.6., while its actual position on the test rig in Figure 2.7. The Drawings for the positioner can be seen in Appendix 1.

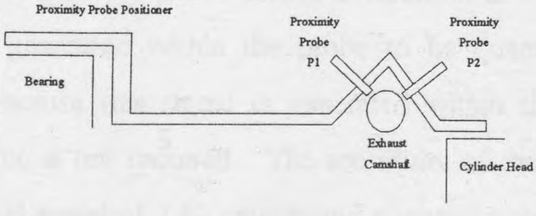

Figure 2.6. : A schematic of the Proximity Probe Positioner.

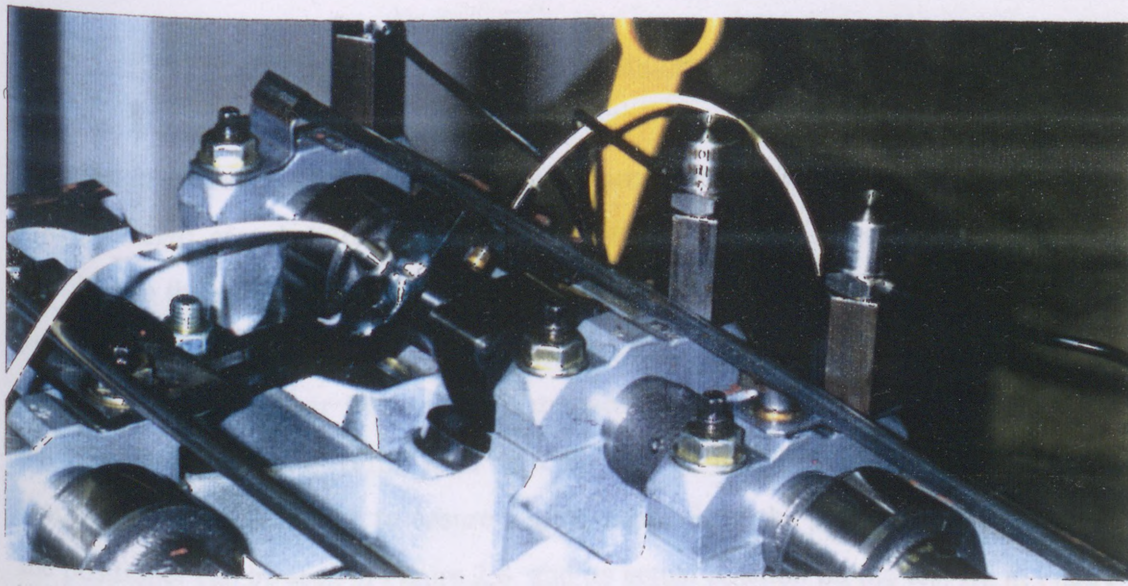

Figure 2.7.: The Proximity Probe set up.

2.4.1.6. Key Phasor Proximity Probe.

The proximity probe chosen to act as the reference pulse was the Stewart-Warner Instruments Limited model number IK4054. This type of probe is a magnetic proximity detector. When the probe senses a variation in the magnetic flux then a frequency signal is generated within the probe to be quantified using appropriate instrumentation. Because this signal is generated within the probe itself then an external power source is not required. The sensitivity of the probe is 150 millivolts peak with a peripheral speed of 7.62 cm/sec and a working temperature range of -40° C to +140° C. The probe casing is ½" x 26 Whitworth threaded for a length of 40 mm. It has a 2.5 mm tip length.

This make and model of proximity probe has been used for this type of application before, and so is known to be suitable for this purpose. It was also part of the existing laboratory equipment and thus was not necessary to purchase, keeping cost to a minimum.

2.4.1.7. Key Phasor Pulse Proximity Probe Positioner.

The design of this positioner ensured that the proximity probe was in position over the inlet camshaft sprocket, or to be more precise the distributor rotor shaft which is attached to the sprocket. This has a small 5x5 mm keyway in it that was used for the pulse. Each time the break in the material passes the proximity probe a pulse is created. The positioner was securely attached to the cylinder head. The distance between the distributor rotor shaft and the tip of the probe was adjustable and therefore was small enough to ensure a good signal from the probe. A schematic for the positioner can be seen in Figure 2.8. and its actual position on the test rig in Figure 2.9. The drawings for the positioner can be seen in Appendix 1.

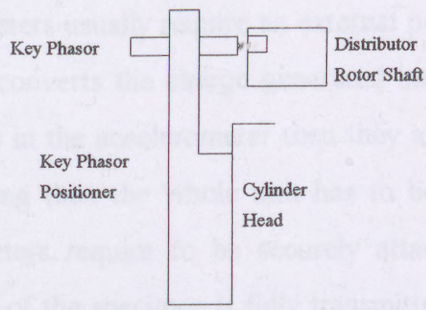

Figure 2.8. : A Schematic of the Key Phasor Positioner

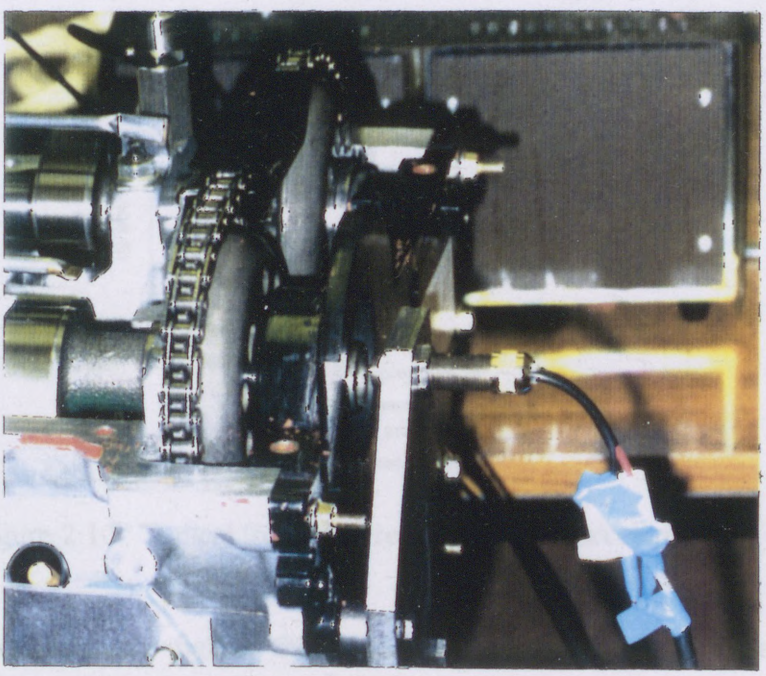

Figure 2.9.: The key phasor proximity probe.

2.4.2. Accelerometers.

2.4.2.1. Introduction.

Accelerometers are transducers that respond to changes in acceleration in one or more directions, depending upon the versatility of the accelerometer used.

Piezoelectric accelerometers have a piezoelectric material (one that develops an electrical charge when it is subjected to a force) connected to an inertial mass, so when the mass is vibrated the piezoelectric material is also vibrated and a measurable electric charge is produced. The piezoelectric charge generated is proportional to the force and as the inertial mass is constant then the charge is directly proportional to the acceleration. Accelerometers usually require an external power source in the form of a charge amplifier which converts the charge generated into a voltage signal. Because there is no moving parts in the accelerometer then they are very reliable. However, if something does go wrong then the whole unit has to be replaced and not just one component. Accelerometers require to be securely attached to the test subject to ensure that the vibration of the specimen is fully transmitted to the accelerometer. The frequency range of a typical accelerometer, is shown in Figure 2.10.

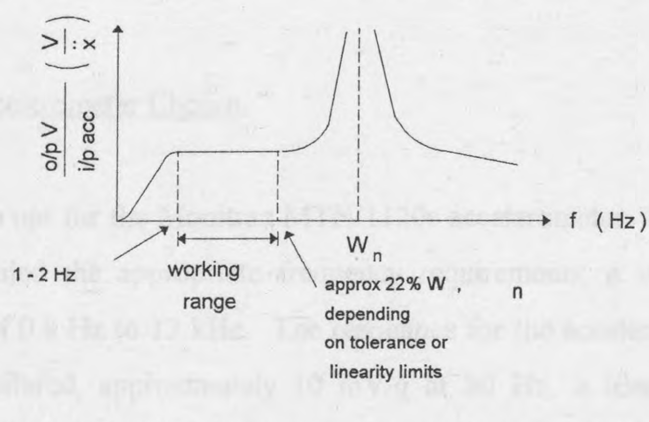

Figure 2.10.: Typical frequency response for an accelerometer.

As can be seen from the figure, the frequency levels are very poor at very low frequencies. The amplitude levels off at about 2 Hz and stays level until it reaches about 30 % of the natural frequency, where the graph then becomes an asymptote to its resonance frequency. The working range of the accelerometer is the flat portion of the graph to within the typical boundary limits of ± 5 %. This is the portion of the graph that does not deviate by 5 %.

2.4.2.2. Accelerometer Requirements.

When choosing an accelerometer it was important to determine all the requirements needed. In brief these were ;

- The frequency range required to be measured by the accelerometer has to be less than approximately 22 % of the natural frequency.
- The accelerometer has to have low sensitivity, to lessen any effects of the impact between the cam and tappets.
- The accelerometer has to be protected from the lubrication in the cylinder head.
- The accelerator has to be small enough to fit in the cylinder head.
- The accelerometer has to be securely attached to the bearings to ensure the best transmission of the vibration signal.
- The accelerometer has to be compatible with existing laboratory equipment.
- It has to be able to successfully meets the above requirements at a minimum cost.

2.4.2.3. The Accelerometer Chosen.

It was decided to opt for the Monitran MTN/1120s accelerometer. This accelerometer adequately provided the appropriate frequency requirements, a working frequency response range of 0.8 Hz to 13 kHz. The resonance for the accelerometer is 20 kHz. The sensitivity offered, approximately 10 mV/g at 80 Hz, is ideal in the event of possible impact forces. The accelerometer is hermetically sealed to IP67, which offers total protection in water up to a depth of 1 meter, and the connection is sealed to IP34, splash proof, and comes with 5 m of PVC coated cable. The accelerometer could be manufactured to give the required height of 20 mm, the cable is side entry which also helps keep the overall height of the unit down. It has a 10-32 UNF threaded female connection for stud connection, allowing good vibration transmission and permanent installation. The accelerometer is compatible with existing laboratory equipment. The overall cost for each accelerometer; £149.00 (£178.60 including V.A.T.) is reasonable for this type of accelerometer.

The serial numbers and sensitivities for the accelerometers are shown in Table 2.2.:

Accelerometer Serial Number	Sensitivity (mV/g)
22222	9.7
22223	9.3
22224	9.9
22225	9.2

Table 2.2.: Accelerometer serial numbers and corresponding serial numbers.

2.4.2.4. Accelerator Platform Design.

The design of the accelerator platform ensured that there was a good connection between the accelerometer and the bearing. This ensured that the best vibration transmission, from the shaft to the accelerometer, was achieved.

The overall height of the platform and the accelerometer was restricted to 75 mm, the internal height allowed by the perspex cover, with an accelerometer height of 20 mm. A schematic of the positioner can be seen in Figure 2.11. The accelerometers on bearings 3L and 4L can be seen in Figure 2.12. The drawing for this positioner can be seen in Appendix 1.

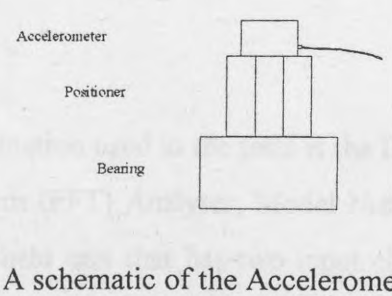

Figure 2.11. : A schematic of the Accelerometer positioner

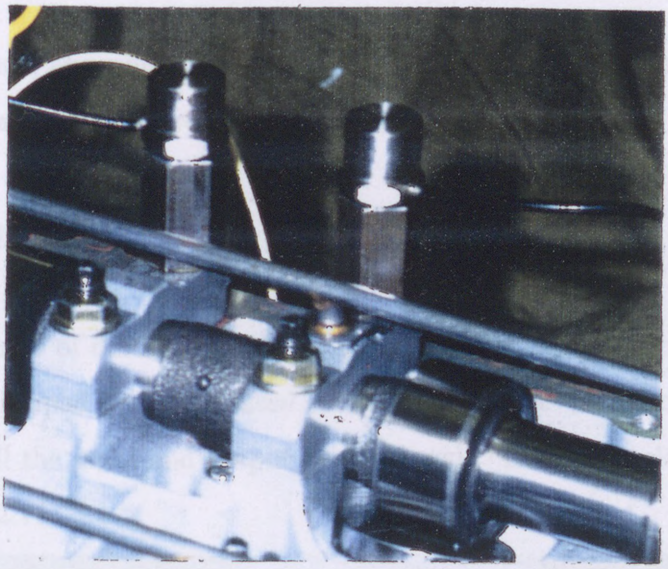

Figure 2.12.: The accelerometers on bearings 3L and 4L.

The positions of the accelerometers and the proximity probes can be seen in the schematic as shown in Figure 2.13.

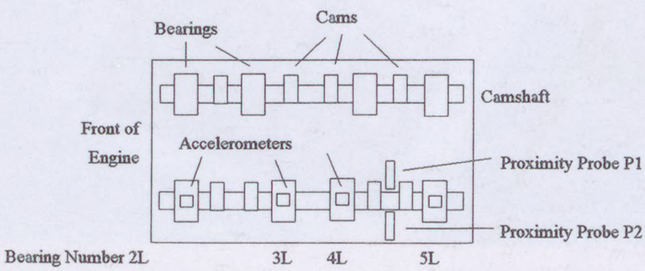

Figure 2.13. : Schematic of the transducer positions on the engine.

2.4.3. FFT Analyser.

The main piece of instrumentation used in the tests is the Diagnostic Instruments Real-Time Fast Fourier Transform (FFT) Analyser; Model Number PL202, Serial Number 123. This is a small hand held unit that has two input channels and can be used for various applications, ranging from vibration measurement to structural and acoustic analysis. This unit is portable and can be powered by a mains adapter or its own internal battery pack, ensuring that the unit is versatile. It is controlled by a series of menus, which are straight forward to understand and use.

2.4.3.1. Construction of the FFT analyser.

The physical make up of the PL202 is in three parts; the screen (which displays all the information), the keypad (which is used to set up the analyser) and the backpanel (which contains all the input and output connections). These can clearly be seen in Figures 2.14. and 2.15.

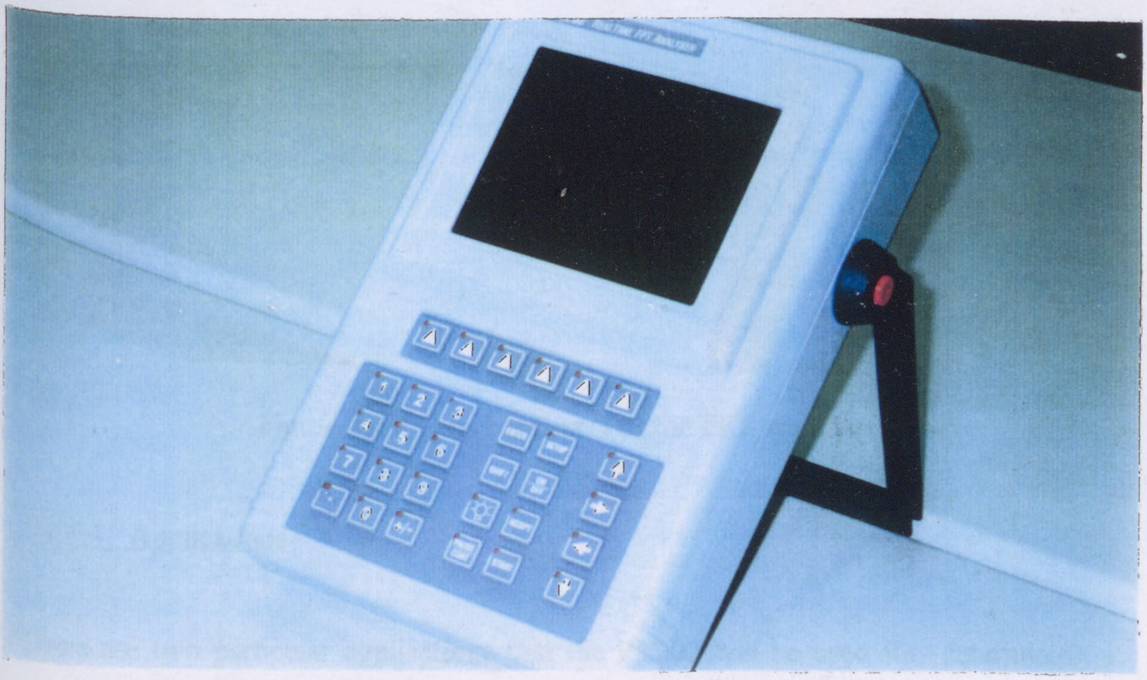

Figure 2.14.: The FFT analyser as seen from the front.

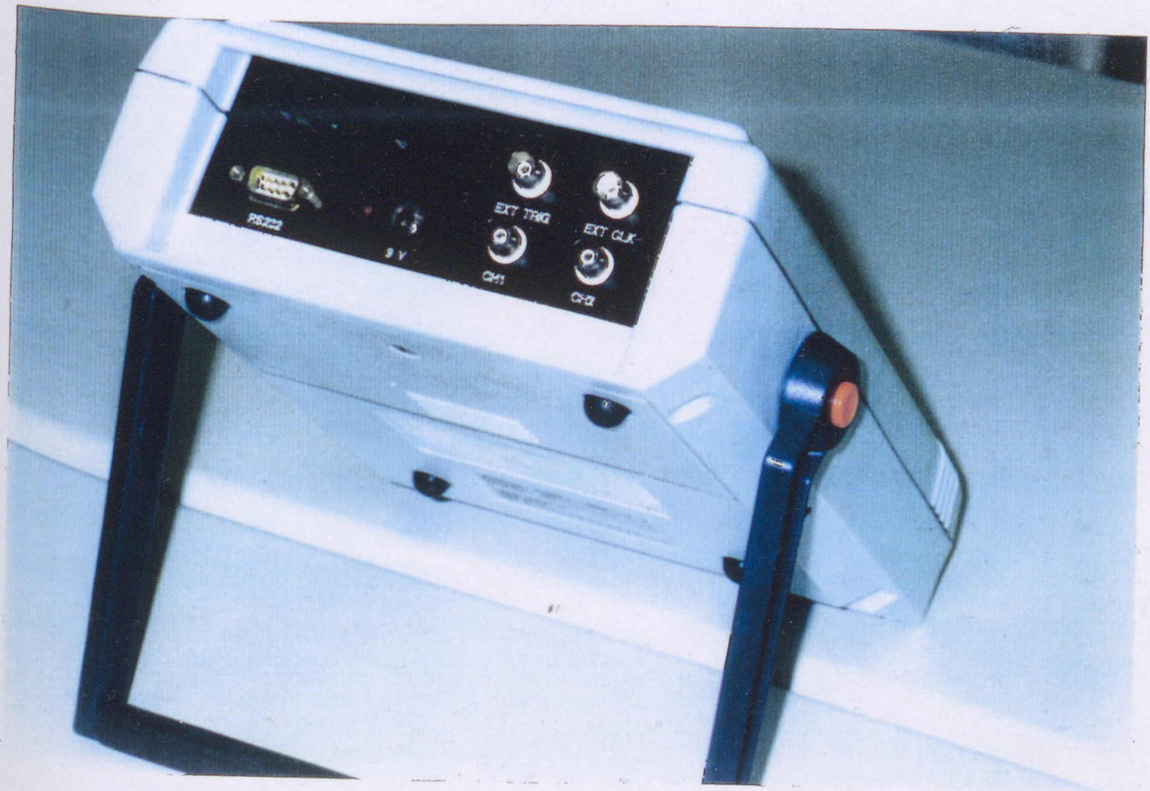

Figure 2.15.: The backpanel of the FFT analyser.

2.4.3.4. Applications.

There are two particular applications that the PL202 will be used for, determining a modal analysis of particular parts of the test rig and determining the vibratory response of the camshaft area using accelerometers and proximity transducers.

The structural resonance test will be in the form of the hammer impact test. This uses an impact (by the hammer) to excite the structure. An accelerometer attached to the test subject will analyse the response of the structure. The FREQ RESP function is used to relate the level of the response to the level of the impact and a spectrum is derived showing the most excitable frequencies (the resonance frequencies) of the structure.

The vibratory response of the transducers will use two functions available. The SPEC function will determine the magnitude of particular vibration frequencies at the positions tested, whereas the FREQ RESP function will relate these frequencies to a particular point (the key-phasor) for comparison.

Chapter 3

Experimental Work

3.1. Introduction.

In this chapter all the experimental work utilised in this research project will be described in great detail.

There were five main tests undertaken., these were;

- Two calibration tests of transducers that were bought for the test rig, the proximity probes and the accelerometers
- A resonance test (in the form of a hammer impact test) to determine whether any of the transducers positioners would induce resonance, thus invalidating their results.
- A spectral analysis of the camshaft using all the transducers for all the speeds under consideration will be performed. The data will be shown in a 'waterfall plot' format.
- Several frequency response tests will be completed incorporating the key phasor and all the transducers for all camshaft speeds.

3.2. Calibration of the Proximity Transducer System.

3.2.1. Introduction.

The specification for the 7200 Proximity Transducer System provided by Bentley Nevada states that the scale factor is 200 mV/mil if calibrated as a system. This calibration is dependent upon the material of the target because the level of eddy currents produced is dependent on the type of material. It was therefore necessary to determine experimentally the scaling calibration for the transducer system in this application.

3.2.2. Equipment.

Thurlby K1 Module Serial Number: 43637 SMOE No.: CP/028/12

Gould Digital Storage Oscilloscope Type 4035 Serial Number: 1895

Hewlett-Packard 7470A Plotter Serial Number: 2517A 00503

Fluke 8840A Multimeter Serial Number: 3948057

Moore and Wright Imperial Feeler Gauges SMOE No.: ME 16/061

3.2.3. Procedure.

The equipment was set up as shown in Figure 3.1.

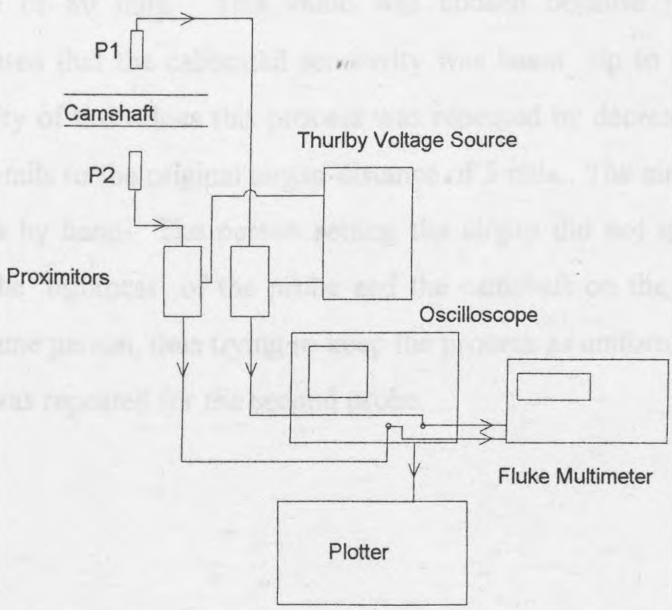

Figure 3.1: Schematic of the calibration test layout

The two proximity probes were designated as proximity probe 1 and proximity probe 2. Where probe 1 is the probe on the left hand side of the camshaft, looking from the front the engine, and probe 2 is the probe on the right hand side of the camshaft. They are at an angle of 45° to the vertical of the camshaft and at an angle of 90° to each other.

The proximity probe was adjusted to a distance of 5 mils between the probe tip and the camshaft using a feeler gauge. The feeler gauge was placed in the airgap between the probe and the shaft and the probe was moved so that it was tight against the gauge, though not so tight that the gauge could not be removed, and the probe locking nut was tightened finger tight.

A voltage reading and a plot of the voltage step, (the difference in voltages between the datum voltage, 0 volts, and the voltage reading) were taken. The airgap distance was increased to 10 mils and the voltage reading noted and plotted.

This process was repeated by increasing the airgap in increments of 5 mils up to a total airgap distance of 80 mils. This value was chosen because the manufacturers specification stated that the calibrated sensitivity was linear up to this distance. To check the validity of the values this process was repeated by decreasing the airgap in increments of 5 mils to the original airgap distance of 5 mils. The airgap was set using the feeler gauge by hand. The person setting the airgap did not change during this procedure, so the 'tightness' of the probe and the camshaft on the feeler gauge was judged by the same person, thus trying to keep the process as uniform as possible. The whole process was repeated for the second probe.

3.2.4. Results.

The following table shows the voltage readings noted during the calibration process.

Airgap (mils)	Probe 1 (volts ± 0.005)	Probe 2 (volts ± 0.005)
5	-1.56	-0.96
10	-2.32	-1.80
15	-3.19	-2.75
20	-4.23	-3.63
25	-5.20	-4.53
30	-6.07	-5.36
35	-6.95	-6.15
40	-7.56	-6.95
45	-8.49	-7.47
50	-9.21	-8.10
55	-9.95	-8.60
60	-10.39	-8.98
65	-10.92	-9.16
70	-11.17	-9.29
75	-11.38	-9.31
80	-11.47	-9.21
75	-11.38	-9.31
70	-11.22	-9.30
65	-10.90	-9.20
60	-10.31	-8.95
55	-9.80	-8.54
50	-9.18	-8.11
45	-8.54	-7.58
40	-7.80	-6.79
35	-6.90	-6.11
30	-6.09	-5.32
25	-5.29	-4.55
20	-4.28	-3.74
15	-3.22	-2.83
10	-2.27	-1.82
5	-1.60	-0.88

Table 3.1.: Experimental Voltage Readings for both Transducer Systems.

3.2.5. Discussion of results.

When these values are plotted in a graph of probe voltage against airgap, Graphs 3.1 and 3.2, it can be seen that the sensitivity is linear over approximately the first 40 mils.

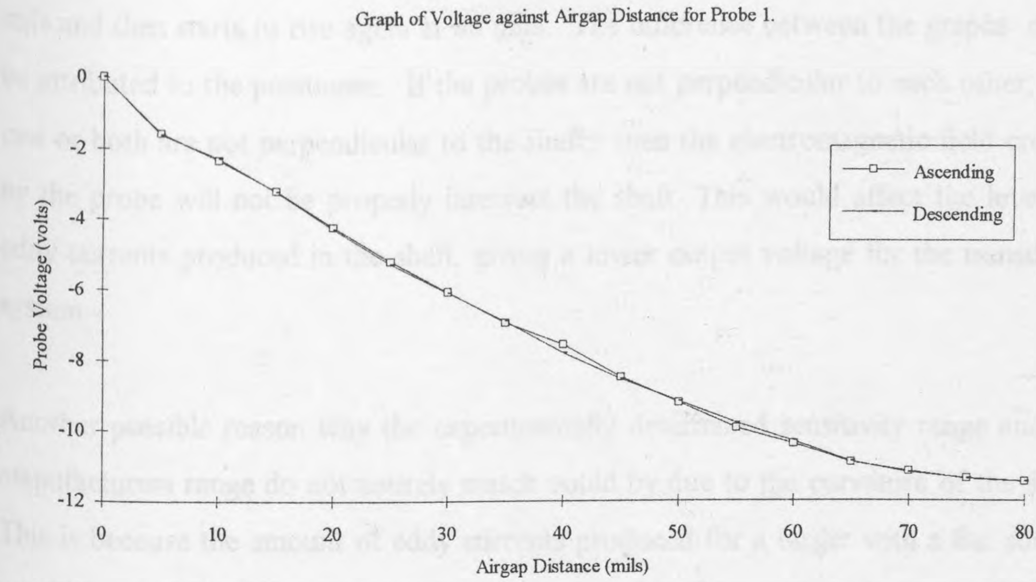

Graph 3.1: Graph of Voltage against Airgap Distance for Probe 1.

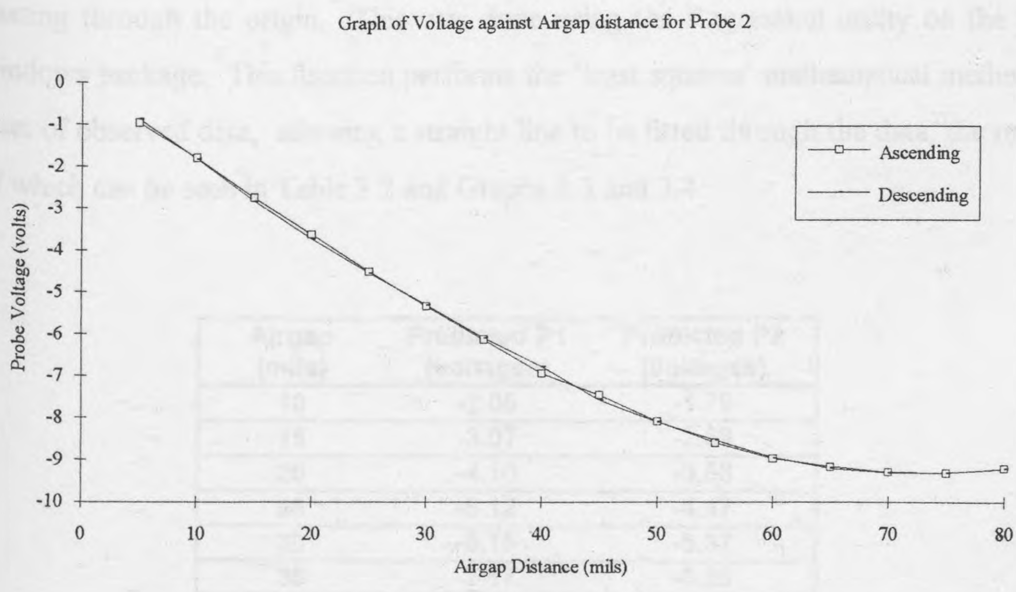

Graph 3.2: Graph of Voltage against Airgap Distance for Probe 2.

It can be seen that both the graphs of voltage against airgap distance for the probes have similar characteristics, with probe 1 giving a larger negative voltage than probe 2. Starting at the origin, they are relatively linear up to approximately 40 mils where they start to level off into a peak. The graph for probe 2 shows that the voltage peaks at 75 mils and then starts to rise again at 80 mils. The difference between the graphs could be attributed to the positioner. If the probes are not perpendicular to each other, thus one or both are not perpendicular to the shaft, then the electromagnetic field created by the probe will not be properly intersect the shaft. This would affect the levels of eddy currents produced in the shaft, giving a lower output voltage for the transducer system.

Another possible reason why the experimentally determined sensitivity range and the manufacturers range do not entirely match could by due to the curvature of the shaft. This is because the amount of eddy currents produced for a target with a flat surface would be slightly different from the amount produced by a curved target, and thus would give a slightly different output voltage.

It was possible to achieve a best fitting straight line over the range 10 - 35 mils, passing through the origin. This was done using the Regression utility on the Exel windows package. This function performs the 'least squares' mathematical method on a set of observed data, allowing a straight line to be fitted through the data, the results of which can be seen in Table 3.2 and Graphs 3.3 and 3.4.

Airgap (mils)	Predicted P1 (voltages)	Predicted P2 (voltages)
10	-2.05	-1.79
15	-3.07	-2.68
20	-4.10	-3.58
25	-5.12	-4.47
30	-6.15	-5.37
35	-7.17	-6.26

Table 3.2: Table of predicted voltages for the probes using the 'least squares' mathematical method.

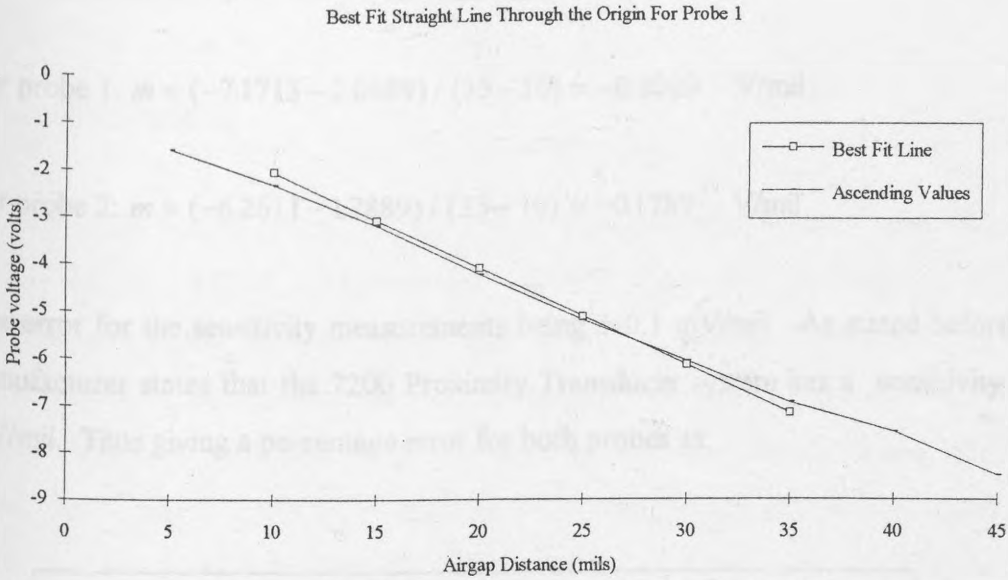

Graph 3.3: Graph of the best fit straight line passing through the origin for probe 1

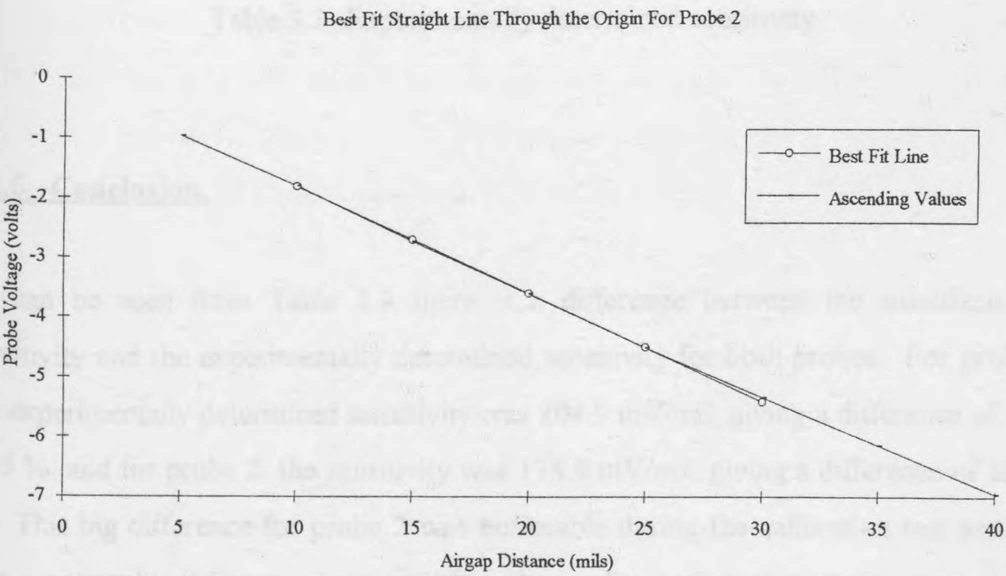

Graph 3.4: Graph of the best fitting straight line passing through the origin for probe 2

The sensitivity of the probes can be determine by finding the gradient of the best fitting lines.

From the gradient equation for a straight line: $m = \Delta y / \Delta x$

For probe 1: $m = (-7.1713 - 2.0489) / (35 - 10) = -0.2049$ V/mil

For probe 2: $m = (-6.2611 - 1.7889) / (35 - 10) = -0.1789$ V/mil

The error for the sensitivity measurements being ± 0.1 mV/mil. As stated before the manufacturer states that the 7200 Proximity Transducer system has a sensitivity 200 mV/mil. Thus giving a percentage error for both probes as;

	Experimental Sensitivity (mV / mil)	Manufacturer Sensitivity (mV / mil)	Percentage Difference %
Probe 1	204.9	200	2.45
Probe 2	178.9	200	10.55

Table 3.3: Experimentally determined sensitivity

3.2.6. Conclusion.

As can be seen from Table 3.3 there is a difference between the manufacturers sensitivity and the experimentally determined sensitivity for both probes. For probe 1 the experimentally determined sensitivity was 204.9 mV/mil, giving a difference of only 2.45 %, and for probe 2 the sensitivity was 178.9 mV/mil, giving a difference of 10.55 %. This big difference for probe 2 was noticeable during the calibration test as there was a noticeable difference between the voltages for both probes at the same airgap distance. These differences were decided to be within an acceptable level, as the experimental values would be used during the experimentation and would remain relatively constant. It was decided to set the airgap distance for both the probes to 20 mils, (0.508 mm). This would ensure that the probes estimated working range of 10 - 30 mils, (0.254 - 0.762 mm), was within the linear range experimentally determined for each probe.

3.3. Calibration of the accelerometers.

3.3.1. Introduction.

As mentioned before in Chapter 2.4.2., the accelerometers chosen were Monitran limited MTN / 1120S accelerometers. These accelerometers were specifically manufactured smaller than the normal type of MTN / 1120S, to a height of 20 mm. the sensitivity of each accelerometer was correspondingly reduced to approximately 10 mV/g. Monitran performed calibration tests on each accelerometer; the values of which can be seen in Table 3.4 on page 36, but it was necessary to perform a separate calibration test to check whether any of them had been damaged since the original test.

3.3.2. Experimental Theory.

If an accelerometer is vibrated at an exact frequency then the spectrum of its response should show up as a peak at that frequency alone, as shown in Figure 3.2, assuming that there is minimal leakage (i.e. the components of that frequency has not influenced the immediate frequencies, causing them to show as a signal).

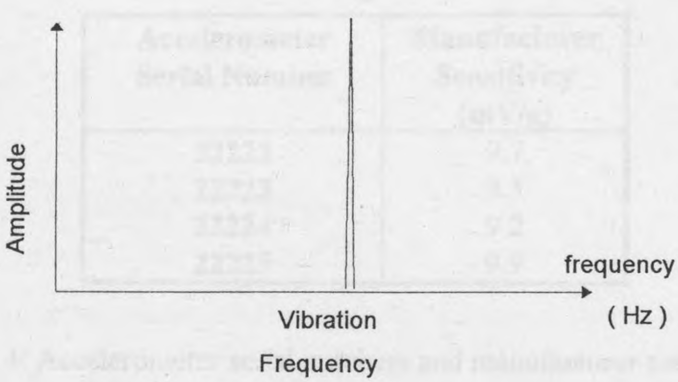

Figure 3.2: Frequency response for a vibration at an exact frequency.

It is possible to determine the power of this signal by measuring the area under this peak. This can be achieved by using the root mean square (RMS) mathematical method. The RMS value of y stands for "the square Root of the Mean value of the Squares of y" between some stated limits. In this case a set limit range with its centre based upon the discrete frequency.

The calibration exciter used to in this check provides an acceleration excitation level of 10 m/s^2 (RMS value) at a frequency of 159.2 Hz ($\omega = 1000$ rad/s). The accelerometers given sensitivity is in mV/g (millivolts per gravity), therefore it is necessary to determine how many 'g's (gravity's) that the exciter provides. The acceleration due to gravity, g, is taken in SI units to be 9.81 m/s^s.

Therefore; g level produced by the exciter = 10/9.81 = 1.019 g.

3.3.3. Equipment.

Diagnostic Instruments PL202 FFT Analyser Model PL202 Serial Number:123

4 Monitran Ltd. MTN/1120S/137 Accelerometers Serial Numbers and sensitivities are shown in Table 3.4.

Brüel and Kjær Calibration Exciter Type 4294 Serial Number; 1154481

Monitran Ltd. MTN/1120D Accelerometer. Serial Number; 5172

Gould Colorwritwer Plotter model 6120-3111-06 Serial Number; N5F02109

Accelerometer Serial Number	Manufacturer Sensitivity (mV/g)
22222	9.7
22223	9.3
22224	9.2
22225	9.9

Table 3.4: Accelerometer serial numbers and manufacturer sensitivities.

3.3.4. Procedure.

The apparatus was set up as shown in Figure 3.3.

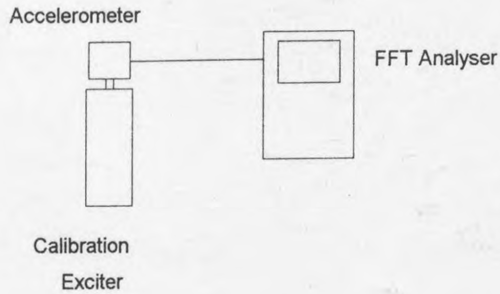

Figure 3.3.: Schematic of the calibration test layout.

An accelerometer was securely connected onto the calibration exciter by a small threaded bar. This was to ensure good vibration transmission from the exciter to the accelerometer. The FFT analyser settings were altered appropriately for each different accelerometer, these settings can be seen in Appendix 2. The calibration exciter was switched on and left for approximately five seconds before readings were taken by the FFT analyser. This delay ensured that the exciter achieved working stability after being switched on from rest. Once the appropriate data had been captured, processed and saved by the FFT analyser the exciter was switched off and the accelerometer was removed. This process was repeated for each accelerometer tested.

3.3.5. Results.

3.3.5.1 Test for accelerometer on bearing 2L.

Accelerometer tested was; MTN/1120S/137 Serial Number 22223

Monitran calibration test states that the sensitivity for this accelerometer is 9.3 mV/g at 80 Hz.

The RMS value obtained from the FFT analyser = 992.436 mg, giving a percentage difference from the expected value of 2.65 %. This percentage difference is the difference from the calculated value in section 3.3.2. The frequency response can be seen in Graph 3.5.

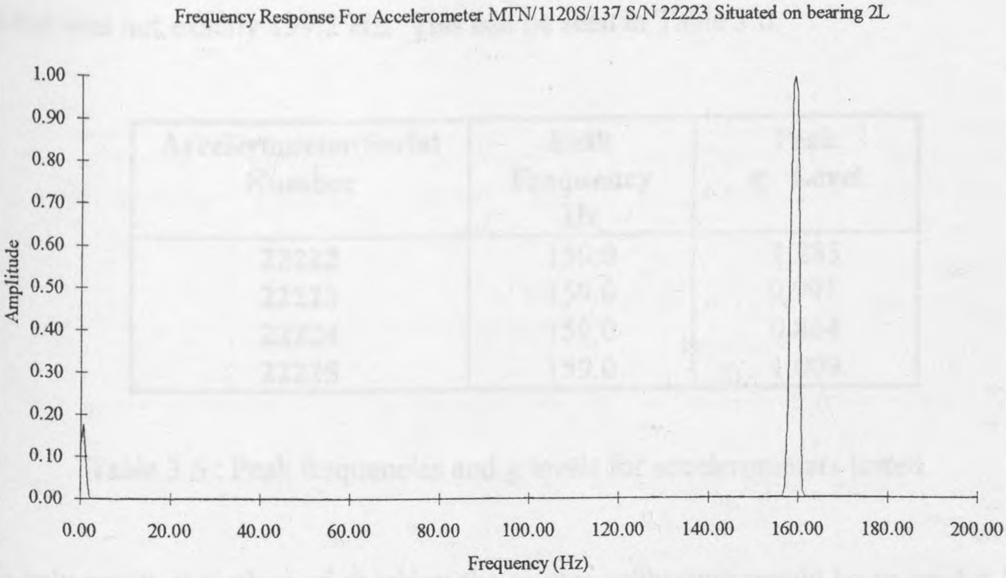

Graph 3.5.: Frequency response for accelerometer MTN/1120S/137 S/N 22223

The other three accelerometers were tested in the same method, with the results shown in Table 3.5

It can be seen from a table of the results, Table 3.5, that two of the accelerometers used on the test rig give quite close values to the theoretical value expected.

Accelerometer Serial Number	Bearing Situated On Test Rig	Experimentally Determined g Level	Percentage Difference from Manufacturer Specification
22222	3L	1.287	26.25
22223	2L	0.992	2.56
22224	5L	0.865	15.10
22225	4L	1.011	0.82

Table 3.5.: Accelerometer calibration test results.

It is unknown when the calibration exciter was itself last calibrated. It is known however, that it has not been checked in the last eight years. This leads to doubt in the exact level and frequency of the vibration produced by the exciter. One indication that the exciter is not producing the exact values was the fact that the peak frequencies for the test was not exactly 159.2 Hz. This can be seen in Table 3.6.

Accelerometer Serial Number	Peak Frequency Hz	Peak g Level
22222	159.0	1.285
22223	159.0	0.991
22224	159.0	0.864
22225	159.0	1.009

Table 3.6.: Peak frequencies and g levels for accelerometers tested.

The only practical method of checking the exciter calibration would be to send it back to its manufacturer, Brüel and Kjær, for re-calibration. It was decided to continue with the equipment as there was not enough time to return the calibration exciter to the manufacture.

This did not however explain the vast difference in the calibration for accelerometers 22222 and 22224 (having a difference from the theoretical of 26.25 % and 15.10 % respectively). This could only be attributed to one of two problems.

Firstly, the initial calibration tests were in error. The accelerometers were not of the 'off the shelf' variety and were specifically manufactured, altering their sensitivity from 100 mV/g for the norm to 10 mV/g.

The most probable cause for the difference would be that they have been damaged in some way during the time between the tests. The only certain way that the extent of this damage could be assessed would be to send the accelerometers in question back to the manufacturer for re-calibration. This would however take time, so it was decided to try and experimentally determine the sensitivity of each accelerometer using the equipment available. This was basically achieved by trial and error. The sensitivity level on the SCALE CH1 menu on the display screen was slightly altered from the stated sensitivity and a reading taken. Once the g RMS value was found to be within 1% (1.019 g ±0.0102) of the theoretical then the test was finished. The new sensitivity for accelerometer 22222 was found to be 12.2. mV/g and accelerometer 22224 was found to be 8.4 mV/g, as shown in Table 3.7, Graph 3.6 and Graph 3.7.

Acc. Serial No.	Original Sensitivity (mV/g)	Original g Level	Experimental Sensitivity (mV/g)	Experimental g Level	Percentage Difference From Manufacturer Specification
22222	9.7	1.287	12.2	1.024	0.45
22224	9.9	0.865	8.4	1.015	0.43

Table 3.7: Experimentally determined sensitivity for accelerometers 22222 and 22224

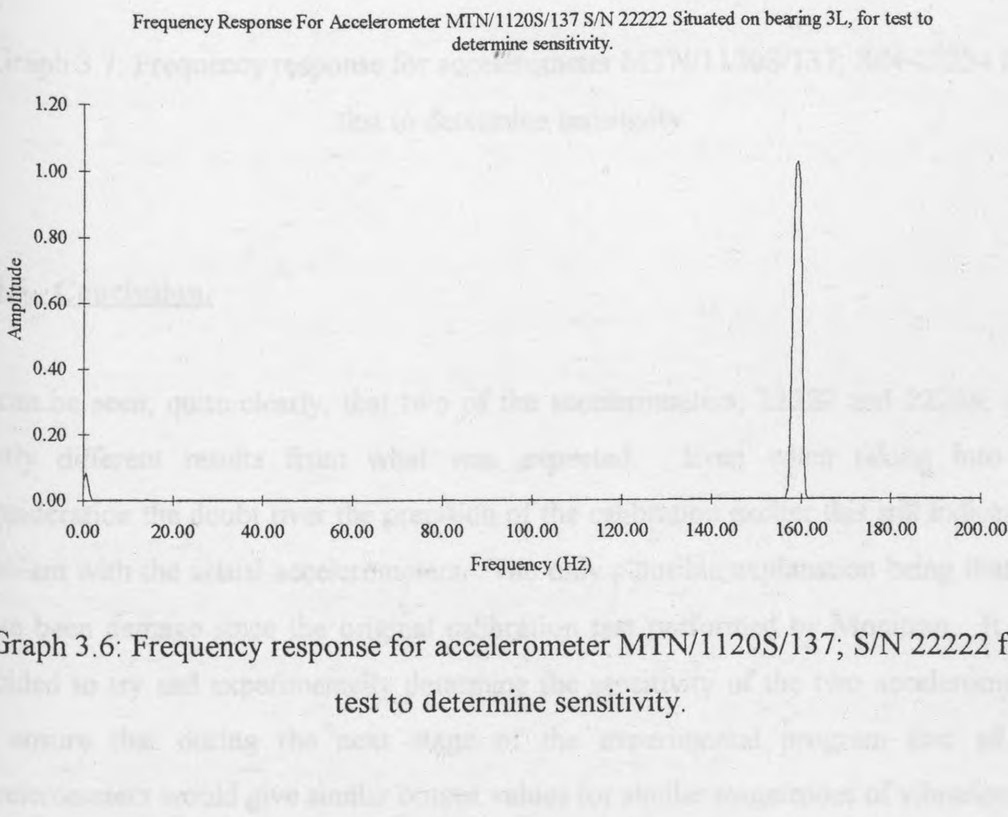

Graph 3.6: Frequency response for accelerometer MTN/1120S/137; S/N 22222 for test to determine sensitivity.

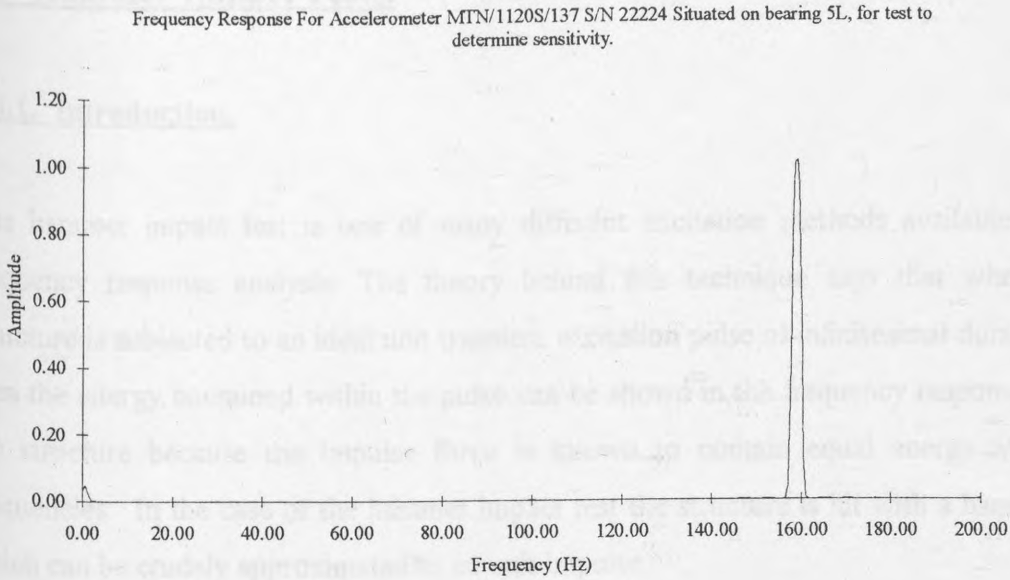

Graph 3.7: Frequency response for accelerometer MTN/1120S/137; S/N 22224 for test to determine sensitivity.

3.3.6. Conclusion.

It can be seen, quite clearly, that two of the accelerometers, 22222 and 22224, gave vastly different results from what was expected. Even when taking into the consideration the doubt over the precision of the calibration exciter this still indicates a problem with the actual accelerometers. The only plausible explanation being that the have been damage since the original calibration test performed by Monitran. It was decided to try and experimentally determine the sensitivity of the two accelerometers to ensure that during the next stage of the experimental program that all the accelerometers would give similar output values for similar magnitudes of vibration.
It must be determined whether this damage was just one off damage or if it is continual degradation to the accelerometer, therefore it would be necessary to undertake calibration tests on the accelerometers on a regular basis.

3.4. Hammer Impact Tests.

3.4.1. Introduction.

The hammer impact test is one of many different excitation methods available for frequency response analysis. The theory behind this technique says that when a structure is subjected to an ideal unit transient excitation pulse of infinitesimal duration then the energy contained within the pulse can be shown in the frequency response of the structure because the impulse force is known to contain equal energy at all frequencies. In the case of the hammer impact test the structure is hit with a hammer which can be crudely approximated to an unit impulse.

This technique was used to try and crudely determine the transducer positioners natural frequencies, and give an indication whether the positioners themselves would be cause of vibration, in normal working speed, thus affecting the transducers' reading.

The basic equipment required is an impactor (usually in the form of a hammer) possibly containing a force transducer, a response transducer and the appropriate signal processing equipment. The simplicity of this set up means that a minimum set up time is required.

3.4.2. Equipment.

Diagnostic Instruments PL202 FFT Analyser Model PL202 Serial No:123

2 x Brüel and Kjær Charge Amplifier Type 2651 Serial Nos: 721259 and 985758
SMOE Nos: CP/082/03 and CP/083/03

Brüel and Kjær Accelerometer Type 4374 Serial No: 983509

Brüel and Kjær Power Supply Type 2805 Serial No 370250
SMOE No: CP/079/3

Brüel and Kjær Hammer Type 8202 Serial No: 1271132
SMOE No: CP/073/9

Includes Force Transducer Type 8200 Serial No: 1288522

Gould Digital Storage Oscilloscope Type 4035 Serial No: 1895

3.4.3. Procedure.

The equipment was set up as shown in Figure 3.4.

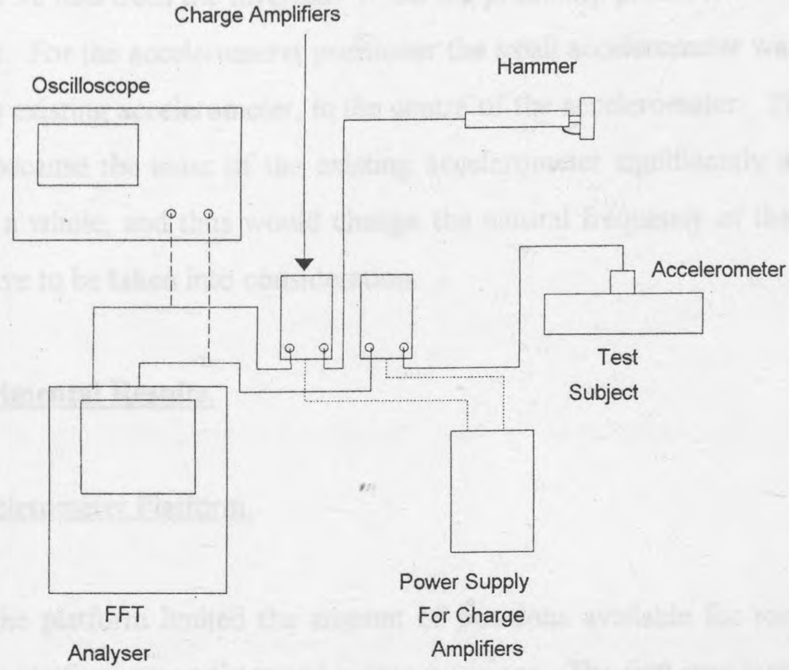

Figure 3.4.: The equipment configuration.

The outputs from both charge amplifiers were connected into the oscilloscope. The hammer was lightly tapped to examine the output signal on the oscilloscope screen. This was to ensure that the hammer had been set up properly and that it was providing a suitable signal. The accelerometer was also lightly tapped for the same reasons. The output leads were then connected to the FFT analyser, with the hammer connected to channel 1 and the accelerometer connected to channel 2. The FFT analyser setting were altered to those required for the hammer impact test. The actual FFT settings can be seen in Appendix 2. The accelerometer was attached to the test subject using beeswax. The test subject was tapped at position 1 with the hammer and the signal was held on the FFT analyser. The signal was checked to ensure that the signal was of adequate strength for the settings, i.e. the tap was not too small so that it gave too small a signal or the tap was not too large that it overloaded the FFT input settings, and that other problems such as a double impact did not occur. The test subject was tapped a total of 10 times at position 1 and the average values processed. This process was repeated for the various different positions, as required.

The whole process was repeated for both the different types of transducer positioners, the proximity probe positioner and the accelerometer positioner. The accelerometer was placed at 32 mm from the inverted 'V' on the proximity probe, near the centre of the positioner. For the accelerometer positioner the small accelerometer was placed on the top of the existing accelerometer, in the centre of the accelerometer. This position was chosen because the mass of the existing accelerometer significantly affected the positioner as a whole, and thus would change the natural frequency of the positioner and would have to be taken into consideration.

3.4.4. Experimental Results.

3.4.4.1. Accelerometer Platform.

The size of the platform limited the amount of positions available for testing so the accelerometer platform was only tested in two positions. The first was located 10 mm from the bottom of the platform, in the centre of one of the sides, and the other was located 10 mm from the top of the platform, again in the centre of the same side. This can be seen in the schematic shown in Figure 3.5. The frequency response graphs can be seen in Graphs 3.8 to 3.11.

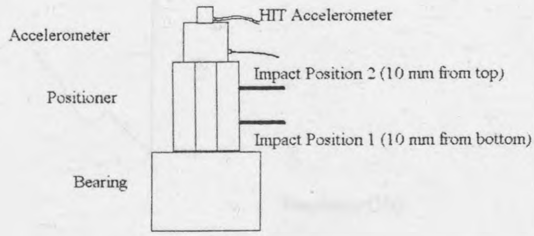

Figure 3.5. : Schematic of Hammer Impact test Impact Positions.

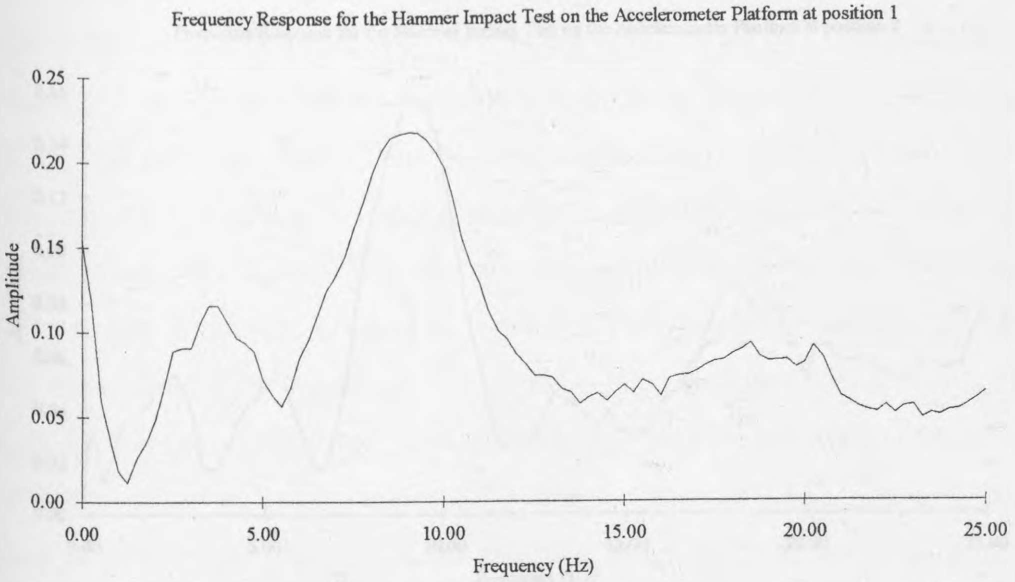

Graph 3.8: The amplitude frequency response graph for the accelerometer platform at position 1

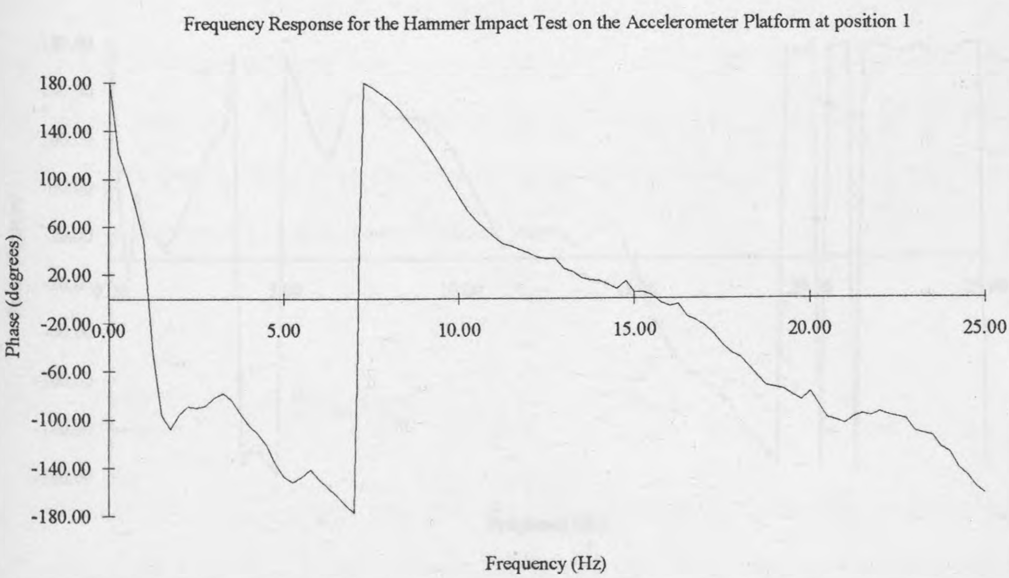

Graph 3.9.: The phase frequency response graph for the accelerometer platform at position 1

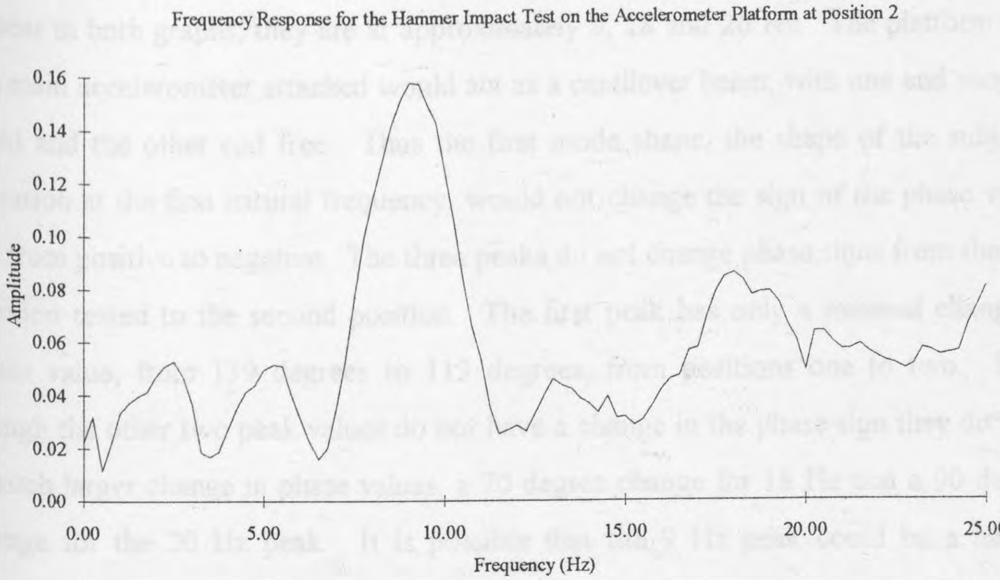

Graph 3.10.: The amplitude frequency response graph for the accelerometer platform at position 2

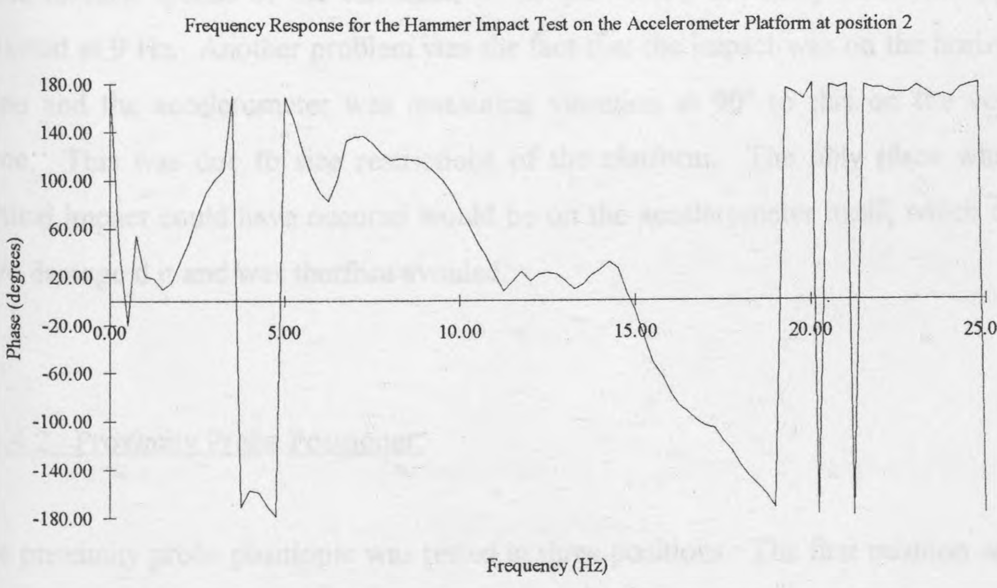

Graph 3.11: The phase frequency response graph for the accelerometer platform at position 2

The graph of amplitude against frequency for position 1 clearly shows four distinct peaks. Whereas the graph of position 2 clearly shows six peaks. For a peak to signify the natural frequency then it would have to appear in both graphs, with the same frequency but different amplitude and phase values. There are only three peaks that appear in both graphs; they are at approximately 9, 18 and 20 Hz. The platform with the main accelerometer attached would act as a cantilever beam, with one end securely fixed and the other end free. Thus the first mode shape, the shape of the subject's vibration at the first natural frequency, would not change the sign of the phase value, i.e. from positive to negative. The three peaks do not change phase signs from the first position tested to the second position. The first peak has only a minimal change in phase value, from 139 degrees to 113 degrees, from positions one to two. Even though the other two peak values do not have a change in the phase sign they do have a much larger change in phase values, a 70 degree change for 18 Hz and a 90 degree change for the 20 Hz peak. It is possible that the 9 Hz peak could be a natural frequency value, though this is unlikely because the positioner is a short, solid bar of metal and would have a large value for its first natural frequency. This frequency value must be looked at closely in the further experiments that use the accelerometers to see if the running speeds of the camshaft, or its harmonics, adversely affect the signals obtained at 9 Hz. Another problem was the fact that the impact was on the horizontal plane and the accelerometer was measuring vibration at 90° to this on the vertical plane. This was due to size restrictions of the platform. The only place where a vertical impact could have occured would be on the accelerometer itself, which could have damage d it and was therfore avoided.

3.4.4.2. Proximity Probe Positioner.

The proximity probe positioner was tested in three positions. The first position was at the centre of the second half of the positioner, this part was the part that was attached to the inlet camshaft bearings. Position two was 18 mm away from the accelerometer at the bottom of the inverted 'V'. The third position was 7 mm from the top of the inverted 'V' on the proximity probe 2 side. These positions can be seen in Figure 3.6. The results of the tests can be seen in Graphs 3.12. to 3.17.

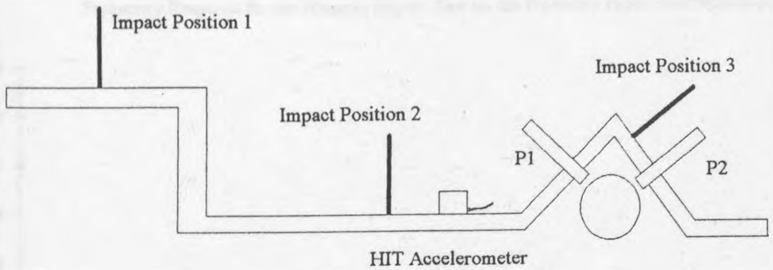

Figure 3.6. : Schematic of the Hammer Impact Test Impact positions

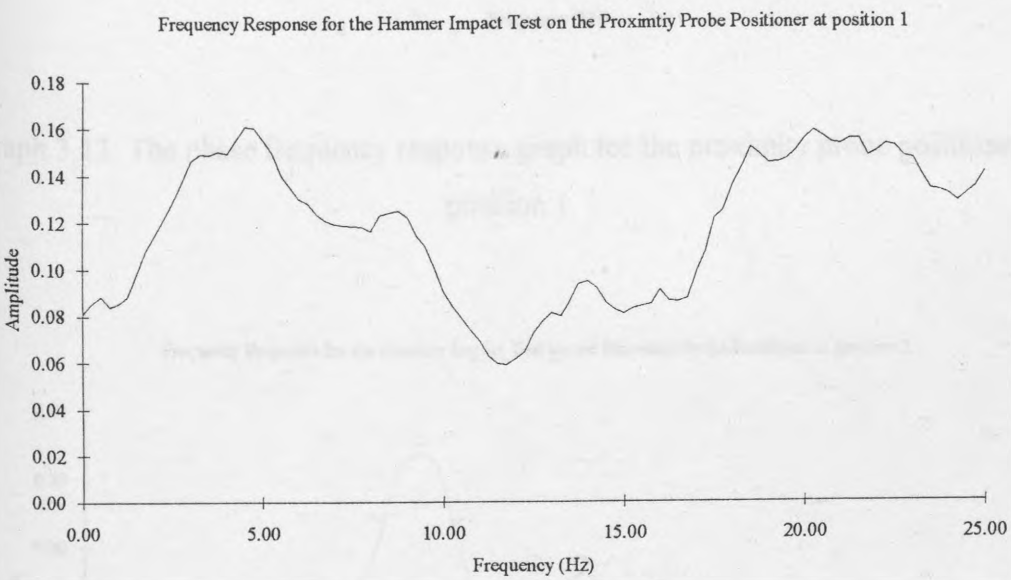

Graph 3.12: The amplitude frequency response graph for the proximity probe positioner at position 1.

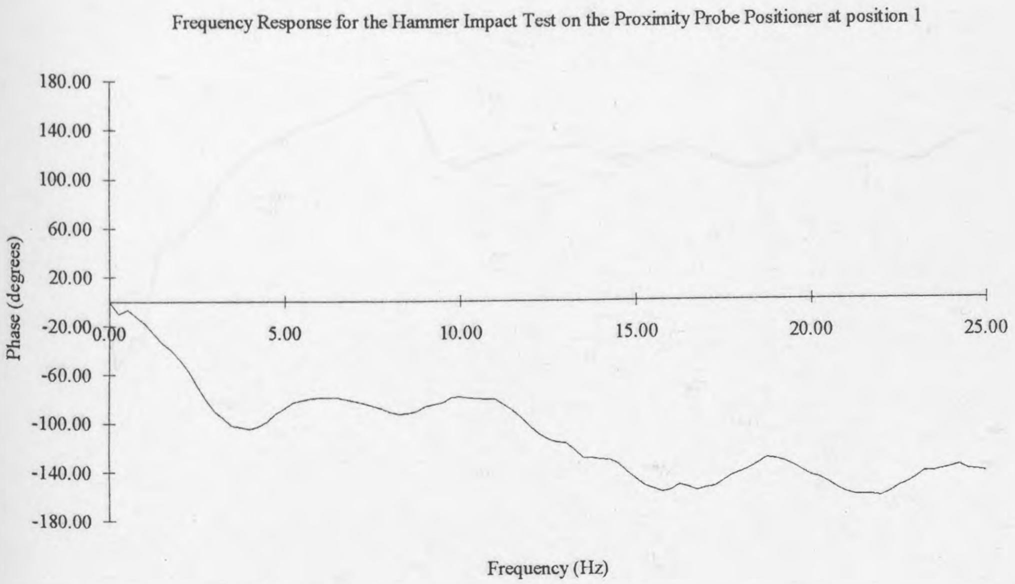

Graph 3.13: The phase frequency response graph for the proximity probe positioner at position 1.

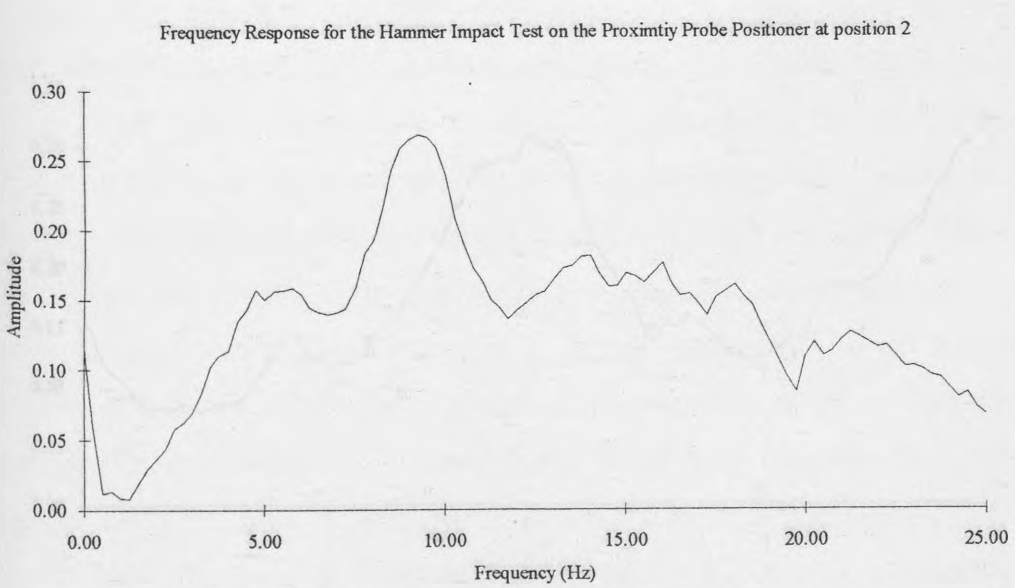

Graph 3.14: The amplitude frequency response graph for the proximity probe positioner at position 2.

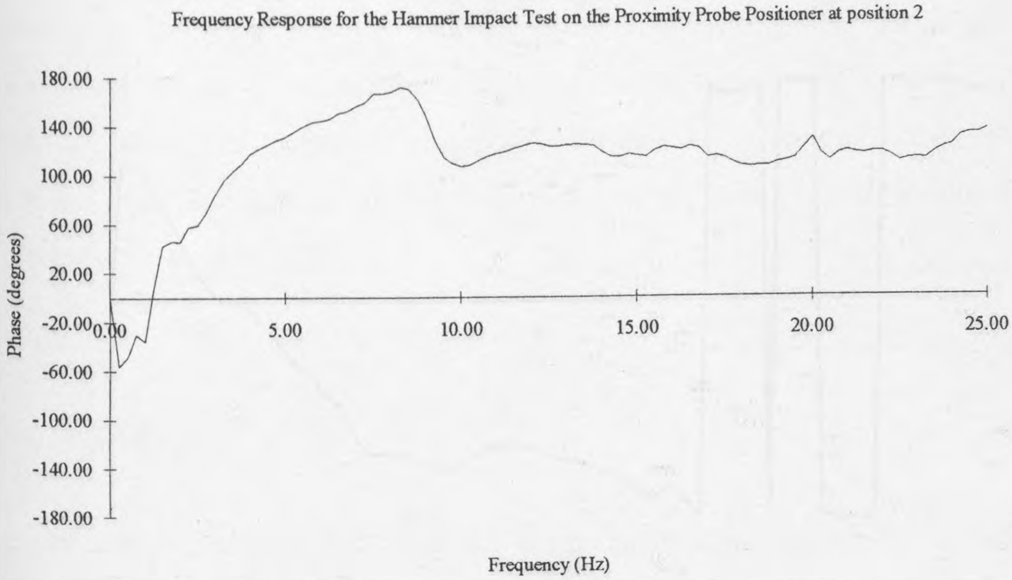

Graph 3.15: The phase frequency response graph for the proximity probe positioner at position 2.

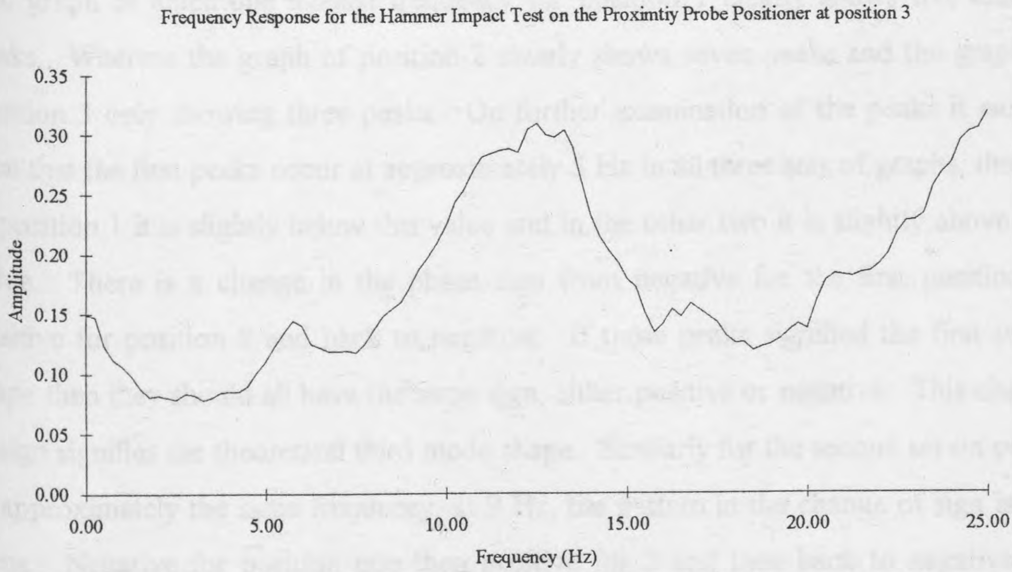

Graph 3.16: The amplitude frequency response graph for the proximity probe positioner at position 3.

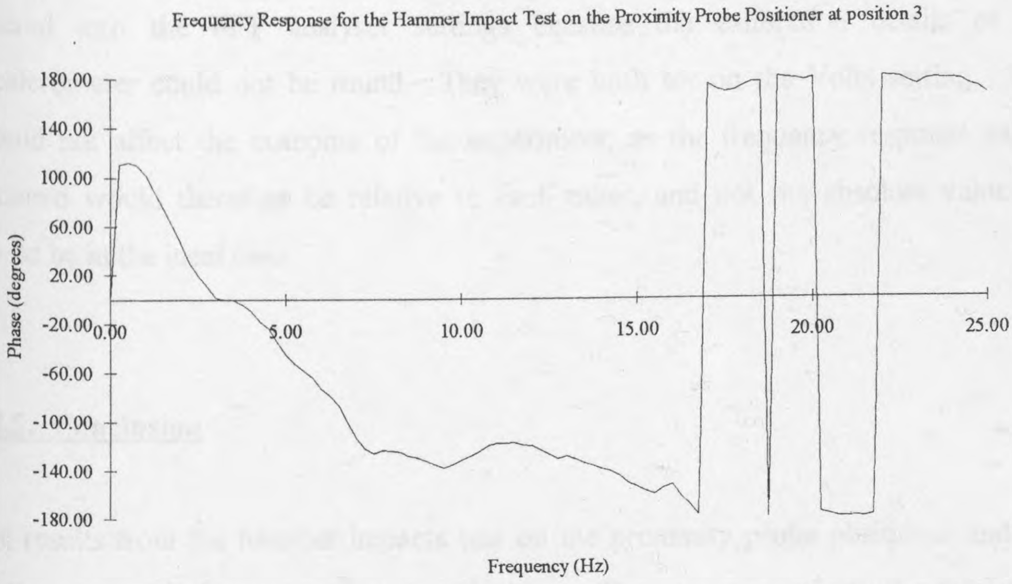

Graph 3.17: The phase frequency response graph for the proximity probe positioner at position 3.

The graph of amplitude against frequency for position 1 clearly shows five distinct peaks. Whereas the graph of position 2 clearly shows seven peaks and the graph of position 3 only showing three peaks. On further examination of the peaks it can be seen that the first peaks occur at approximately 5 Hz in all three sets of graphs, though in position 1 it is slightly below this value and in the other two it is slightly above this value. There is a change in the phase sign from negative for the first position to positive for position 2 and back to negative. If these peaks signified the first mode shape then they should all have the same sign, either positive or negative. This change in sign signifies the theoretical third mode shape. Similarly for the second set on peaks at approximately the same frequency, at 9 Hz, the pattern in the change of sign is the same. Negative for position one then positive for 2 and then back to negative for position 3. Another aspect of the phase value is that for the mode shapes they should be approximately - 90 ° or + 90°, though this may not be the case because of possible errors in the experimentation.

The sensitivities of the hammer force transducer and the accelerometer were not entered into the FFT analyser settings because the calibration details of the accelerometer could not be found. They were both set on the Volts setting. This should not affect the outcome of the experiment, as the frequency response values obtained would therefore be relative to each other, and not the absolute values as would be in the ideal case.

3.4.5. Conclusion

The results from the hammer impacts test on the proximity probe positioner and the accelerometer platform were not very decisive. There was a peak on the frequency response graphs for the accelerometer platform that may have been due to a natural frequency. This occurred at about 9 Hz. This is unlikely though due to the fact that the platform would act as a very stiff cantilever beam and thus the natural frequency of the platform would be high. One possible way to determine more information about this peak would be to make hammer impact tests of the area around the accelerometer platform, to determine whether it was a part of the engine immediately adjacent to the platform that was the cause of this peak. Another would be to test all the accelerometer platforms in the same positions. Even though the platforms have an identical design they would be manufactured slightly differently, but would provide an good indication of the frequencies that peaks may occur. The proximity probe positioner did not give any indication that any of the peaks were due to its natural frequency, but again because of the quality of the results this should be treated with caution.

The hammer impact test was undertaken, because of severe time constraints, very quickly. Because of this a full modal survey could not be undertaken thus leading to inconclusive results that were obtained.

3.5. Spectral Analysis

3.5.1. Introduction.

A spectral analysis basically takes a time domain signal and breaks it down into its main components. This is achieved by using fourier transforms to interpret the signal into its frequency and amplitude terms. This can be clearly demonstrated by two examples. In the first case a simple sine wave is analysed. The sine wave has an amplitude A and a frequency ωt, as seen in Figure 3.7. When analysed the sine wave will show up as a single spike, of amplitude A at a frequency of ωt.

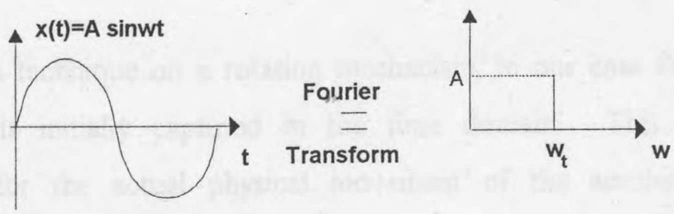

Figure 3.7.: A simple sine wave in the time domain and the frequency domain.

For a more complex signal, as shown in Figure 3.8. Where the signal is the sum of three different sine wave such that:

$$x(t) = A^*\sin \omega_1 t + B^*\sin \omega_2 t + C^*\sin \omega_3 t$$

The signal would be analysed and broken down into its three components and shown in the frequency domain as three spikes, one for each part of the signal.

This analysing technique is particularly useful when dealing with very complex signals as they can be transformed into the frequency domain for easier interpretation.

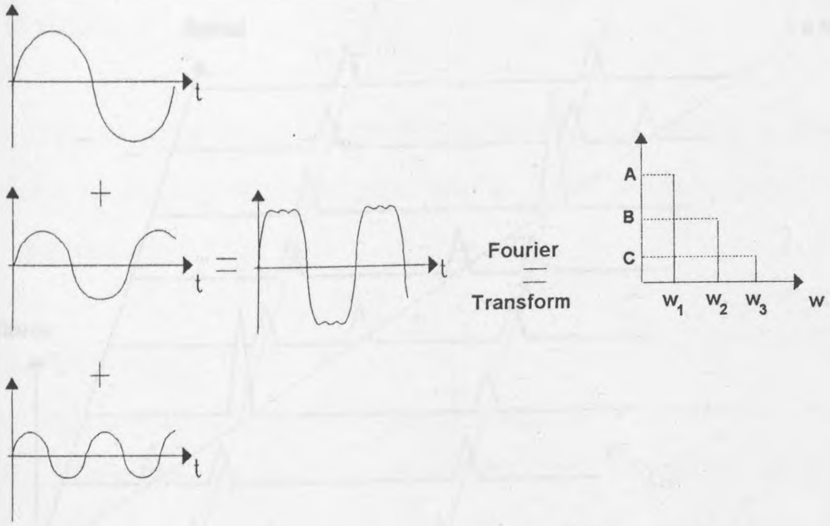

Figure 3.8: A complex wave made from three individual sine waves in the time domain and the frequency domain.

When using this technique on a rotating mechanism, in our case the camshaft, the vibration data is initially captured in the time domain. This gives a voltage representation for the actual physical movement of the accelerometer (for the accelerometer) and the camshaft (for the proximity transducers). Once this data has been transferred into the frequency domain then it is possible to determine, from the peaks, the running speed and its harmonics and any resonance frequencies in the system induced by them for the speed that the data was captured at.

If this data capture process is done at different speeds then a 'Waterfall Plot' can be constructed. This is achieved by accelerating a rotating machine through a range of speeds and carrying out spectral analysis at regular speed intervals. This allows for a more detailed analysis of vibratory response for the mechanism over the speed range under consideration. It will clearly show whether any particular speeds or their harmonics induce resonance frequencies in the system, i.e. where the peaks attributed to the running speed coincide with those due to the modes, as can be seen in Figure 3.9.

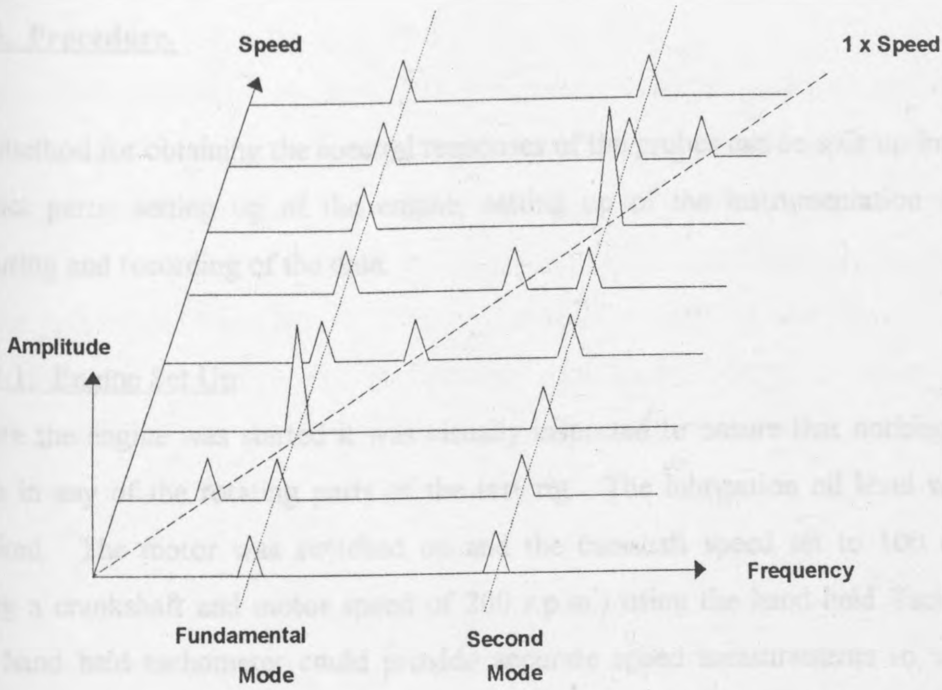

Figure 3.9.: An example of a waterfall plot showing the effect of varying running speed on the resonance frequencies.

3.5.2. Equipment.

Thurlby K1 Module Serial No: 43637 SMOE No.: CP/028/12

Gould Digital Storage Oscilloscope Type 4035 Serial No: 1895

Diagnostics Instruments Real Time FFT Analyser Model PL202 Serial No:123

2 x Bentley Nevada Proximity Probe Part No. 21500-00-08-10-02
Serial Nos: JULU440763 and JULU440765

2 x Bentley Nevada Extension Cable Part No.: 21747-040-00

2 x Bentley Nevada Proximitor Part No.: 18745-03
Serial No: JUNU118860 and JUNU118865

4 x Monitran Accelerometer Serial Nos: MTN/1120S/22222 to MTN/1120S/22225

RS Components Ltd. Optical Tacho Model TM-2011 Serial No: 0468
SMOE No.: CP/043/4

3.5.3. Procedure.

The method for obtaining the spectral responses of the probes can be split up into three distinct parts; setting up of the engine, setting up of the instrumentation and the capturing and recording of the data.

3.5.3.1. Engine Set Up:

Before the engine was started it was visually inspected to ensure that nothing would catch in any of the rotating parts of the test rig. The lubrication oil level was also checked. The motor was switched on and the camshaft speed set to 100 r.p.m. (giving a crankshaft and motor speed of 200 r.p.m.) using the hand held Tachometer (the hand held tachometer could provide accurate speed measurements to within 2 r.p.m. of the desired value). The lubrication oil pressure reading on the oil pressure dial was checked to ensure an adequate flow of lubrication oil.

3.5.3.2. Instrumentation Set Up:

The FFT Analyser settings were set for the capture of data from the particular transducer to be used, the actual settings for all the accelerometers and proximity probes can be seen in Appendix 2. The power source for the proximitor was set to -18.01 volts and the pulse created by the key phasor display on the digital oscilloscope. The INPUT 1 and COUP 1 menu settings on the Input Screen and the SCALE CH1 and TYPE menu settings on the Display Screen were double checked to ensure they were set at the appropriate value for the probe being tested. The probe lead was connected into the Channel 1 connection on the back panel of the FFT Analyser and the capture process started. The engine was only going to be run up to camshaft speeds of 350 r.p.m., which is approximately 6 Hz. It was decided to only investigate a small frequency range, from 0 - 25 Hz, for two reasons. Firstly this would adequately provide information for up to four times running speed, for maximum running speed, and secondly 0 - 25 Hz is the smallest frequency range available on the FFT analyser.

3.5.3.3. Capturing and Recording Data:

Because of the number of averages taken for each set of results each data capture takes approximately 2 minutes 30 seconds. The data is then stored under its appropriate filename on the DIRECTORY and FILENAME menus on the Memory Screen. The FFT Analyser settings were altered to accommodate the next transducer to be tested and the data captured and stored. This was repeated until all the transducers had been tested for that camshaft speed, this process took approximately 20 minutes for a complete set of data. The series of tests were repeated for camshaft speeds of 150 r.p.m., 200 r.p.m., 250 r.p.m., 300 r.p.m. and 350 r.p.m.

As mentioned before the engine has been modified and the cooling system removed. It was therefore only practical to have the engine running for an hour before the engine started to heat up. This allowed three complete sets of data (data for speeds 100 - 200 r.p.m.) to be captured and processed before the engine had to be stopped. The final three sets of data had to be captured later, once the engine had cooled down to a sufficient temperature.

When all the data has been captured for all the tests it is possible to print out each trace on either a plotter or a laser printer. This option can be seen on the Utility Screen and by using the Hardcopy 'Hardkey' on the keypad.

The data can also be downloaded to a computer for use in various software packages. This is achieved using the DEC2L V1.11 PL202 Download Support Program provided by the Analyser's manufacturer, Diagnostic Instruments. Each spectrum trace is downloaded as a magnitude trace (in the form of a .TRA file). Each file gives the X and Y co-ordinates of the appropriate trace.

3.5.4. Results.

Please note that because of equipment restrictions that these plots are not true waterfall plots, but are individual traces that have been merged onto a single graph. This is explained more clearly in the next section, immediately after the graphs.

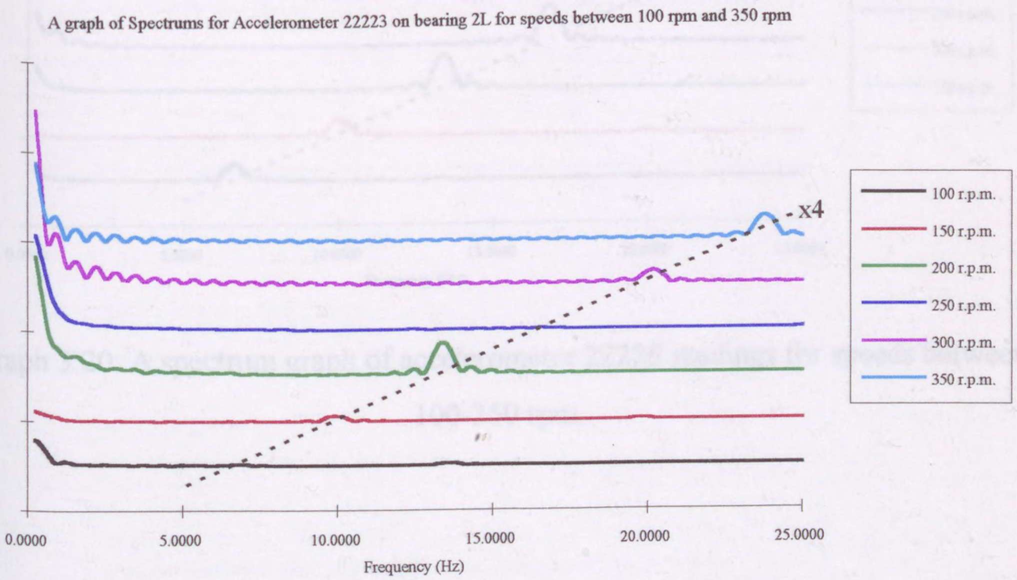

Graph 3.18.: A spectrum graph of accelerometer 22223 readings for speeds between 100-350 rpm.

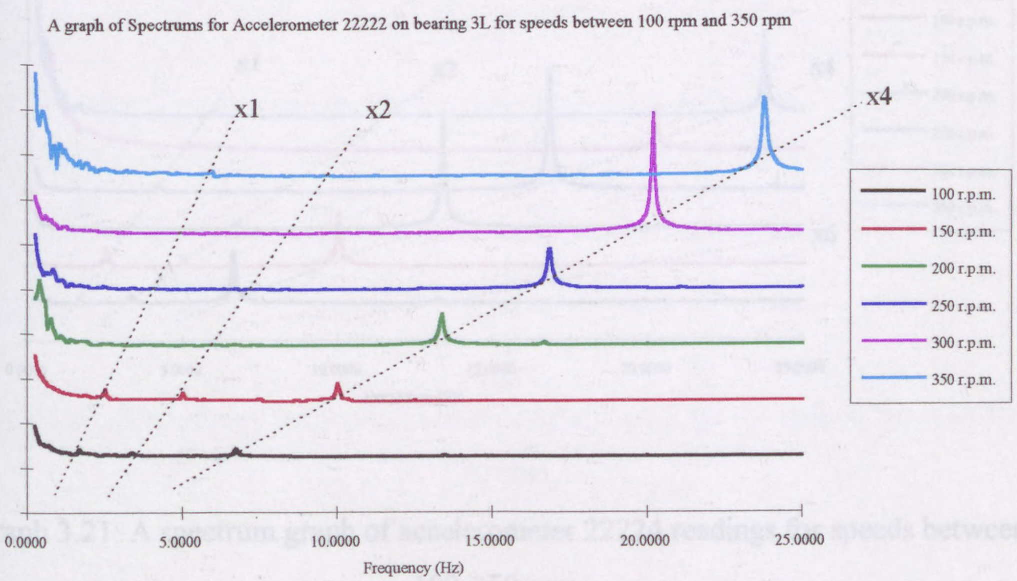

Graph 3.19: A spectrum graph of accelerometer 22222 readings for speeds between 100-350 rpm.

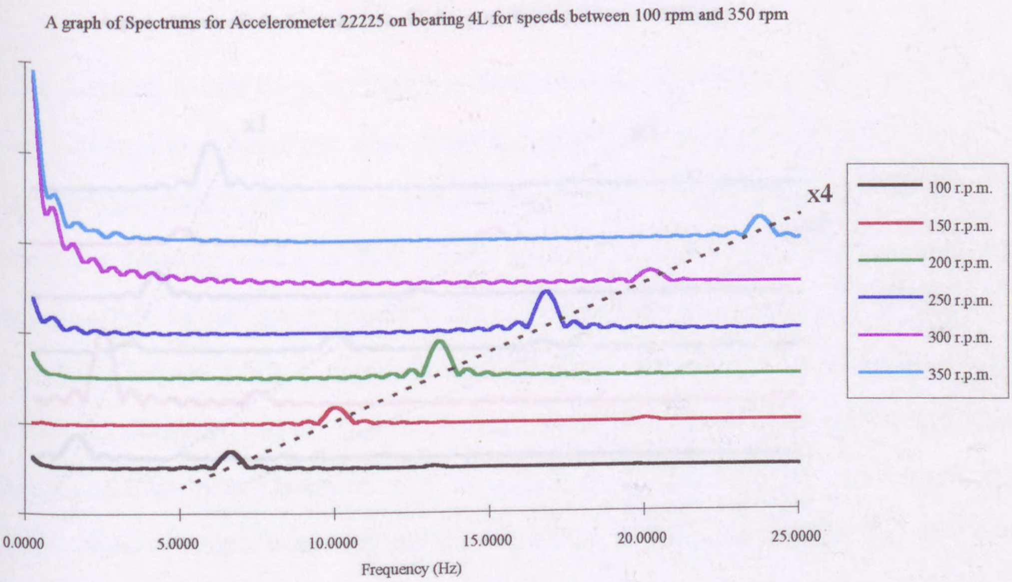

Graph 3.20: A spectrum graph of accelerometer 22225 readings for speeds between 100-350 rpm.

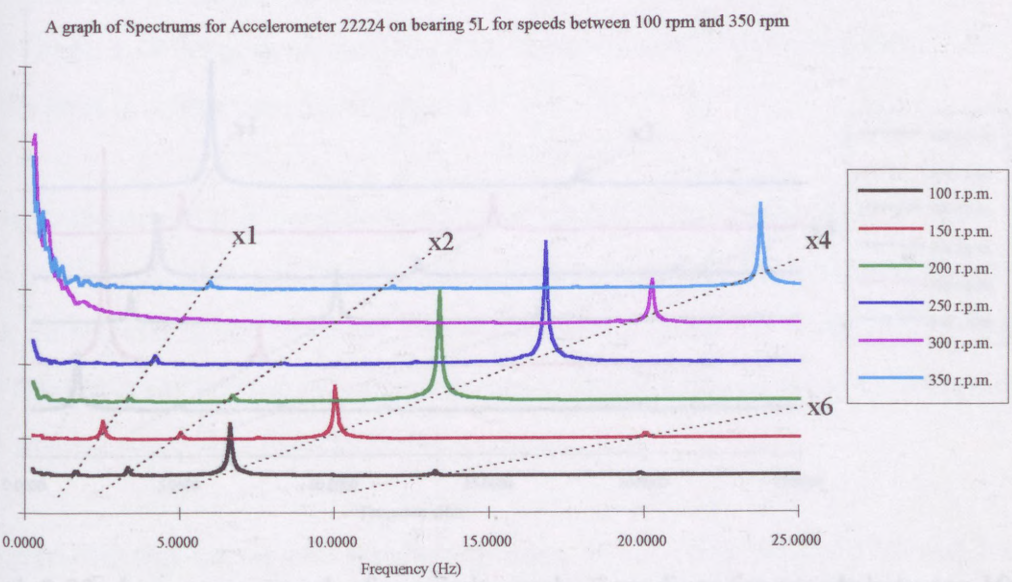

Graph 3.21: A spectrum graph of accelerometer 22224 readings for speeds between 100-350 rpm.

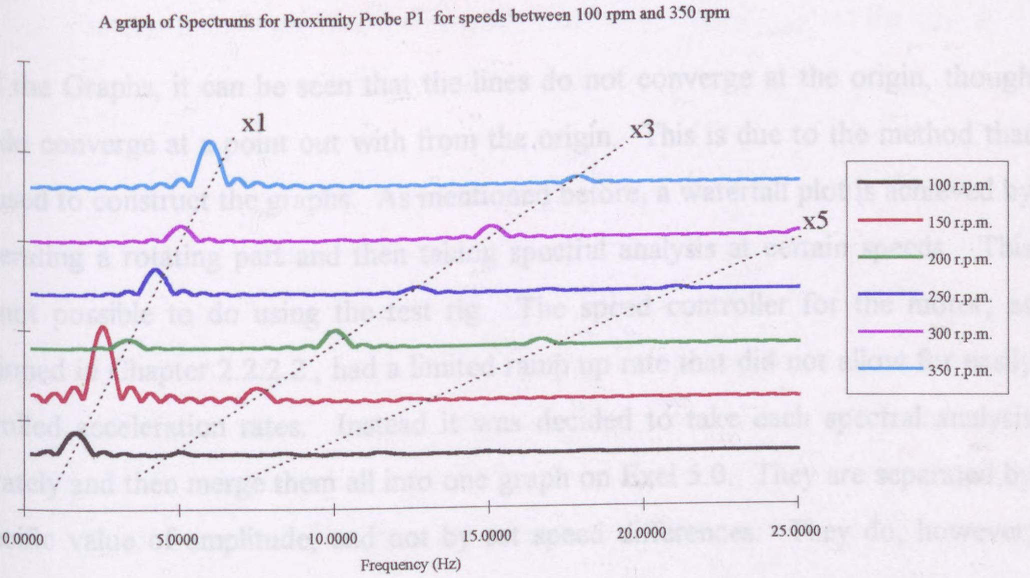

Graph 3.22: A spectrum graph of proximity probe 1 readings for speeds between 100-350 rpm.

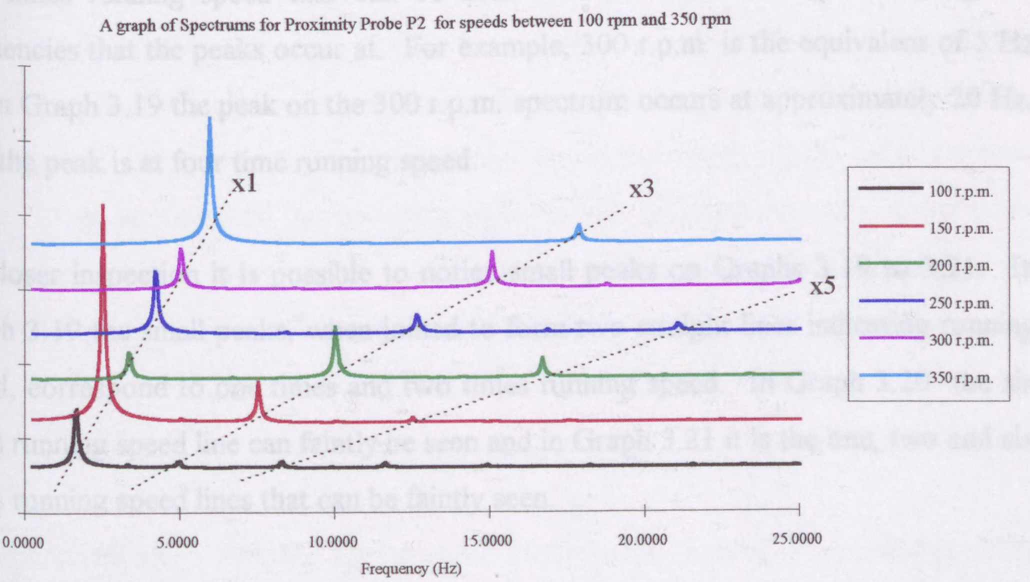

Graph 3.23: A spectrum graph of proximity probe 2 readings for speeds between 100-350 rpm.

3.5.5. Spectral Analysis Observations.

In all the Graphs, it can be seen that the lines do not converge at the origin, though they do converge at a point out with from the origin. This is due to the method that was used to construct the graphs. As mentioned before, a waterfall plot is achieved by accelerating a rotating part and then taking spectral analysis at certain speeds. This was not possible to do using the test rig. The speed controller for the motor, as mentioned in Chapter 2.2.2.2., had a limited ramp up rate that did not allow for easily controlled acceleration rates. Instead it was decided to take each spectral analysis separately and then merge them all into one graph on Exel 5.0. They are separated by a specific value of amplitude, and not by set speed differences. They do, however, provide good running speed information.

It can be quite clearly seen from Graphs 3.18 to 3.21 , for the accelerometers, that a line can be drawn through the peaks to indicate a running speed. In these cases it is the four times running speed that can be seen. This can be told by examining the frequencies that the peaks occur at. For example, 300 r.p.m. is the equivalent of 5 Hz and in Graph 3.19 the peak on the 300 r.p.m. spectrum occurs at approximately 20 Hz, thus the peak is at four time running speed.

On closer inspection it is possible to notice small peaks on Graphs 3.19 to 3.21. In Graph 3.19 the small peaks, when joined to form two straight lines indicating running speed, correspond to one times and two times running speed. In Graph 3.20 the six times running speed line can faintly be seen and in Graph 3.21 it is the one, two and six times running speed lines that can be faintly seen.

It is quite different for the two proximity probes, as shown in Graphs 3.22 and 3.23. In both diagrams the most prominent running speed line is the one times running speed, with the three and five times faintly showing in both figures.

The proximity probes show the most prominent values for the one times running speed. This could be due to the fact that they read the vibrations directly form the camshaft, and the most prominent measurement would be from the running speed.

It is also possible that there are some resonance values showing in the graphs. In Graph 3.18. The 4 x running speed peaks increase until 200 rpm at approximately 13 Hz, then decrease again. For Graphs 3.20. and 3.21. the peak is at approximately 16 Hz and then starts to decay again. For Graph 3.19. the peaks slowly increase in magnitude until 350 rpm, at approximately 20 Hz. For the two proximity probe graphs, Graphs 3.22. and 3.23. the magnitudes of the 1 x running speed increases until 150 rpm at approximately 2 Hz then falls away again. These are possible resonance values but they are unclear because of the fact that there aren't enough traces available to provide a clear picture. If enough traces were available then the peak at the first natural frequency would be most prominent than over, say the fourth natural frequency.

The accelerometer specification states a frequency range of 0.8 Hz to 13 kHz. It can be seen that at low frequencies within this range, especially at the higher speeds under investigation, the accelerometer gives a very large signal which rapidly falls to normal levels. This implies that the accelerometers do not function properly at very low frequencies, even in the specified working range and thus the values obtained at the very low frequencies should be treated with scepticism.

<u>3.5.6. Conclusion.</u>

The spectral analysis plots for the proximity probes clearly show the running speed of the camshaft. The accelerometers, however, do not. The most prominent running speed for them is the four times running speed. Other running speed lines can be seen , though they are very small in comparison to the main peaks, for most of the transducers.

There are possible resonance frequencies showing on each graph, but because of the limited number of traces it is not clear whether they are resonances or not.

CHAPTER 4

INFLUENCE COEFFICIENTS

4.1. Introduction.

In this chapter data experimentally using frequency response tests will be utilised to determine the validity of the initial premise of the research; the influence coefficients connecting the vibration measured at the camshaft to the vibration measured on the camshaft bearings. This will be achieved in several stages:

- The theory behind the premise will be explained and the equations to be used by the theory will be derived.
- Experimental data from the frequency response tests shall be measured.
- A sample calculation will be shown using the experimentally determined values of amplitude and phase to determine the value of the influence coefficient at one particular frequency for one speed. Sample calculations for the same frequency at the other speeds can be seen in Appendix 5.
- There shall be a further examination one of the original assumptions of the theory and to show its effect on the influence coefficient.
- Only a small number of combinations will be examined in detail, even though there are a large number of possible combinations. Each set will be further looked at and this shall be used to determine whether the initial premise was valid or not.

4.2. Theory.

The premise for this research study was to try and determine whether there was a direct relationship between the vibration measured on the camshaft and the vibrations transmitted through the bearings, or not.

It was decided to try and adapt the method of influence coefficients from the static deflection case to use in this rotational dynamic case. From the theory, as described in Appendix 4 for the static case, the force at a certain point in a system is related to the total potential energy in the system by an influence coefficient. In adapting this theory to our particular case it was decided to use influence coefficients to relate vibration transmitted through the bearings to the vibration measured from the camshaft.

The test rig incorporated two proximity probes, measuring camshaft vibration between the two cams between the bearings classified as 4L and 5L. The rig also incorporated four accelerometers, one on each bearing from 2L to 5L. These can be seen in Figure 4.1.

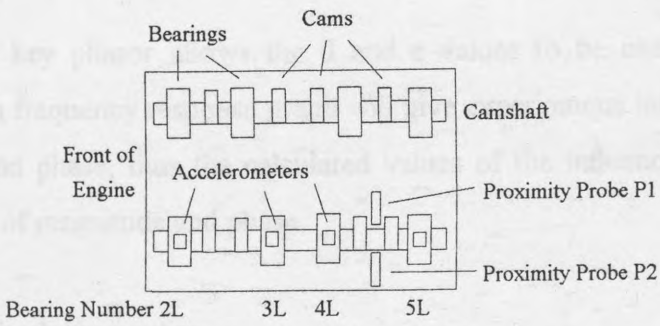

Figure 4.1.: A schematic of the transducer layout.

This allowed for the possibility of using the following two equations:

$$d_1 = a_1\alpha_{11} + a_2\alpha_{12} + a_3\alpha_{13} + a_4\alpha_{14} \qquad - (4.1)$$

and

$$d_2 = a_1\alpha_{21} + a_2\alpha_{22} + a_3\alpha_{23} + a_4\alpha_{24} \qquad - (4.2)$$

In this case d is measured experimentally as a frequency response transfer function between the appropriate proximity probe and the key phasor i.e. $d_n. = P_n / K.P.$ Where n signifies the proximity probe number.

Similarly a is measured experimentally as a frequency response transfer function between the appropriate accelerometer and the key phasor i.e. $a_n = A_n / K.P.$ Where n signifies the appropriate accelerometer number.

As mentioned in Chapter 2.4 the key phasor is a proximity probe detecting a keyway on the distributor rotor shaft. Because it is at a fixed point the amplitude and frequency of the generated pulse does not change, as long as the rotational speed of the camshaft does not alter. Therefore each set of capture of the frequency response values will be related to a common starting point. For ease of writing the /K.P. part of the equation has been left out. and D_n and a_n used

The influence coefficient α_{1n} is the coefficient relating d_1 and a_n, where α_{2n} is the coefficient relating d_2 and a_n.

The use of the key phasor allows the d and a values to be used together in the equations. Each frequency response graph will give experimental information in terms of magnitude and phase, thus the calculated values of the influence coefficients will also be in terms of magnitude and phase.

A simple units check shows that:

For the proximity probe P_n:

Output = Input x Sensitivity. = mils x volts/mil = volts

For the accelerometer A_n:

Output = Input x Sensitivity = g x volt/g = volts.

For the key-phasor output is in volts.

Therefore both d_n and a_n are unitless.

The two equations, (4.1) and (4.2) as shown on the previous page, present a problem with the number of unknowns. There are two equations and eight unknowns, which is impossible to solve in its current form. It was decided to reduce the amount of terms in order to overcome this problem. The two equations were reduced to a manageable size:

$$d_1 = a_1\alpha_{11} + a_2\alpha_{12}$$
$$d_2 = a_1\alpha_{21} + a_2\alpha_{22}$$

Another assumption of the conversion from the static deflection case to the dynamic case that has been altered is the assumption that each influence coefficient is independent from the other. In the case of vibration analysis this would not be the true. Vibration from one part of the camshaft, if slightly different from another part, would be transmitted through the shaft and be noticeable at the other point. So any determination of one influence coefficient would have to incorporate the other coefficient. Now looking at the first equation.

$$d_1 = a_1\alpha_{11} + a_2\alpha_{12}$$

For the initial calculations it will be assumed that α_{12} is a unity vector, i.e. it has a magnitude of 1 at 0 degrees. This is assumed for the following calculations and shall be looked at more closely in Chapter 4.5. Therefore there is only one unknown in the equation for d_1,that is α_{11} and can be determined relatively easily.

$$d_1 = a_1\alpha_{11} + a_2\alpha_{12}$$

$$\Rightarrow a_{11}\alpha_{11} = d_1 - a_2\alpha_{12}$$

$$\Rightarrow \alpha_{11} = \frac{d_1 - a_2\alpha_{12}}{a_1}$$

Using the notation M for magnitude and θ for phase then $a_2\alpha_{12}$ has magnitude $M_{a2\alpha12}$ and phase $\theta_{a2\alpha12}$ such that

$$M_{a2\alpha 12} = M_{a2} * M_{\alpha 12}$$
$$\theta_{a2\alpha 12} = \theta_{a2} + \theta_{\alpha 12}$$

changing into its real and imaginary parts

$$r_{a2\alpha 12} = M_{a2\alpha 12} * \cos(\theta_{a2\alpha 12})$$
$$i_{a2\alpha 12} = M_{a2\alpha 12} * \sin(\theta_{a2\alpha 12})$$

changing d_1 into its real and imaginary parts

$$r_{d2} = M_{d1} * \cos(\theta_{d1})$$
$$i_{d2} = M_{d2} * \sin(\theta_{d1})$$

$$\Rightarrow d_1 - a_2\alpha_{12} = (r_{d1} + i_{d1}) - (r_{a2\alpha 12} + i_{a2\alpha 12})$$
$$= (r_{d1} - r_{a2\alpha 12}) + (i_{d1} - i_{a2\alpha 12})$$

Now changing back into vector notation for magnitude and phase

$$M_{d1-a2\alpha 12} = \sqrt{(r_{d1} - r_{a2\alpha 12})^2 + (i_{d1} - i_{a2\alpha 12})^2}$$
$$\theta_{d1-a2\alpha 12} = \tan^{-1}\left(\frac{i_{d1} - i_{a2\alpha 12}}{r_{d1} - r_{a2\alpha 12}}\right)$$

Now

$$\alpha_{11} = \frac{d_1 - a_2\alpha_{12}}{a_1}$$

Therefore

$$M_{\alpha 11} = \frac{M_{d1-a2\alpha 12}}{M_{a1}}$$

$$\theta_{\alpha 11} = \theta_{d1-a2\alpha 12} - \theta_{a1}$$

Similarly

$$\alpha_{22} = \frac{d_2 - a_1\alpha_{21}}{a_{21}}$$

Therefore

$$M_{\alpha 22} = \frac{M_{d2 - a2\alpha 21}}{M_{a2}}$$

$$\theta_{\alpha 22} = \theta_{d2 - a1\alpha 21} - \theta_{a2}$$

Where M is unitless and θ is in degrees.

4.3. Frequency Response Tests.

4.3.1. Equipment.

Thurlby K1 Module Serial No: 43637 SMOE No.: CP/028/12

Gould Digital Storage Oscilloscope Type 4035 Serial No: 1895

Diagnostics Instruments Real Time FFT Analyser Model PL202 Serial No:123

2 x Bentley Nevada Proximity Probe Part No. 21500-00-08-10-02
Serial Nos: JULU440763 and JULU440765

2 x Bentley Nevada Extension Cable Part No.: 21747-040-00

2 x Bentley Nevada Proximitor Part No.: 18745-03
Serial Nos: JUNU118860 and JUNU118865

4 x Monitran Accelerometer Serial Nos: MTN/1120S/22222 to MTN/1120S/22225

RS Components Ltd. Optical Tacho Model TM-2011 Serial No:0468
SMOE No.: CP/043/4

Stewart-Warner Instruments Limited Proximity Probe Model IK4054

4.3.2. Procedure.

The method for obtaining the frequency response graphs was basically the same method as that what was used for the spectral analysis tests, with the main difference being in the instrumentation set up part of the procedure, this was due to the introduction of the key phasor.

4.3.2.1. Engine Set Up:

As before the engine was visually inspected and the motor was set to the appropriate speed. The lubrication oil pressure was noted to ensure an adequate flow of lubrication oil.

4.3.2.2. Instrumentation Set Up:

Again, as with before the FFT Analyser settings were set for the capture of data from the transducer in use, the actual FFT Analyser settings can be seen in Appendix 2. The power source for the proximitor was set to -18 ± 0.01 volts and the pulse created by the key phasor display on the digital oscilloscope. The INPUT 2 and COUP 2 menu settings on the Input Screen and the SCALE CH2 and TYPE menu settings on the Display Screen were double checked to ensure they were set at the appropriate value for the transducer being tested. The transducer lead was connected into the Channel 2 connection on the back panel (Channel 1 was used for the key phasor) of the FFT Analyser and the capture process started. As with the spectrum tests the frequency range under investigation was 0 - 25 Hz. The key phasor pulse was used as the trigger value to start the capture process.

4.3.2.3. Capturing and Recording Data:

Again, as with the spectrum tests each data capture takes approximately 2 minutes 30 seconds. The data is then stored under its appropriate filename on the DIRECTORY and FILENAME menus on the Memory Screen.

The data can also be downloaded to a computer for use in various software packages. This is achieved using the DEC2L V1.11 PL202 Download Support Program provided by the Analyser's manufacturer, Diagnostic Instruments. Each frequency response trace is downloaded in two parts, the magnitude trace (in the form of a .TRA file) and the phase trace (in the form of a .TRB file). Each file gives the X and Y co-ordinates of the appropriate trace.

4.3.3. The Key Phasor Pulse.

As mentioned before the key phasor is used as a reference pulse, in order to relate all the frequency response graphs together for the calculations. This pulse is also used to trigger the data capturing process and if the trigger settings on the FFT analyser remain constant for all the tests then all the data should be referenced to the same point. This pulse, on its own, is basically in the form of a voltage against time graph. The real time plots for the pulse at 100 r.p.m. and at 200 r.p.m. can be seen in Graphs 4.1. and 4.2. respectively.

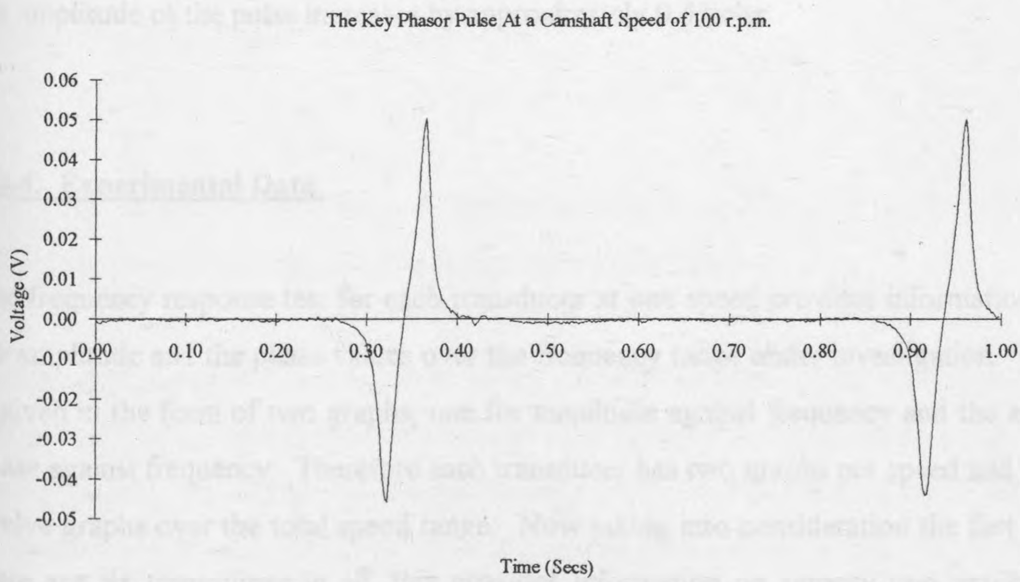

Graph 4.1: A graph of the real time key phasor pulse at 100 r.p.m.

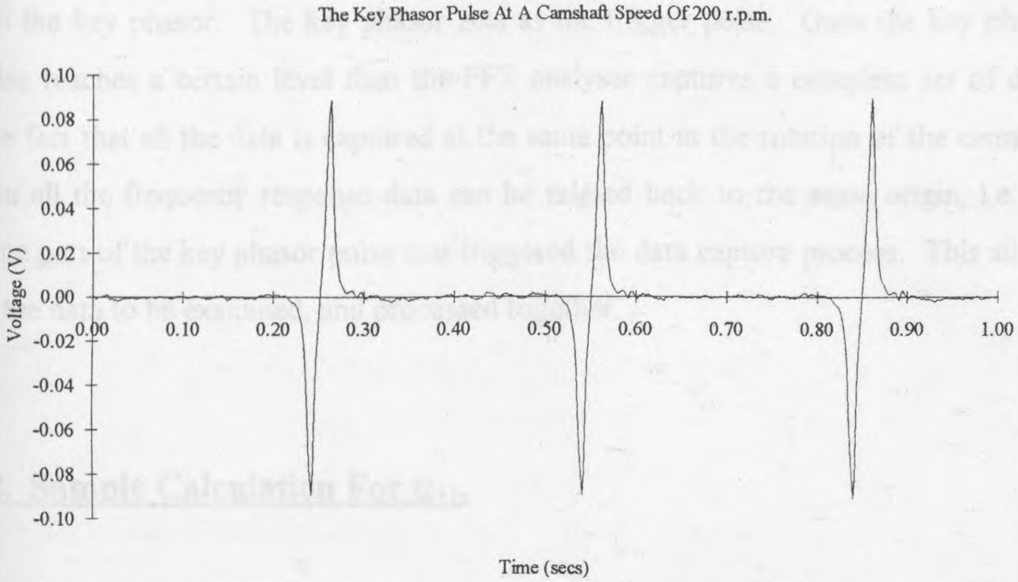

Graph 4.2..: A graph of the real time key phasor pulse at 200 r.p.m.

It can be clearly seen from the two figures that the frequency of the pulse increases with the increase of camshaft speed, as would be expected. It can also be noticed that the amplitude of the pulse increases by approximately 0.4 volts.

4.3.4. Experimental Data.

The frequency response test for each transducer at one speed provides information on the amplitude and the phase values over the frequency range under investigation. This is given in the form of two graphs, one for amplitude against frequency and the other phase against frequency. Therefore each transducer has two graphs per speed and thus twelve graphs over the total speed range. Now taking into consideration the fact that there are six transducers in all, this provides information on seventy two graphs in total. The graphs for all the frequency response tests at 150 r.p.m. can be seen in Appendix 3. The other graphs have been left out, though the main information from them has been extracted and used later on in this Chapter.

Each frequency response test provides information between the transducer in question and the key phasor. The key phasor acts as the trigger pulse. Once the key phasor pulse reaches a certain level then the FFT analyser captures a complete set of data. The fact that all the data is captured at the same point in the rotation of the camshaft then all the frequency response data can be related back to the same origin, i.e. the same part of the key phasor pulse that triggered the data capture process. This allows all the data to be examined, and processed together.

4.4. Sample Calculation For α_{11}.

It was important to determine initially, by hand, the values of α_{11} at one particular frequency at all speeds. These values would be used as a guide when constructing an appropriate spreadsheet on the spreadsheet package, Microsoft Exel 5.0, to determine all the values of α_{11} for all the different combinations of a_1, a_2 and d_1.

The proposed equation involving α_{11} was:

$$d_1 = a_1\alpha_{11} + a_2\alpha_{12}$$

The variables are the same as those that were defined in Chapter 4.2. Where each variable is a vector quantity, i.e. has a magnitude and phase.

For camshaft speed at 100 rpm, the d_1 values taken between proximity probe 1 and the key phasor, the a_1 values taken between the accelerometer situated on bearing 2L and the key phasor, and the a_2 values taken between the accelerometer situated on bearing 5L and the key phasor. These values are taken at a frequency of 10 Hz. These values were obtained from the frequency response graphs as obtained from the frequency response tests in Chapter 4.3. The positions for P1, 2L and 5L can be seen in figure 4.1

	Magnitude	Phase
P1	0.000134	106.30
2L	0.117	-79.70
5L	0.105	180.00

Using the notation M for magnitude and θ for phase then $a_2\alpha_{12}$ has magnitude $M_{a2\alpha12}$ and phase $\theta_{a2\alpha12}$ such that

$$M_{a2\alpha12} = M_{a2} * M_{\alpha12} = 0.1046 * 1 = 0.1046$$
$$\theta_{a2\alpha12} = \theta_{a2} + \theta_{\alpha12} = 180 + 0 = 180$$

changing into its real and imaginary parts

$$r_{a2\alpha12} = M_{a2\alpha12} * \cos(\theta_{a2\alpha12}) = 0.1046 * \cos(180) = -0.1046$$
$$i_{a2\alpha12} = M_{a2\alpha12} * \sin(\theta_{a2\alpha12}) = 0.1046 * \sin(180) = 0$$

changing d_1 into its real and imaginary parts

$$r_{d2} = M_{d1} * \cos(\theta_{d1}) = 0.000134 * \cos(106.3017) = -0.0000375$$
$$i_{d2} = M_{d2} * \sin(\theta_{d1}) = 0.000134 * \sin(106.3017) = 0.0001283$$

$$\begin{aligned} \Rightarrow d_1 - a_2\alpha_{12} &= (r_{d1} + i_{d1}) - (r_{a2\alpha12} + i_{a2\alpha12}) = (r_{d1} - r_{a2\alpha12}) + j(i_{d1} - i_{a2\alpha12}) \\ &= (-0.0000375 + 0.1046) + j(0.0001283 - 0) \\ &= 0.1046 + j0.0001283 \end{aligned}$$

Now changing back into vector notation for magnitude and phase

$$M_{d1-a2\alpha12} = \sqrt{(r_{d1} - r_{a2\alpha12})^2 + (i_{d1} - i_{a2\alpha12})^2} = \sqrt{(0.1046)^2 + (0.0001283)^2} = 0.10459$$
$$\theta_{d1-a2\alpha12} = \tan^{-1}\left(\frac{i_{d1} - i_{a2\alpha12}}{r_{d1} - r_{a2\alpha12}}\right) = \tan^{-1}\left(\frac{0.001283}{0.1046}\right) = 0.07029$$

Now from the initial equation

$$\alpha_{11} = \frac{d_1 - a_2\alpha_{12}}{a_1}$$

Therefore

$$M_{\alpha_{11}} = \frac{M_{d_1 - a_2\alpha_{12}}}{M_{a_1}} = \frac{0.1046}{0.11740} = 0.8909$$

$$\theta_{\alpha_{11}} = \theta_{d_1 - a_2\alpha_{12}} - \theta_{a_1} = 0.07029 + 79.6952 = 79.7654$$

Where M is unitless and θ is in degrees.

Sample calculations for the same frequency at the other speeds under consideration can be seen in Appendix 5.

4.5. The Effects Of α_{12} On α_{11}.

In both the initial equations the influence coefficients, α_{11}, α_{12}, α_{21}, α_{22}, were unknown. It was decided to investigate each equation separately, thus reducing the number of unknowns to two for each equation. To further simplify this α_{12} was assumed to be a unity vector, i.e. has a magnitude of 1 at 0 degree phase, in the initial calculations. It was important to discover whether this was a valid assumption or not. The most practical way to determine this was to significantly alter the value of α_{12} and see what effect this would have on the calculated values of α_{11}. This could be easily achieved by incorporating the value of α_{12} as variable in the spreadsheet package, used for calculating the values of α_{11}, and inspecting the effect of any change of α_{12} on the graphs of magnitude and phase of α_{11} .

This process was achieved in two stages, firstly by altering the magnitude only and then by altering the phase only.

The initial value of the magnitude was 1, as shown in Graphs 4.3 and 4.4, then it was changed to 5, as shown in graphs 4.5 and 4.6, and then to a value of 10, as shown in Graphs 4.7 and 4.8, it was easily seen that the graphs of magnitude and phase stayed the same shape, the only difference being that the values of magnitude increased by the amount that the magnitude of α_{12} was increased by. This can easily be explained by referring back to parts of the equations used in the calculations.

$$d_1 = a_1\alpha_{11} + a_2\alpha_{12}$$

$$\Rightarrow a_{11}\alpha_{11} = d_1 - a_2\alpha_{12}$$

$$\Rightarrow \alpha_{11} = \frac{d_1 - a_2\alpha_{12}}{a_1}$$

It was found that the value used for d_1 was usually about one thousandth of the value used for a_2. This means that a_2 would be the most influential value in the equation, and because this was the only value directly influenced by α_{12} any alteration of the magnitude of α_{12} would only increase the magnitude of α_{11} by a factor of whatever the magnitude of α_{12} was.

When the phase value was increased by increments of 30°, from 0° to 150°, then there was no change in the magnitude graph but a change in the phase graph, as shown in Graphs 4.9 to 4.16. This phase change though showing some similarities in the shape of the graph, but not in the actual values, over certain frequency ranges would appear to be more random than anything else. This could possibly be attributed to the fact that the calculation for α_{11} contains the three main trigonimic functions, sin, cos and tan, at various stages of the calculation. Though sin and cos are related to each other through a 90° phase shift, tan does not have such a relationship and as the tan calculation is the last one undertaken to determine the phase value this has the most affect on the final value, making the value to appear to change in an almost random fashion.

Thus in conclusion it was found that the value of α_{12} had little effect on the value of α_{11} because of the difference in values between d and a.

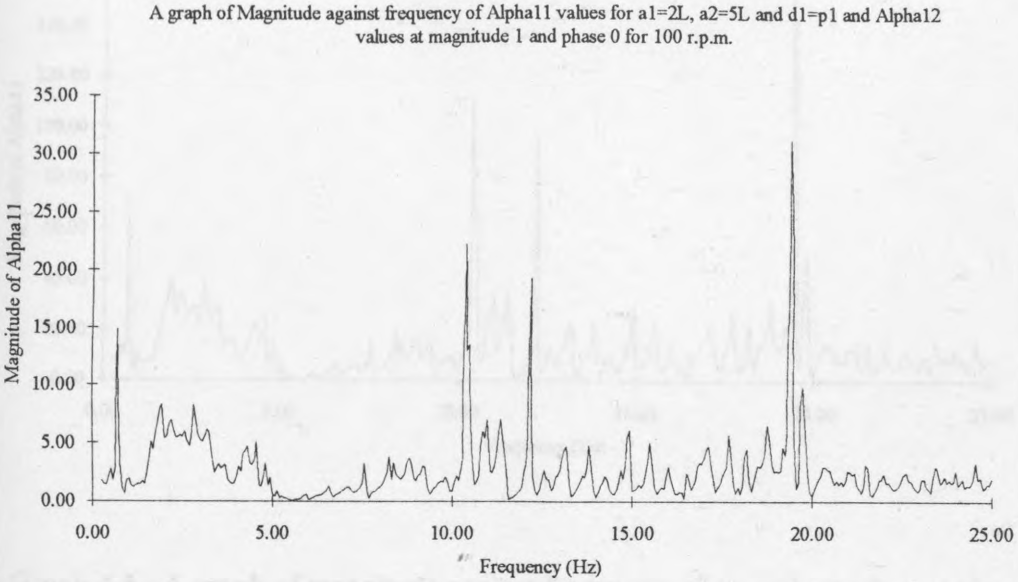

Graph 4.3.: A graph of magnitude against frequency of α_{11} values when α_{12} has magnitude 1 and phase 0^{o}.

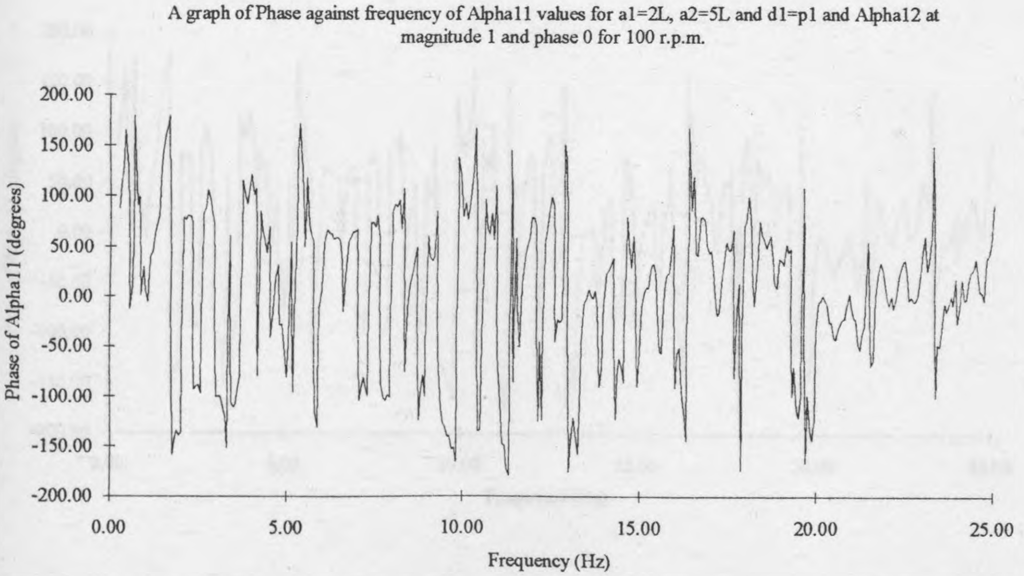

Graph 4.4.: A graph of phase against frequency of α_{11} values when α_{12} has magnitude 1 and phase 0^{o}.

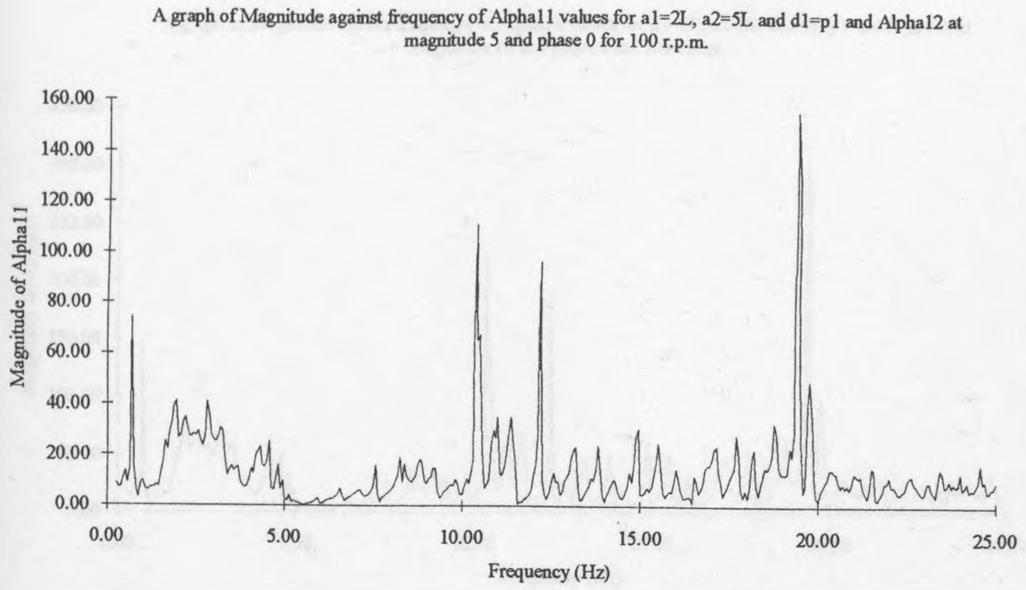

Graph 4.5.: A graph of magnitude against frequency of α_{11} values when α_{12} has magnitude 5 and phase 0°.

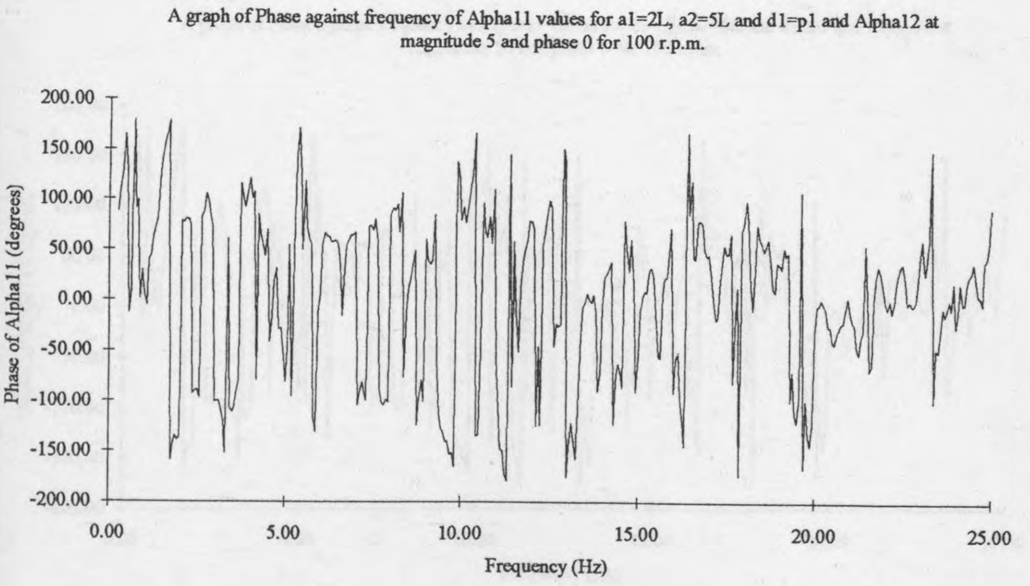

Graph 4.6: A graph of phase against frequency of α_{11} values when α_{12} has magnitude 5 and phase 0°.

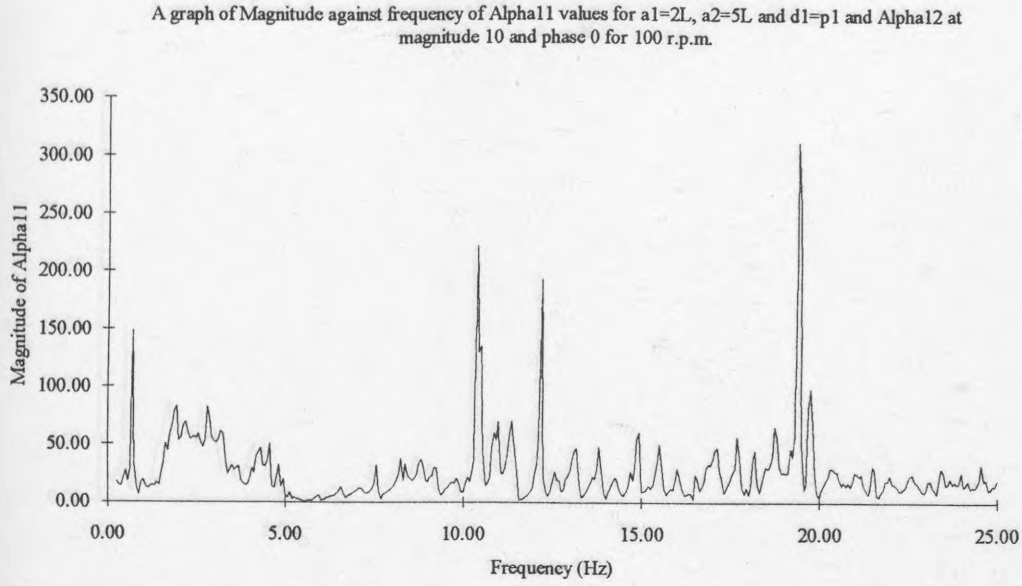

Graph 4.7: A graph of magnitude against frequency of α_{11} values when α_{12} has magnitude 10 and phase 0°.

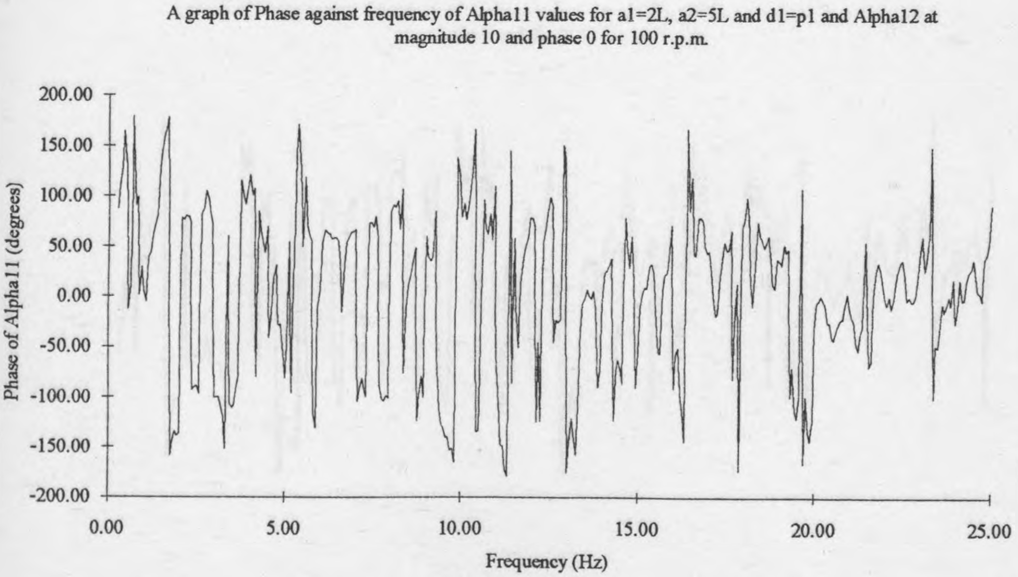

Graph 4.8: A graph of phase against frequency of α_{11} values when α_{12} has magnitude 10 and phase 0°.

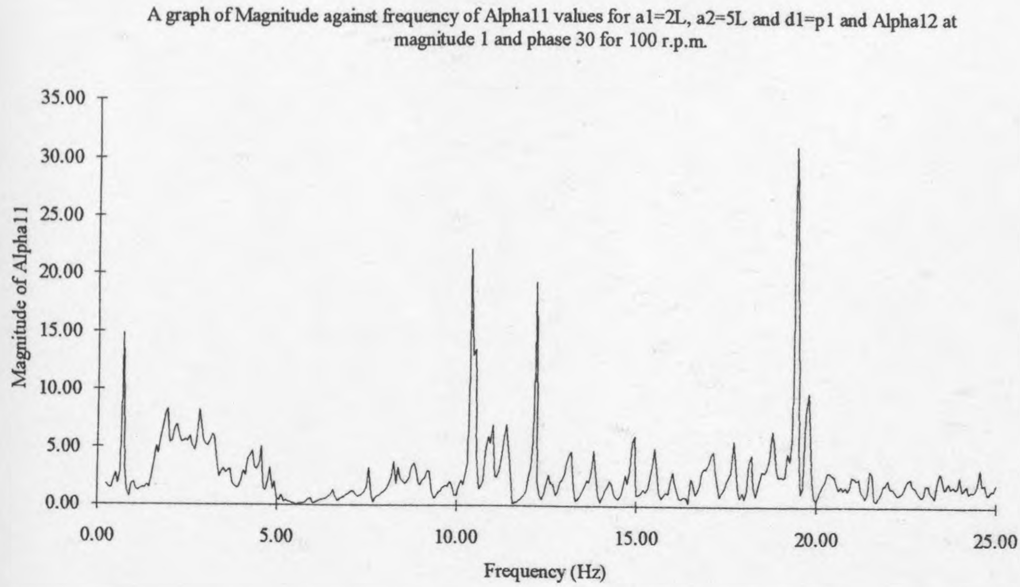

Graph 4.9: A graph of magnitude against frequency of α_{11} values when α_{12} has magnitude 1 and phase 30°.

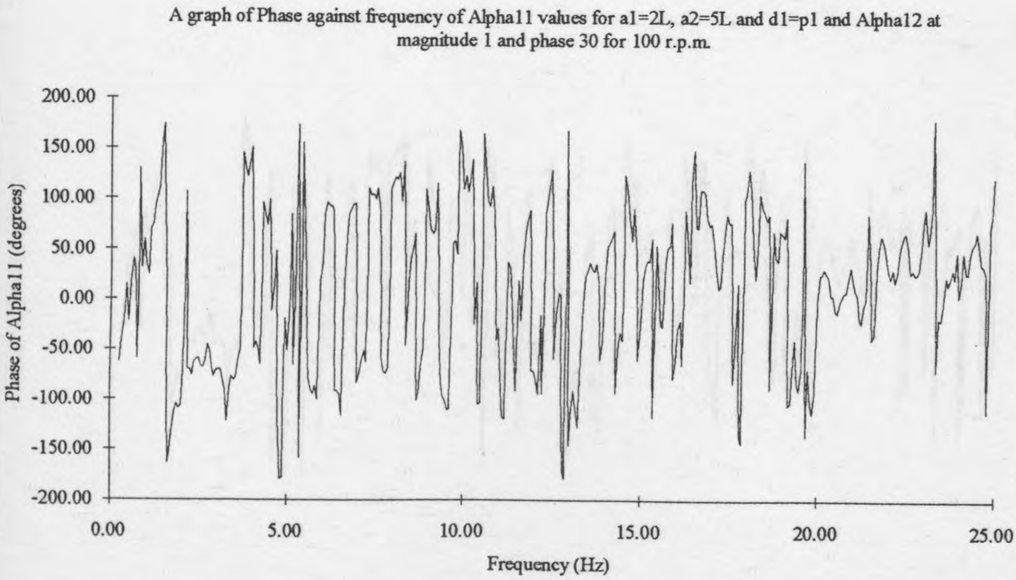

Graph 4.10: A graph of phase against frequency of α_{11} values when α_{12} has magnitude 1 and phase 30°.

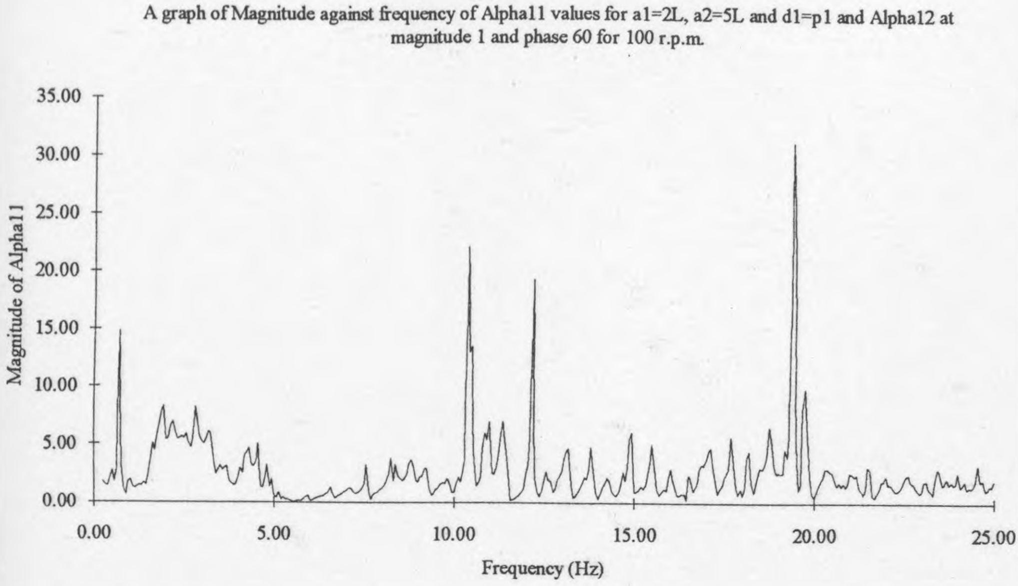

Graph 4.11: A graph of magnitude against frequency of α_{11} values when α_{12} has magnitude 1 and phase 60°.

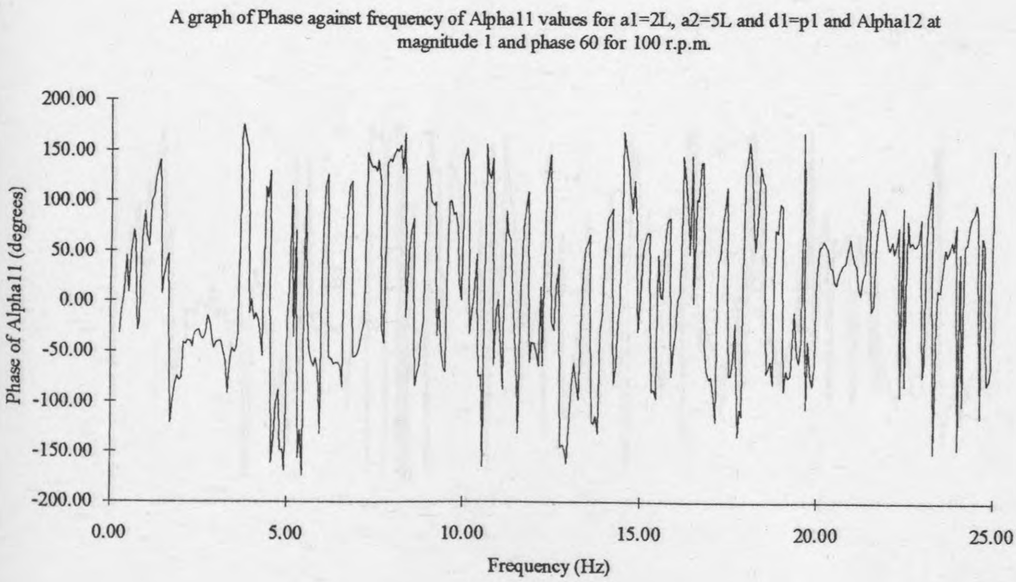

Graph 4.12: A graph of phase against frequency of α_{11} values when α_{12} has magnitude 1 and phase 60°.

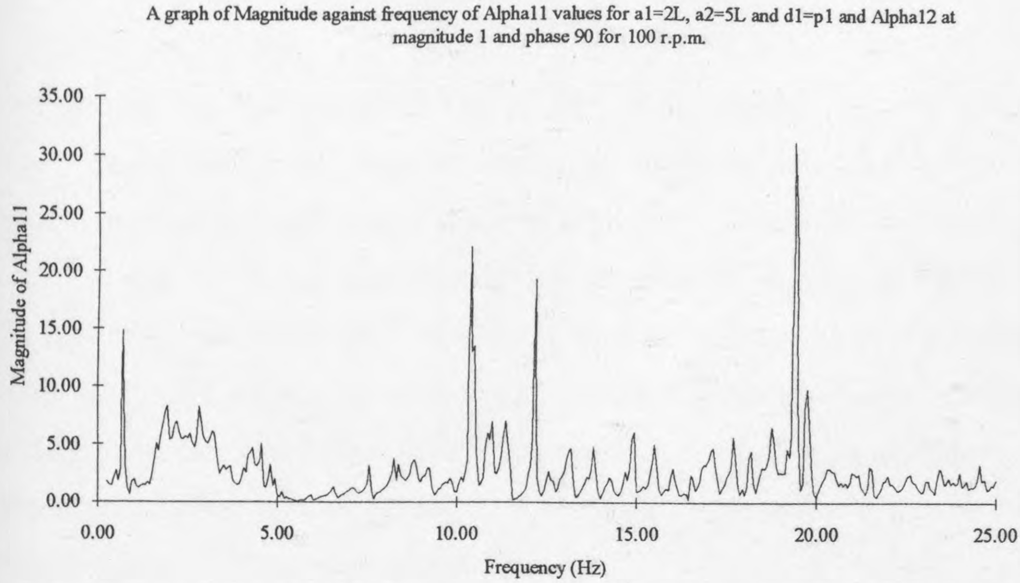

Graph 4.13: A graph of magnitude against frequency of α_{11} values when α_{12} has magnitude 1 and phase 90°.

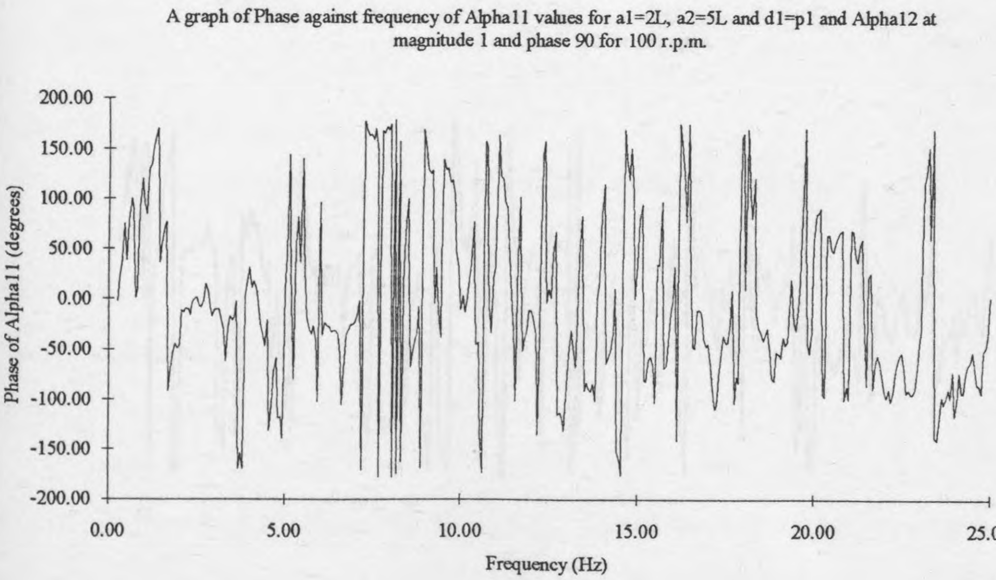

Graph 4.14: A graph of phase against frequency of α_{11} values when α_{12} has magnitude 1 and phase 90°.

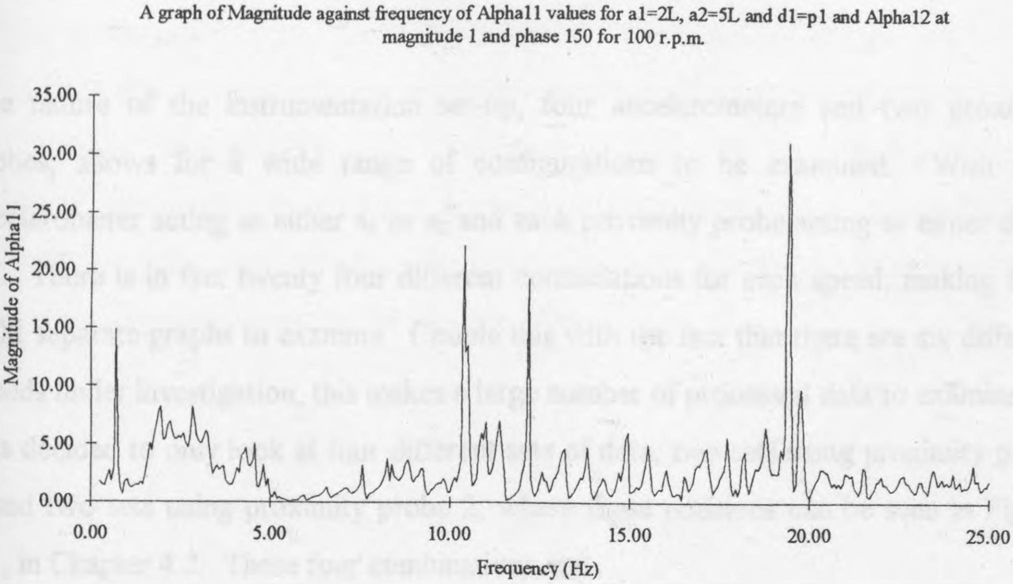

Graph 4.15: A graph of magnitude against frequency of α_{11} values when α_{12} has magnitude 1 and phase 150°.

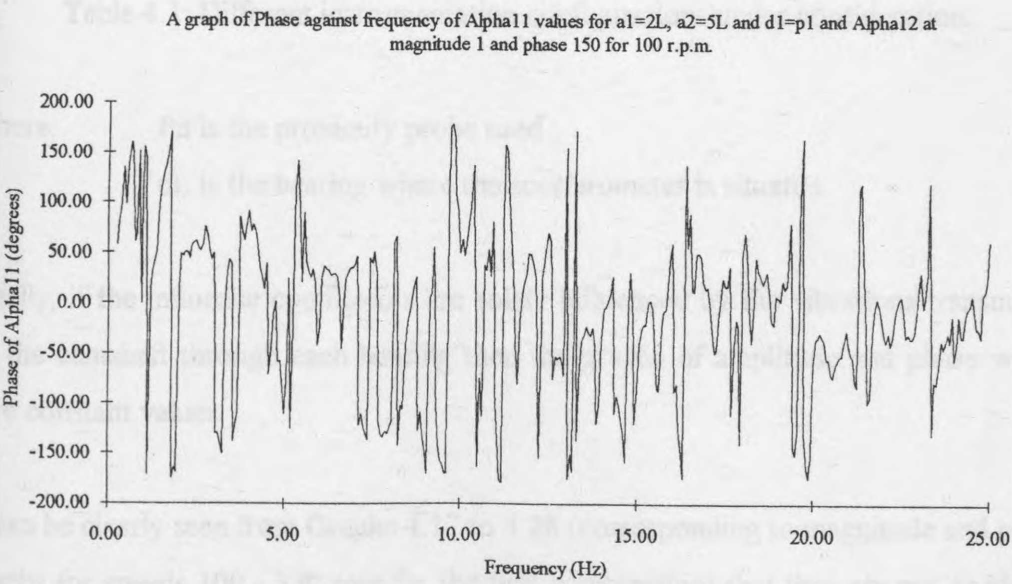

Graph 4.16: A graph of phase against frequency of α_{11} values when α_{12} has magnitude 1 and phase 150°.

4.6. The Different Combinations Of Transducers.

The nature of the instrumentation set-up, four accelerometers and two proximity probes, allows for a wide range of configurations to be examined. With each accelerometer acting as either a_1 or a_2 and each proximity probe acting as either d_1 or d_2. There is in fact twenty four different combinations for each speed, making forty eight separate graphs to examine. Couple this with the fact that there are six different speeds under investigation, this makes a large number of processed data to examine. It was decided to only look at four different sets of data, two sets using proximity probe 1 and two sets using proximity probe 2, where these positions can be seen in Figure 4.1, in Chapter 4.2. These four combinations are:

Combination	d	a_1	a_2
1	P1	2L	5L
2	P1	3L	4L
3	P2	5L	2L
4	P2	4L	3L

Table 4.1: Different instrumentation configurations under consideration.

Where: Pn is the proximity probe used

nL is the bearing where the accelerometer is situated.

Ideally, if the influence coefficients are solely influenced by the vibrations transmitted by the camshaft through each bearing then the graphs of amplitude and phase would give constant values.

It can be clearly seen from Graphs 4.17 to 4.28 (corresponding to magnitude and phase graphs for speeds 100 - 350 rpm for the first combination) that they are not as ideally expected.

It can be seen for each combination and speed that the magnitude graphs peak at different frequencies and at different magnitudes, and the phase graphs also show no similarities. There are parts of the magnitude graphs that show some stability, i.e. little change in value over a certain frequency range. An example of this can adequately be seen from Graphs 4.25 and 4.27, showing the first combination at 300 rpm and 350 rpm. Both graphs show a period where the magnitude has a relatively constant value, i.e. "stability" over the 21 - 23 Hz frequency range. It was decided to further investigate the magnitude graphs to determine whether these periods of stability were of similar magnitude and frequency range for each speed and thus try to show whether the proposed equations were valid for certain frequencies.

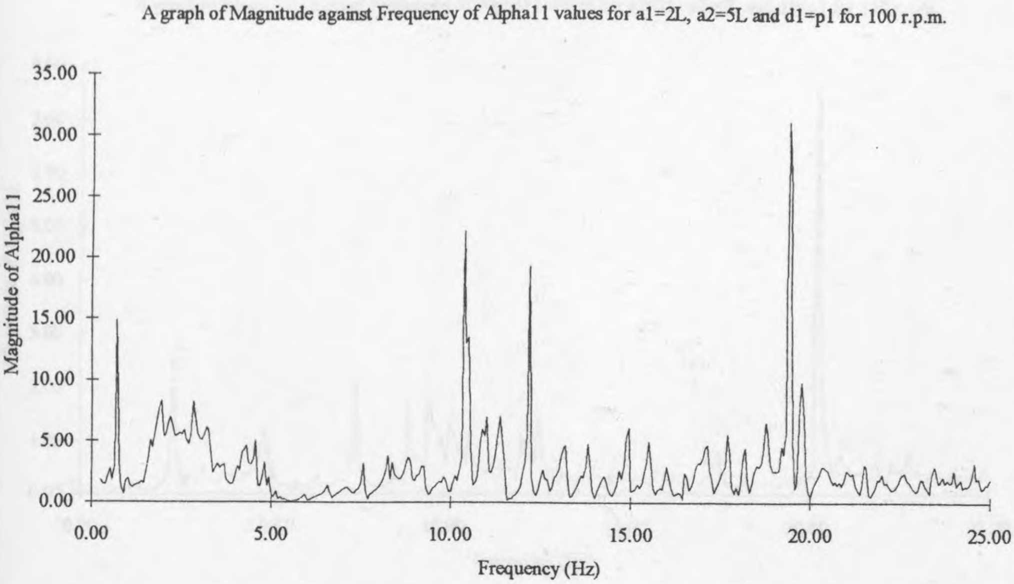

Graph 4.17: A graph of magnitude against frequency for α_{11} values for d1=P1, a1=2L and a2=5L at 100 rpm.

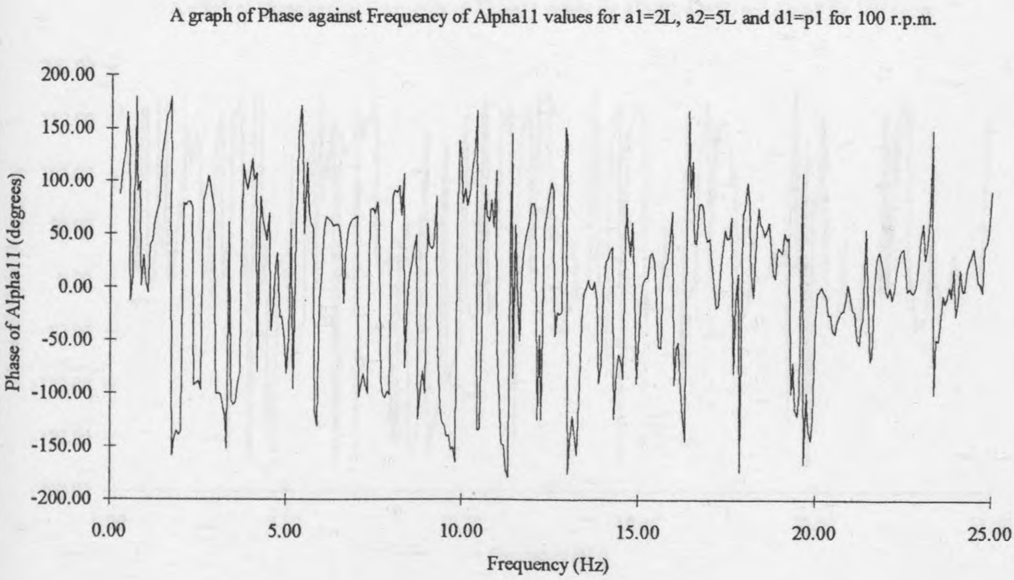

Graph 4.18: A graph of phase against frequency for α_{11} values for d1=P1, a1=2L and a2=5L at 100 rpm.

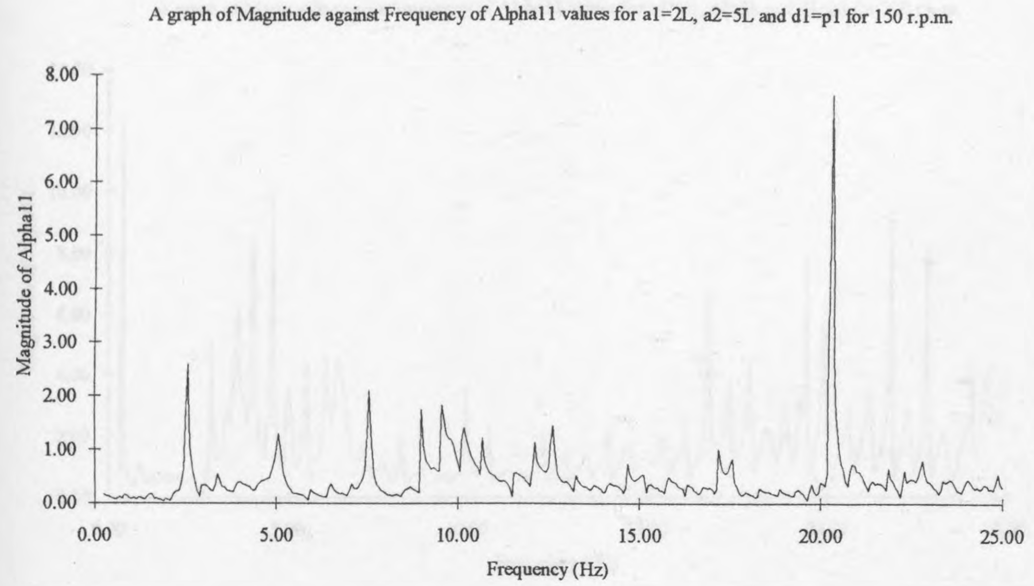

Graph 4.19: A graph of magnitude against frequency for α_{11} values for d1=P1, a1=2L and a2=5L at 150 rpm.

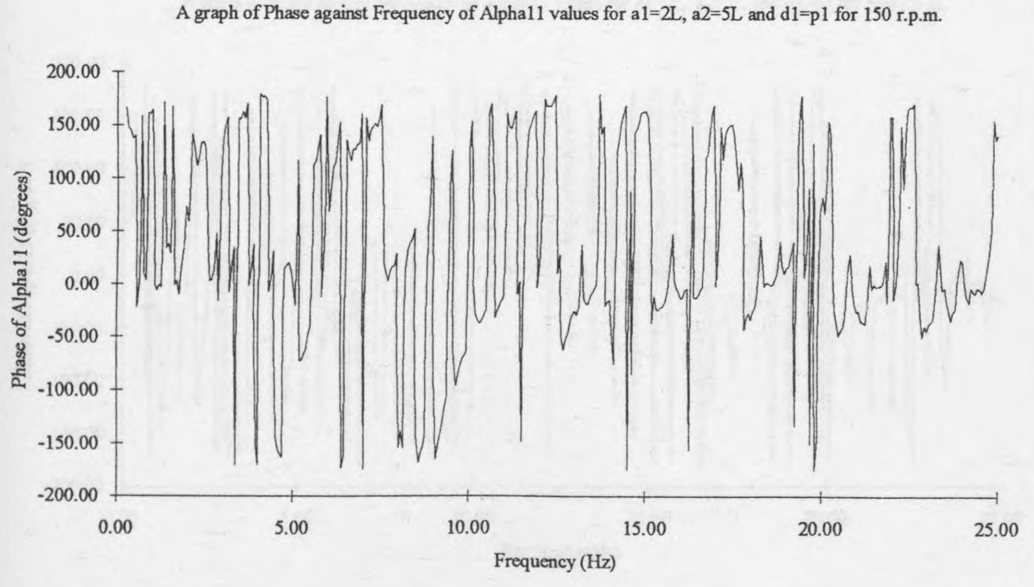

Graph 4.20: A graph of phase against frequency for α_{11} values for d1=P1, a1=2L and a2=5L at 150 rpm.

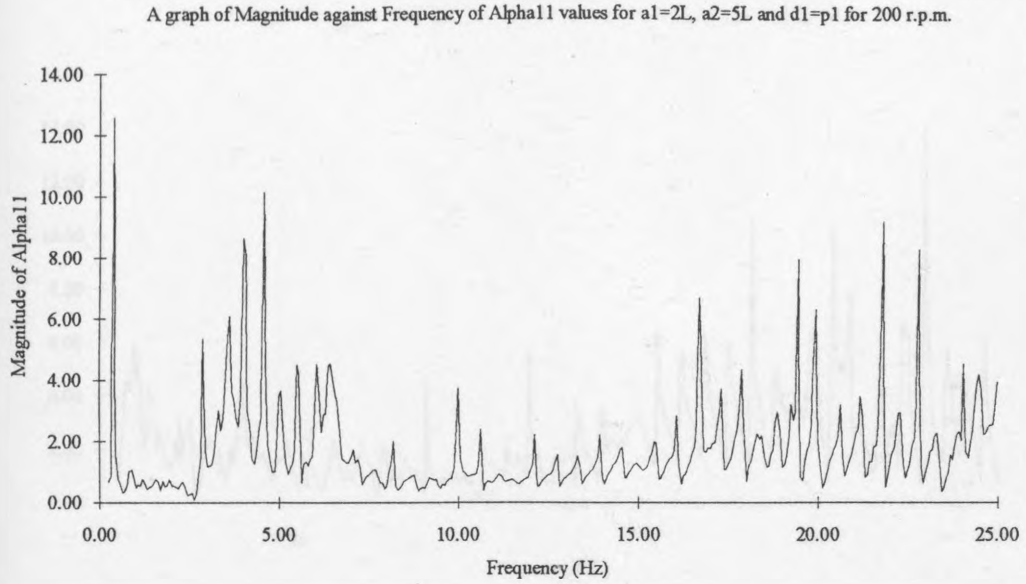

Graph 4.21: A graph of magnitude against frequency for α_{11} values for d1=P1, a1=2L and a2=5L at 200 rpm.

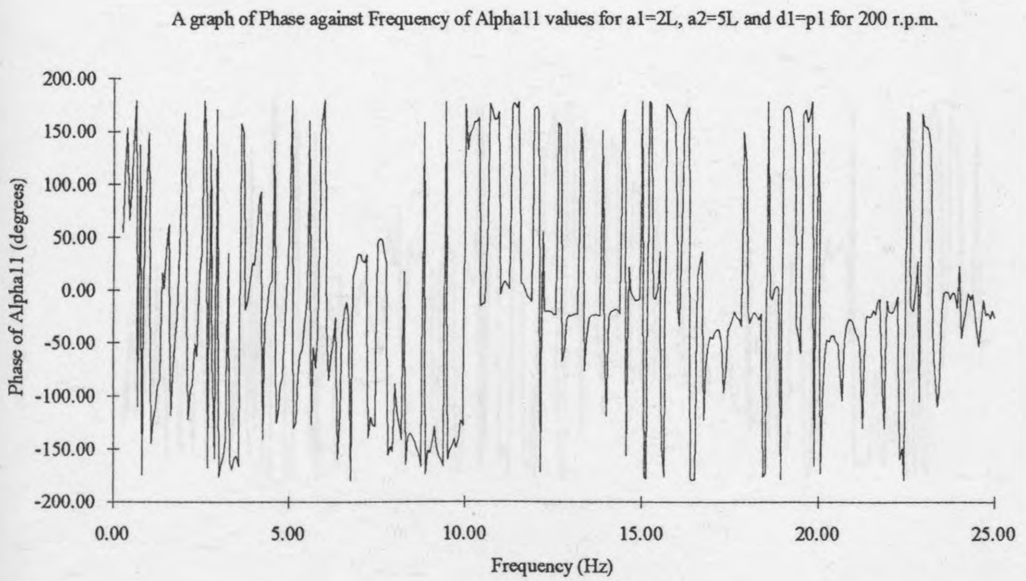

Graph 4.22: A graph of phase against frequency for α_{11} values for d1=P1, a1=2L and a2=5L at 200 rpm.

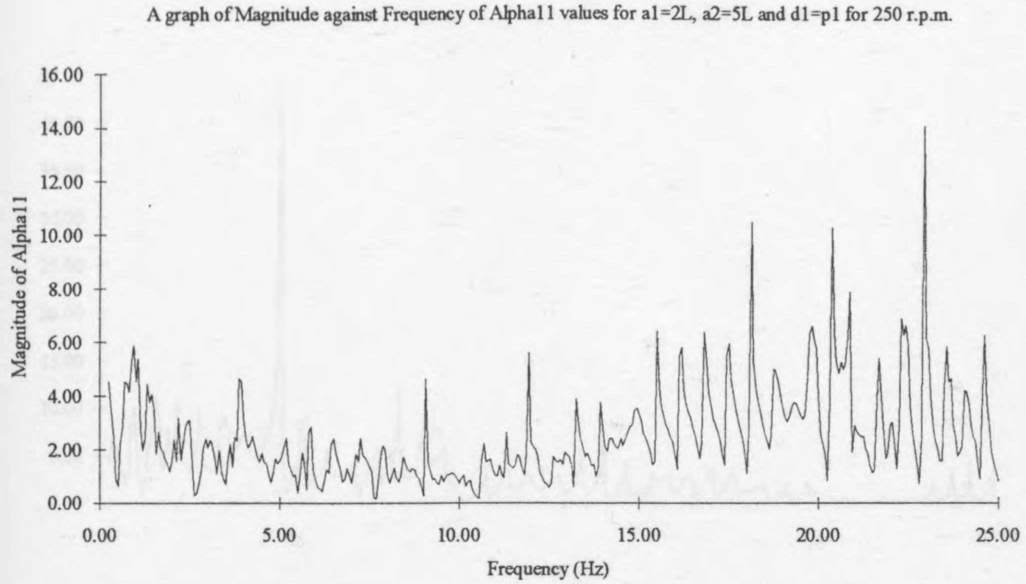

Graph 4.23: A graph of magnitude against frequency for α_{11} values for d1=P1, a1=2L and a2=5L at 250 rpm.

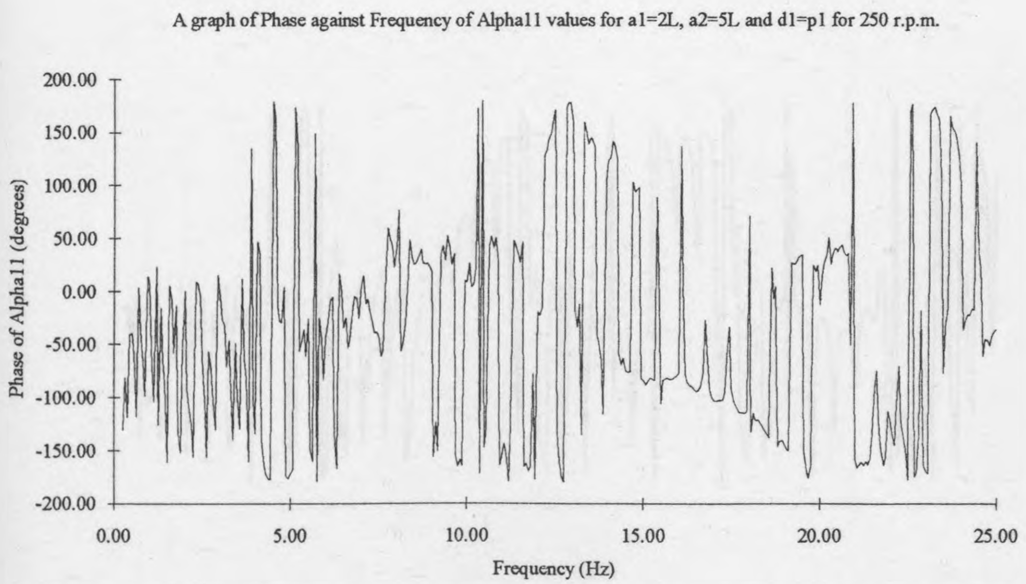

Graph 4.24: A graph of phase against frequency for α_{11} values for d1=P1, a1=2L and a2=5L at 250 rpm.

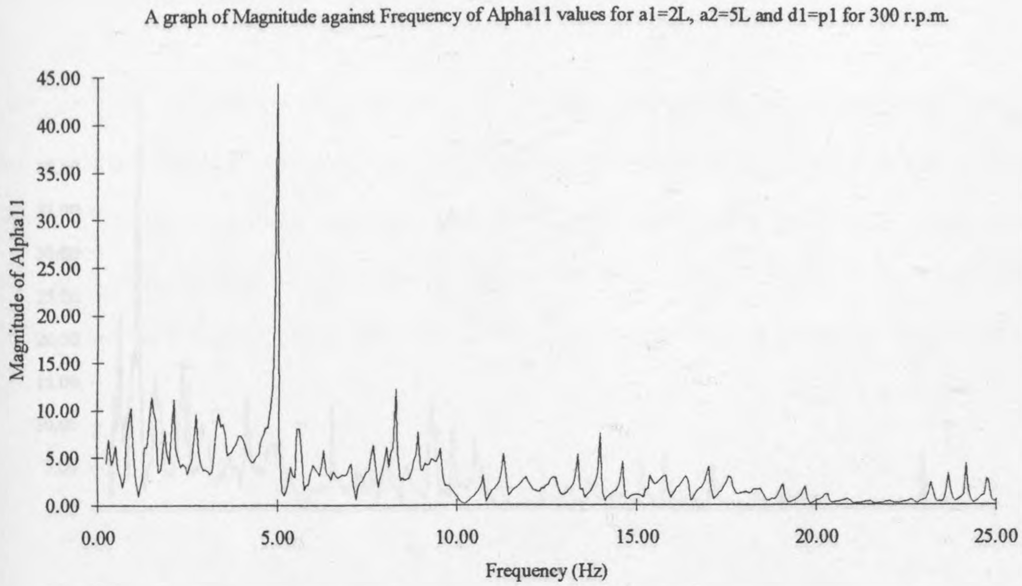

Graph 4.25: A graph of magnitude against frequency for α_{11} values for d1=P1, a1=2L and a2=5L at 300 rpm.

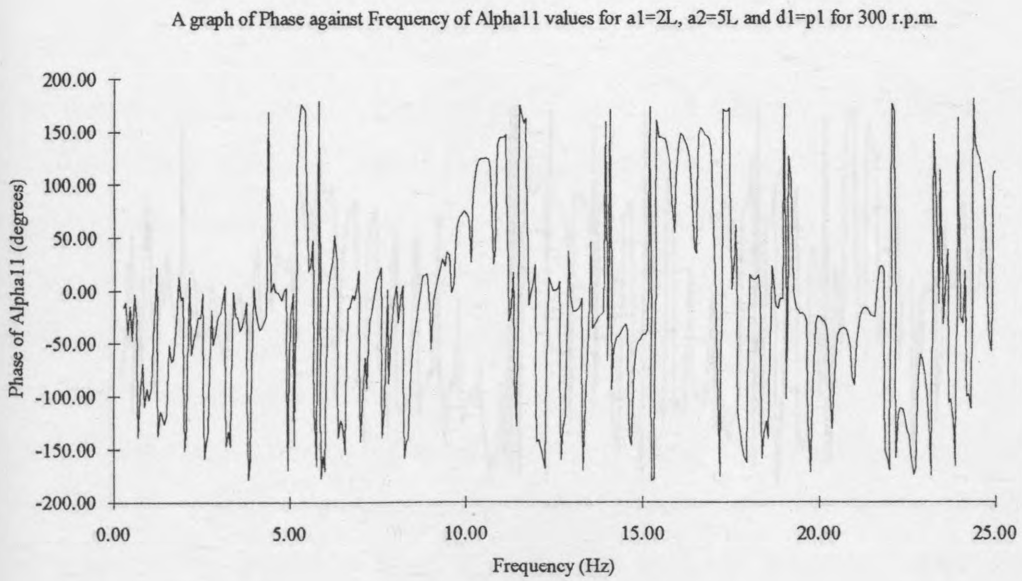

Graph 4.26: A graph of phase against frequency for α_{11} values for d1=P1, a1=2L and a2=5L at 300 rpm.

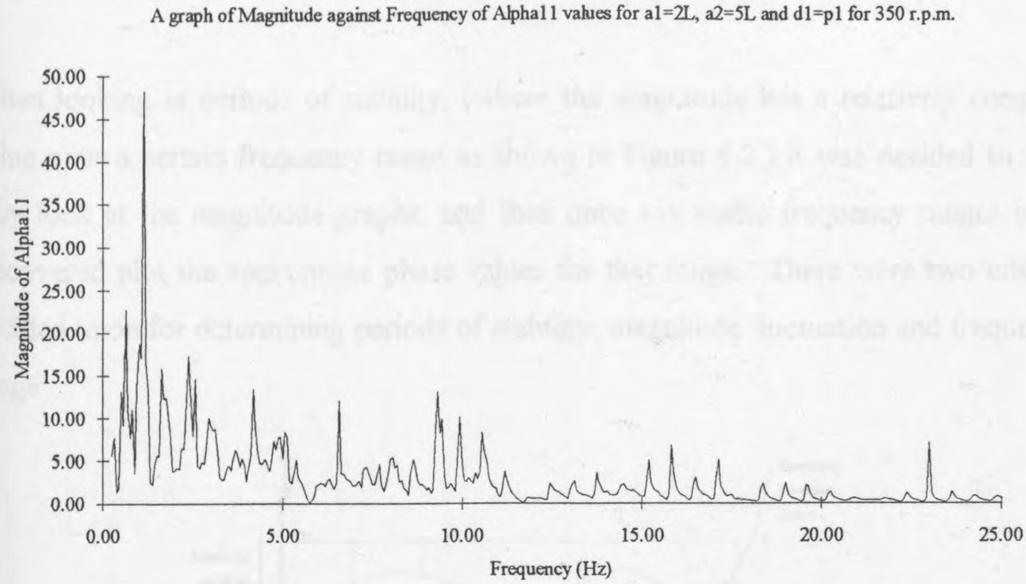

Graph 4.27: A graph of magnitude against frequency for α_{11} values for d1=P1, a1=2L and a2=5L at 350 rpm.

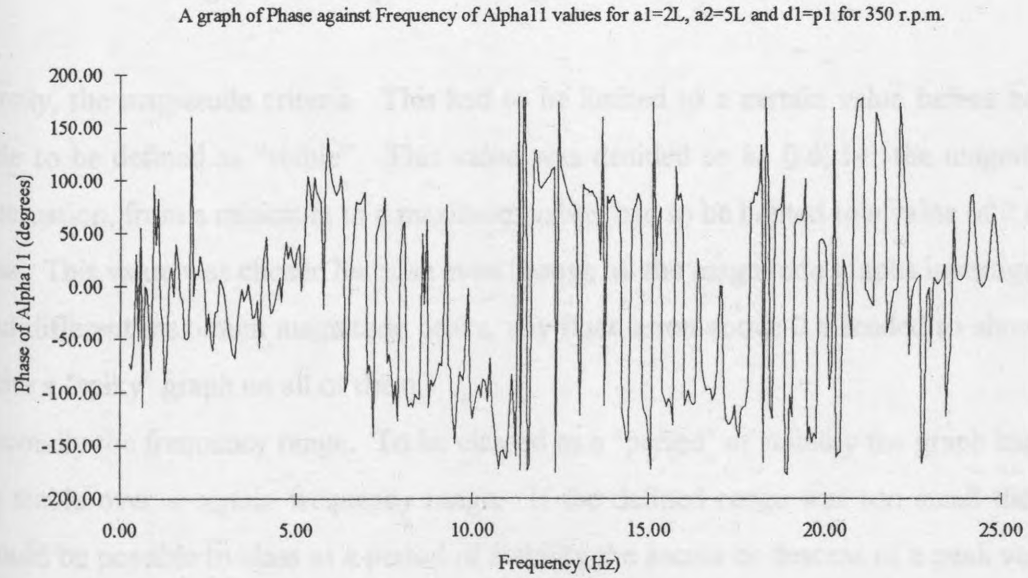

Graph 4.28: A graph of phase against frequency for α_{11} values for d1=P1, a1=2L and a2=5L at 350 rpm.

4.7. Periods Of Stability.

When looking at periods of stability, (where the magnitude has a relatively constant value over a certain frequency range as shown in Figure 4.2.) it was decided to first only look at the magnitude graphs, and then once any stable frequency ranges were discovered plot the appropriate phase values for that range. There were two criteria decided upon for determining periods of stability; magnitude fluctuation and frequency range.

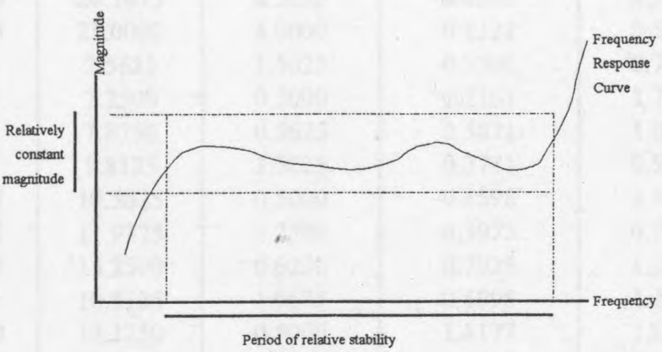

Figure 4.2. : A period having a relative constant value.

Firstly, the magnitude criteria. This had to be limited to a certain value before being able to be defined as "stable". This value was decided to be 0.6, i.e. the magnitude fluctuation, from a minimum to a maximum value, had to be limited to a value of 0.6 or less. This value was chosen because even though all the magnitude graphs investigated had different maximum magnitude peaks, any fluctuation above 0.6 tended to show as quite a 'spiky' graph on all of them.

Secondly the frequency range. To be classed as a 'period' of stability the graph had to be stable over a certain frequency range. If the defined range was too small then it would be possible to class as a period of stability the ascent or descent of a peak value, which is clearly not the case. It would also, when compared over the frequency range under investigation, (0 - 25 Hz), only appear as a very small line on the graph. It was decide to have a minimum frequency range value of 0.5 Hz. This would hopefully eliminate any problems with the peak values and as it is a fiftieth of the total frequency range would be noticeable on the final graph.

The tables for each combination, showing the frequency range and the amplitude range for the periods of stability can be seen in Tables 4.2 to 4.5

Speed (r.p.m)	Minimum Frequency	Maximum Frequency	Frequency Range	Minimum Magnitude	Maximum Magnitude	Magnitude Range
100	5.1875	6.3750	1.1875	0.0855	0.6100	0.5246
150	0.8125	2.4375	1.6250	0.0314	0.6265	0.5951
150	2.6875	4.8750	2.1875	0.1220	0.6067	0.4847
150	5.1875	7.4375	2.2500	0.0569	0.5936	0.5367
150	7.6875	8.9375	1.2500	0.1297	0.5434	0.4137
150	10.8125	12.0625	1.2500	0.1170	0.6529	0.5358
150	12.7500	17.1250	4.3750	0.1426	0.7332	0.5905
150	17.6250	20.1875	2.5625	0.0603	0.5699	0.5096
150	21.0000	25.0000	4.0000	0.1122	0.5949	0.4826
200	1.0000	2.5625	1.5625	0.2306	0.7515	0.5209
200	6.7500	7.2500	0.5000	1.2161	1.7205	0.5044
200	7.3125	7.8750	0.5625	0.5871	1.0747	0.4877
200	8.2500	9.8125	1.5625	0.3781	0.9014	0.5233
200	10.0625	10.5625	0.5000	0.8598	1.4407	0.5810
200	10.6875	11.9375	1.2500	0.3975	0.9196	0.5221
200	14.6250	15.2500	0.6250	0.7925	1.2818	0.4893
250	9.2500	10.3125	1.0625	0.6098	1.1172	0.5073
250	12.6250	13.1250	0.5000	1.4177	1.8980	0.4802
250	14.1875	14.6875	0.5000	2.0511	2.5875	0.5364
300	17.6875	18.5000	0.8125	1.1586	1.7235	0.5649
300	20.3750	23.0625	2.6875	0.1135	0.6753	0.5618
350	11.5000	12.3750	0.8750	0.1480	0.6699	0.5218
350	17.5625	18.2500	0.6875	0.2373	0.5539	0.3166
350	20.3750	22.3125	1.9375	0.1482	0.6479	0.4998
350	24.3125	25.0000	0.6875	0.2281	0.7942	0.5661

Table 4.2: Table showing periods of stability for the first combination.

Speed (rpm)	Minimum Frequency	Maximum Frequency	Frequency Range	Minimum Magnitude	Maximum Magnitude	Magnitude Range
100	1.3125	5.1250	3.8125	0.0053	0.5816	0.5763
100	9.3125	10.1875	0.8750	0.0001	0.5463	0.5462
100	11.0625	11.7500	0.6875	0.0856	0.6736	0.5880
100	16.1250	16.7500	0.6250	0.1375	0.4418	0.3044
100	22.9375	23.6875	0.7500	0.0712	0.5778	0.5067
150	3.1250	4.2500	1.1250	1.6107	2.1874	0.5766
150	4.8125	5.1875	0.3750	0.1719	0.7134	0.5415
150	12.1250	12.7500	0.6250	0.1257	0.7048	0.5791
150	14.9375	15.5625	0.6250	0.0679	0.5274	0.4595
150	17.4375	18.1250	0.6875	0.1608	0.7281	0.5672
150	18.1875	19.0625	0.8750	0.8101	1.1176	0.3074
150	21.2500	21.8125	0.5625	0.6460	1.0353	0.3892
150	22.3750	22.8750	0.5000	0.0880	0.4546	0.3666
200	0.8750	1.3750	0.5000	1.4169	1.8335	0.4167
200	2.8750	3.6250	0.7500	0.2444	0.7482	0.5038
200	4.0000	4.7500	0.7500	0.8669	1.4496	0.5828
200	6.1250	7.3750	1.2500	0.1502	0.7129	0.5627
200	7.4375	7.9375	0.5000	0.7450	1.2404	0.4954

Speed (rpm)	Minimum Frequency	Maximum Frequency	Frequency Range	Minimum Magnitude	Maximum Magnitude	Magnitude Range
200	8.2500	8.7500	0.5000	0.5231	1.0134	0.4903
200	8.8125	9.9375	1.1250	0.2025	0.7513	0.5488
200	11.0000	11.8750	0.8750	1.5071	1.9840	0.4769
250	1.0625	6.3125	5.2500	0.1527	0.6910	0.5383
250	6.3750	8.3125	1.9375	0.0526	0.4992	0.4467
250	8.5625	11.1250	2.5625	0.2788	0.8275	0.5487
250	11.1875	13.1875	2.0000	0.1996	0.6250	0.4255
250	13.3125	14.5000	1.1875	0.3478	0.8641	0.5163
250	14.8750	15.3750	0.5000	0.4555	1.0314	0.5760
250	16.1250	16.7500	0.6250	1.1199	1.4900	0.3701
250	16.8125	17.3750	0.5625	1.5932	1.9706	0.3774
250	17.4375	17.9375	0.5000	2.1591	2.6549	0.4958
250	18.1875	18.6875	0.5000	2.7807	3.3627	0.5820
300	7.1875	7.6875	0.5000	0.1720	0.6384	0.4664
300	7.8125	8.3125	0.5000	0.1453	0.6745	0.5292
300	9.0625	9.9375	0.8750	0.0352	0.5883	0.5530
300	10.6250	11.3125	0.6875	0.1781	0.7747	0.5966
300	11.5000	12.2500	0.7500	0.2546	0.7770	0.5224
300	12.8750	13.3750	0.5000	0.3483	0.8453	0.4970
300	13.5000	14.0000	0.5000	0.1872	0.5145	0.3272
300	14.1250	23.1875	9.0625	0.0578	0.5019	0.4441
300	23.2500	24.7500	1.5000	0.2631	0.8157	0.5525
350	2.0000	2.5625	0.5625	0.1255	0.6788	0.5533
350	3.8125	4.3125	0.5000	0.0830	0.4989	0.4159
350	5.6250	6.7500	1.1250	0.2893	0.7102	0.4209
350	6.8750	8.8125	1.9375	0.1779	0.7289	0.5510
350	8.9375	9.8750	0.9375	0.2685	0.7686	0.5001
350	10.6250	11.6875	1.0625	0.4486	0.8119	0.3633
350	11.7500	12.3750	0.6250	0.1362	0.6069	0.4707
350	13.1875	15.6875	2.5000	0.3574	0.9500	0.5926
350	16.5000	17.0625	0.5625	0.4920	1.0593	0.5673
350	17.6250	18.2500	0.6250	0.0705	0.5663	0.4957
350	18.3750	18.8750	0.5000	0.2384	0.7708	0.5324
350	19.6250	22.8125	3.1875	0.2751	0.8737	0.5986
350	23.0625	25.0000	1.9375	0.2712	0.8250	0.5538

Table 4.3: Table showing periods of stability for the second combination

Speed (rpm)	Minimum Frequency	Maximum Frequency	Frequency Range	Minimum Magnitude	Maximum Magnitude	Magnitude Range
100	5.1875	6.3750	1.1875	0.0861	0.6100	0.5239
100	6.8125	7.4375	0.6250	0.6485	1.2062	0.5577
150	0.8125	2.4375	1.6250	0.0319	0.6261	0.5942
150	2.6875	4.8750	2.1875	0.1228	0.6055	0.4828
150	5.1875	7.4375	2.2500	0.0568	0.5939	0.5371
150	7.6875	8.9375	1.2500	0.1301	0.5238	0.3937
150	10.8125	12.0625	1.2500	0.1170	0.6528	0.5358
150	12.7500	17.1250	4.3750	0.1425	0.7331	0.5906
150	17.6250	20.1875	2.5625	0.0603	0.5699	0.5096
150	20.9375	22.7500	1.8125	0.1122	0.7105	0.5983
150	22.8750	25.0000	2.1250	0.1710	0.5441	0.3731
200	1.0000	2.5625	1.5625	0.2342	0.7513	0.5171

Speed (rpm)	Minimum Frequency	Maximum Frequency	Frequency Range	Minimum Magnitude	Maximum Magnitude	Magnitude Range
200	6.7500	7.2500	0.5000	1.2171	1.7217	0.5046
200	7.3125	8.0625	0.7500	0.5875	1.0754	0.4879
200	8.2500	9.8125	1.5625	0.3782	0.9017	0.5235
200	10.0625	10.5625	0.5000	0.8603	1.4415	0.5812
200	10.6875	11.9375	1.2500	0.3976	0.9199	0.5222
200	14.7500	15.3125	0.5625	0.9884	1.4579	0.4695
250	9.2500	10.3125	1.0625	0.6102	1.1176	0.5074
250	12.6250	13.1250	0.5000	1.3980	1.8985	0.5005
250	14.1875	14.6875	0.5000	2.0513	2.5877	0.5364
300	14.6875	15.1875	0.5000	0.5808	1.0471	0.4663
300	17.6875	18.5000	0.8125	1.1586	1.7238	0.5652
300	20.3750	23.0625	2.6875	0.1135	0.6752	0.5618
350	11.5000	12.3750	0.8750	0.1479	0.6693	0.5214
350	17.5625	18.2500	0.6875	0.2373	0.5540	0.3167
350	20.3750	22.3125	1.9375	0.1482	0.6481	0.4999
350	24.3125	25.0000	0.6875	0.2281	0.8122	0.5841

Table 4.4: Table showing the periods of stability for the third combination.

Speed (rpm)	Minimum Frequency	Maximum Frequency	Frequency Range	Minimum Magnitude	Maximum Magnitude	Magnitude Range
100	1.3125	5.1250	3.8125	0.1108	0.5817	0.4709
100	9.3125	10.1875	0.8750	0.0002	0.5440	0.5438
100	11.0625	11.7500	0.6875	0.0852	0.6726	0.5874
100	16.1250	16.7500	0.6250	0.1373	0.4411	0.3038
100	22.9375	23.6875	0.7500	0.0563	0.5771	0.5208
150	3.1250	4.2500	1.1250	1.6126	2.1795	0.5668
150	11.3125	11.8125	0.5000	1.2838	1.8806	0.5969
150	12.1250	12.7500	0.6250	0.1238	0.7058	0.5820
150	14.9375	15.5625	0.6250	0.0687	0.5279	0.4592
150	17.4375	18.1250	0.6875	0.1608	0.7580	0.5972
150	18.1875	19.0000	0.8125	0.8104	1.1178	0.3074
150	21.2500	21.8125	0.5625	0.6463	1.0359	0.3896
150	22.3750	22.8750	0.5000	0.0881	0.5081	0.4200
200	0.8750	1.3750	0.5000	1.4171	1.8826	0.4655
200	2.8750	3.6250	0.7500	0.2384	0.7386	0.5002
200	4.0000	4.7500	0.7500	0.8652	1.4430	0.5779
200	6.1250	7.3750	1.2500	0.1497	0.7140	0.5642
200	7.4375	8.1250	0.6875	0.5300	0.7450	0.2149
200	8.2500	8.7500	0.5000	0.5235	1.0138	0.4903
200	8.8125	9.9375	1.1250	0.2030	0.7974	0.5944
200	10.5000	11.8750	1.3750	1.5077	1.9277	0.4200
200	12.5625	13.0625	0.5000	2.3397	2.9312	0.5915
200	13.1875	13.6875	0.5000	2.9883	3.4461	0.4578
200	13.7500	14.3125	0.5625	3.6055	4.1619	0.5564
250	0.8125	4.1875	3.3750	0.2291	0.7839	0.5548
250	4.2500	6.3125	2.0625	0.1525	0.6466	0.4941
250	6.3750	8.3125	1.9375	0.0525	0.5628	0.5103
250	8.5625	9.0625	0.5000	0.5314	0.8270	0.2956
250	9.1250	13.1875	4.0625	0.1996	0.6925	0.4929
250	13.2500	14.5000	1.2500	0.3478	0.9068	0.5590
250	16.1250	16.7500	0.6250	1.1199	1.4900	0.3701
250	16.8125	17.3750	0.5625	1.5932	1.9706	0.3774
250	17.4375	17.9375	0.5000	2.1591	2.6549	0.4958

Speed (rpm)	Minimum Frequency	Maximum Frequency	Frequency Range	Minimum Magnitude	Maximum Magnitude	Magnitude Range
300	7.1875	7.6875	0.5000	0.1718	0.6366	0.4648
300	7.8125	8.3125	0.5000	0.1446	0.6733	0.5287
300	9.0625	9.9375	0.8750	0.0357	0.5874	0.5517
300	10.6250	11.2500	0.6250	0.1780	0.7254	0.5475
300	11.5625	12.4375	0.8750	0.2703	0.7440	0.4737
300	12.8750	13.3750	0.5000	0.3484	0.8454	0.4970
300	13.5000	14.0000	0.5000	0.1891	0.5144	0.3253
300	14.1250	23.1875	9.0625	0.0578	0.5211	0.4633
300	23.2500	24.3125	1.0625	0.3613	0.8661	0.5047
350	2.0000	2.5625	0.5625	0.1255	0.6789	0.5533
350	3.8125	4.3125	0.5000	0.1194	0.4974	0.3781
350	5.6250	6.7500	1.1250	0.2908	0.7104	0.4196
350	6.8750	8.8125	1.9375	0.1787	0.7304	0.5518
350	8.9375	9.8750	0.9375	0.2687	0.7695	0.5008
350	10.0625	11.2500	1.1875	0.5352	1.1304	0.5953
350	11.3125	12.3750	1.0625	0.1348	0.6667	0.5319
350	13.1875	15.6875	2.5000	0.3575	0.9504	0.5929
350	16.5000	17.0625	0.5625	0.4920	1.0593	0.5673
350	17.6250	18.2500	0.6250	0.0699	0.5662	0.4963
350	18.3750	18.8750	0.5000	0.2384	0.7708	0.5324
350	19.6875	22.9375	3.2500	0.1810	0.7638	0.5828
350	23.0625	25.0000	1.9375	0.2712	0.8250	0.5538

Table 4.5: Table showing periods of stability for the fourth combination.

Once the periods of stability had been determined for the four combinations of instrumentation then the average values for each period was calculated. This was plotted and can be seen in Graphs 4.29, 4.32, 4.35 and 4.38, for combinations 1 to 4 respectively, with the plotted phase values for that frequency range shown in the two figures immediately following each plot.

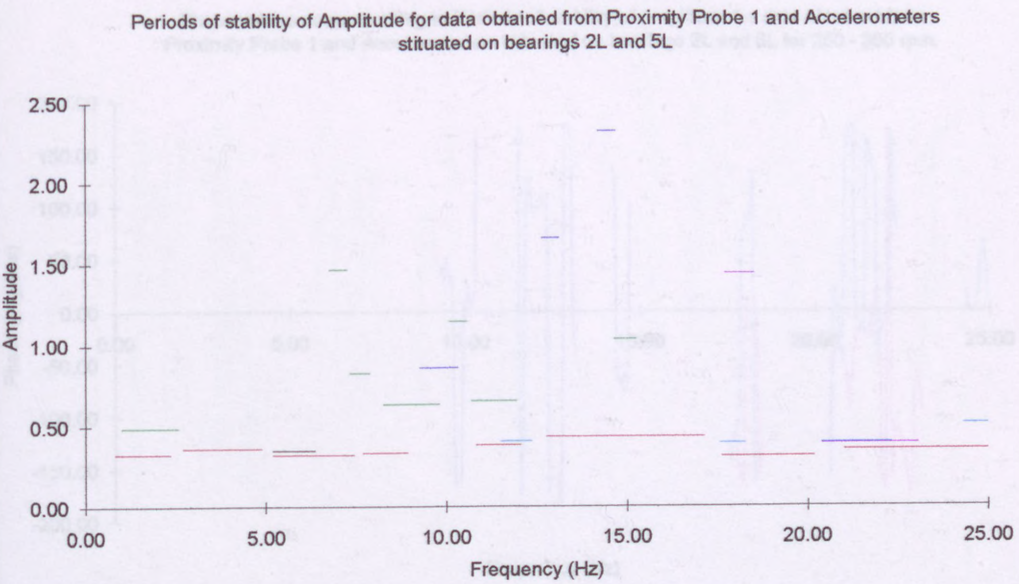

Graph 4.29: A graph of periods of stability for amplitude of $\alpha 11$ for d1=P1, a1=2L and a2=5L.

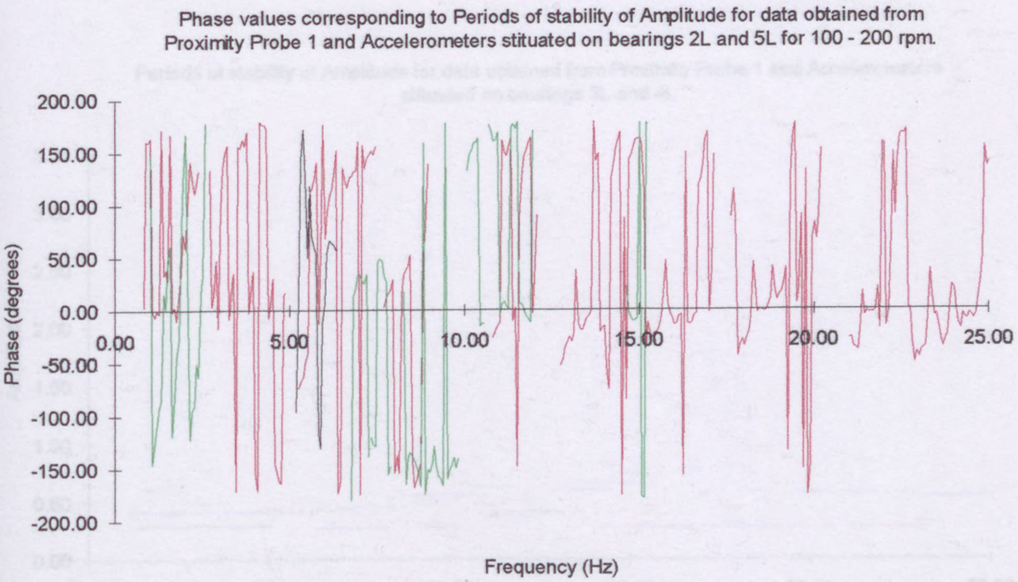

Graph 4.30: A graph of phase values corresponding to periods of stability for the amplitude, for speeds 100 - 200 rpm.

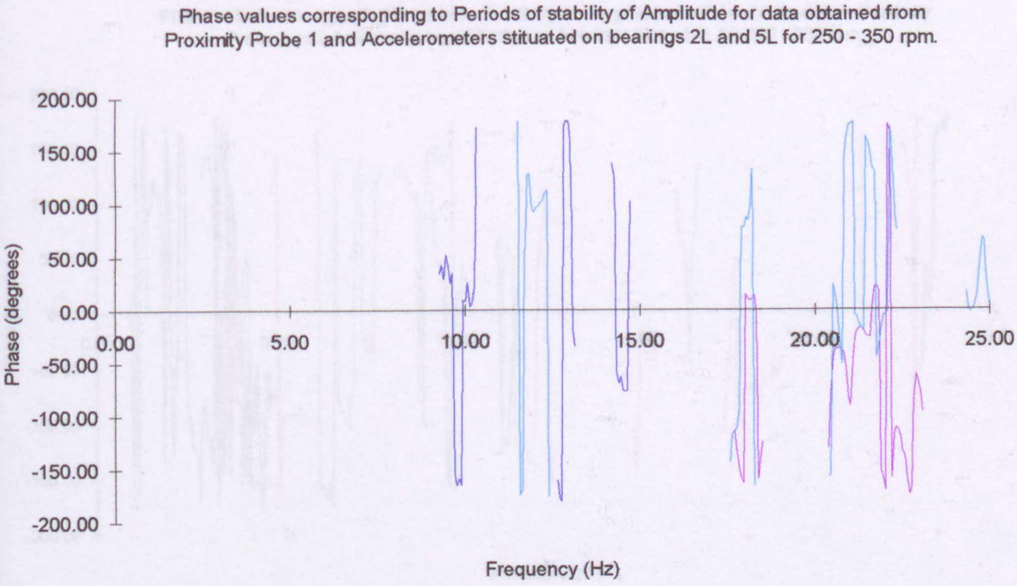

Graph 4.31: A graph of phase values corresponding to periods of stability for the amplitude, for speeds 250 - 350 rpm.

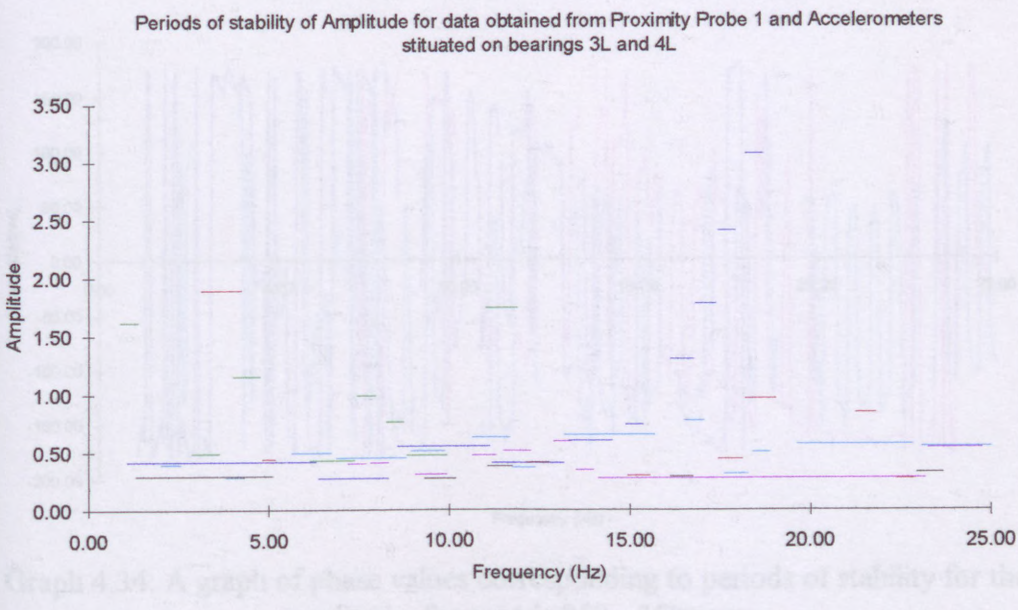

Graph 4.32: A graph of periods of stability for amplitude of $\alpha 11$ for d1=P1, a1=3L and a2=4L.

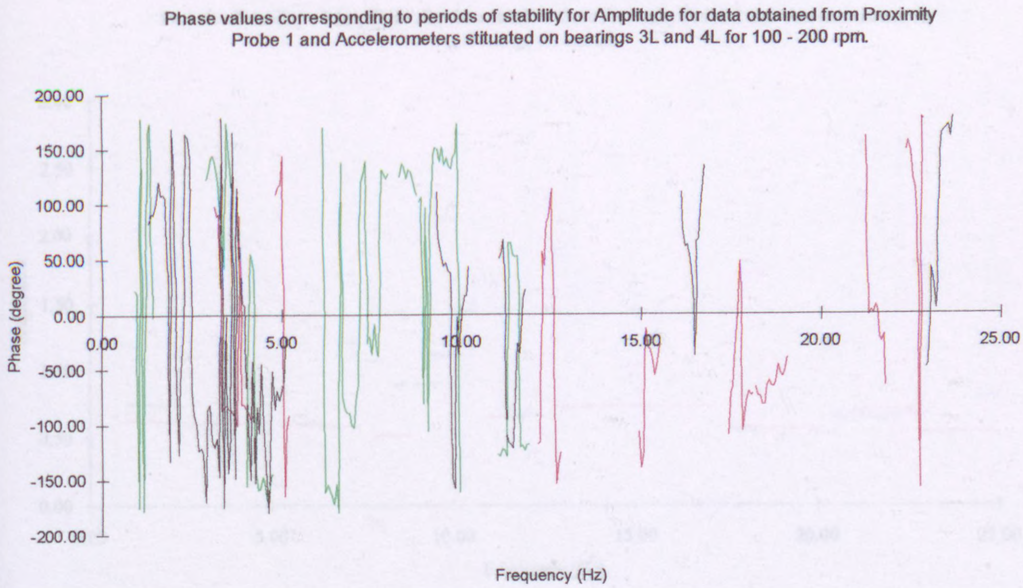

Graph 4.33: A graph of phase values corresponding to periods of stability for the amplitude, for speeds 100 - 200 rpm.

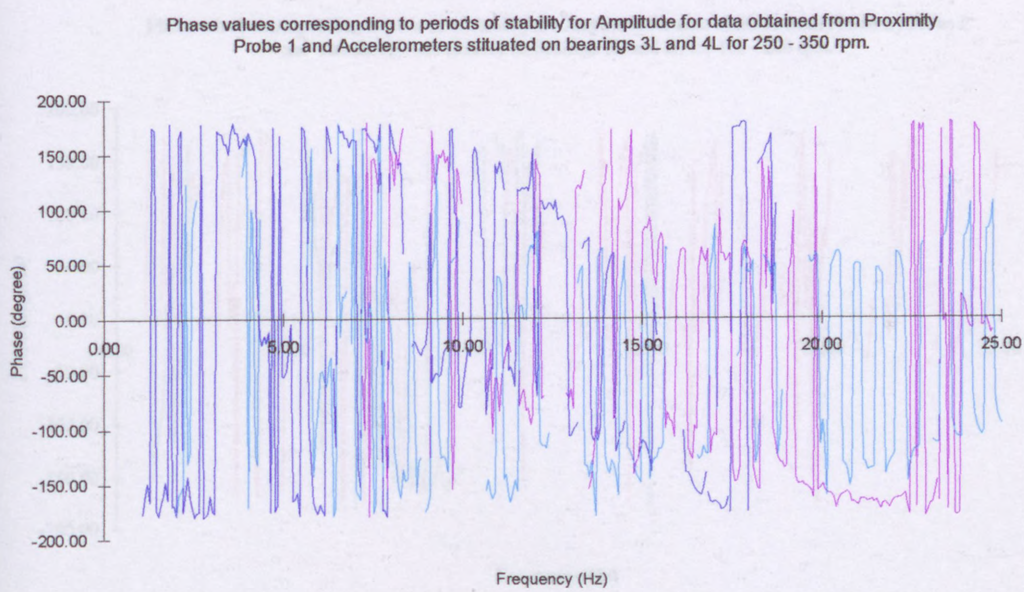

Graph 4.34: A graph of phase values corresponding to periods of stability for the amplitude, for speeds 250 - 350 rpm.

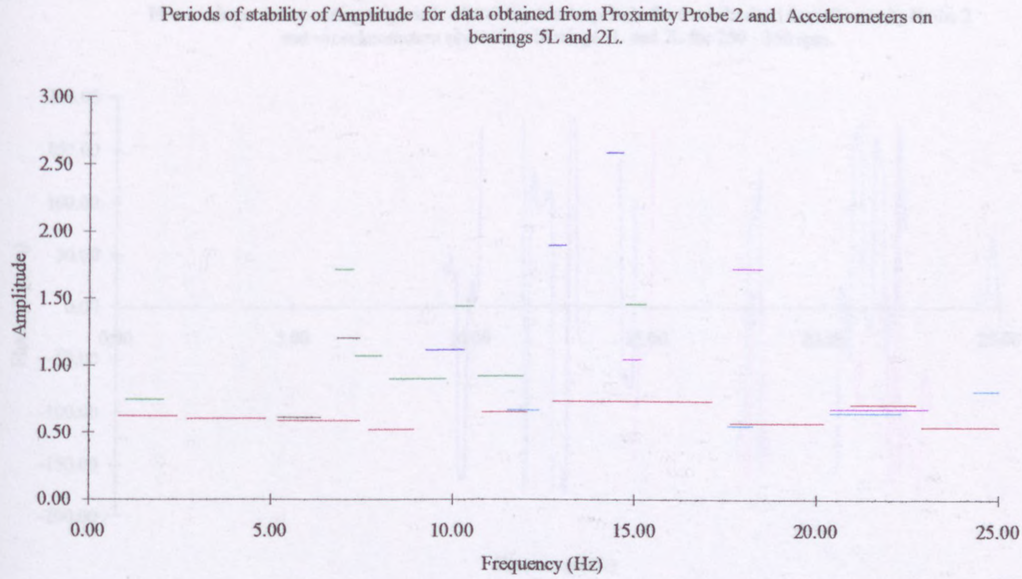

Graph 4.35: A graph of periods of stability for amplitude of $\alpha 11$ for d2=P2, a1=5L and a2=2L.

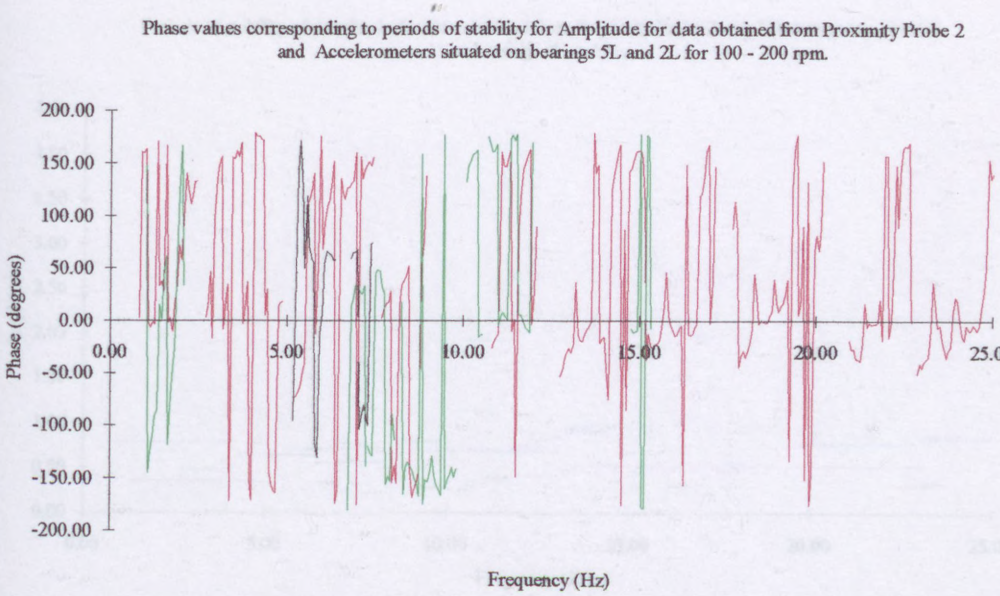

Graph 4.36: A graph of phase values corresponding to periods of stability for the amplitude, for speeds 100 - 200 rpm.

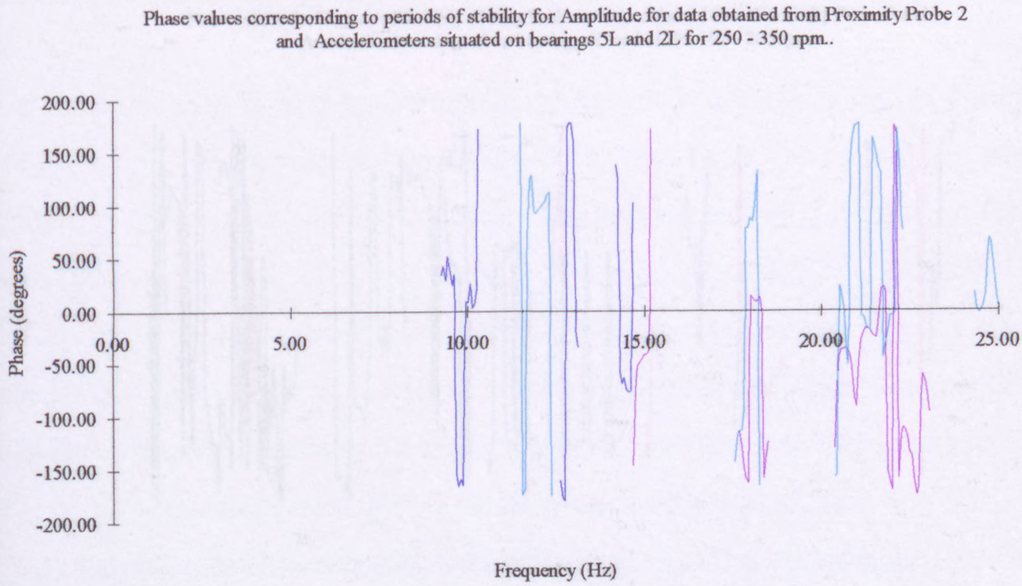

Graph 4.37: A graph of phase values corresponding to periods of stability for the amplitude, for speeds 250 - 350 rpm.

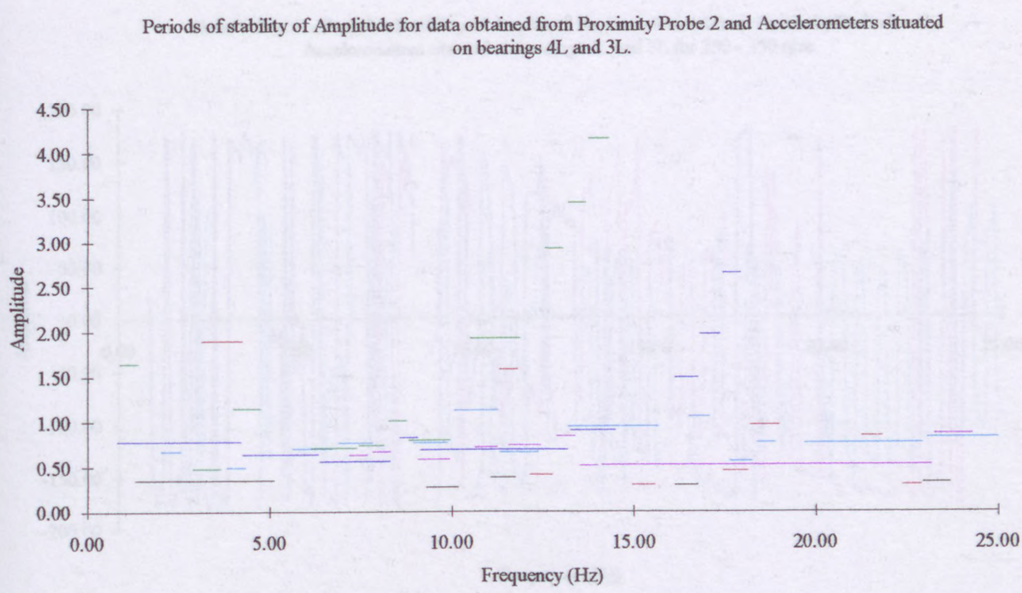

Graph 4.38: A graph of periods of stability for amplitude of $\alpha 11$ for d2=P2, a1=4L and a2=3L.

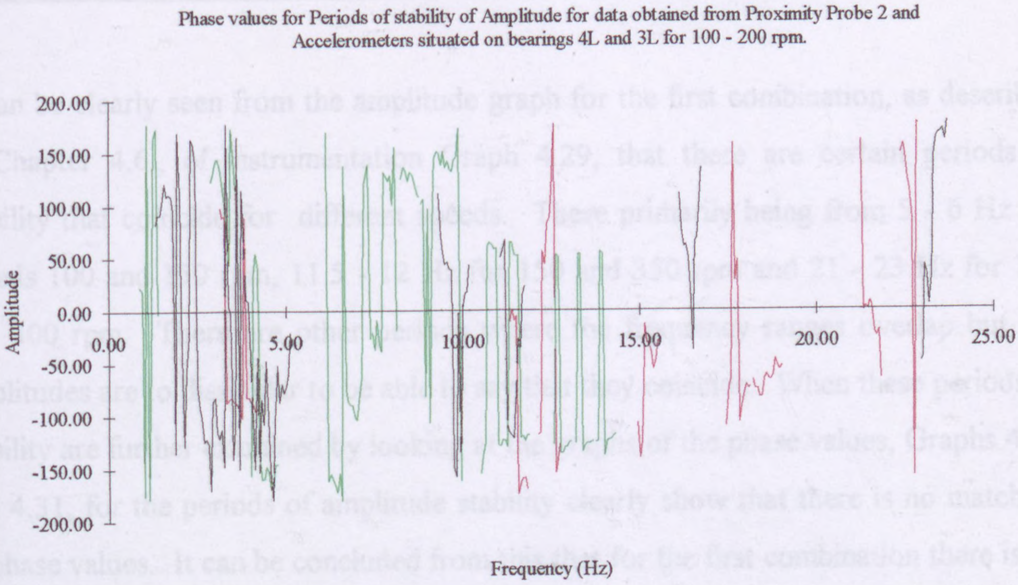

Graph 4.39: A graph of phase values corresponding to periods of stability for the amplitude, for speeds 100 - 200 rpm.

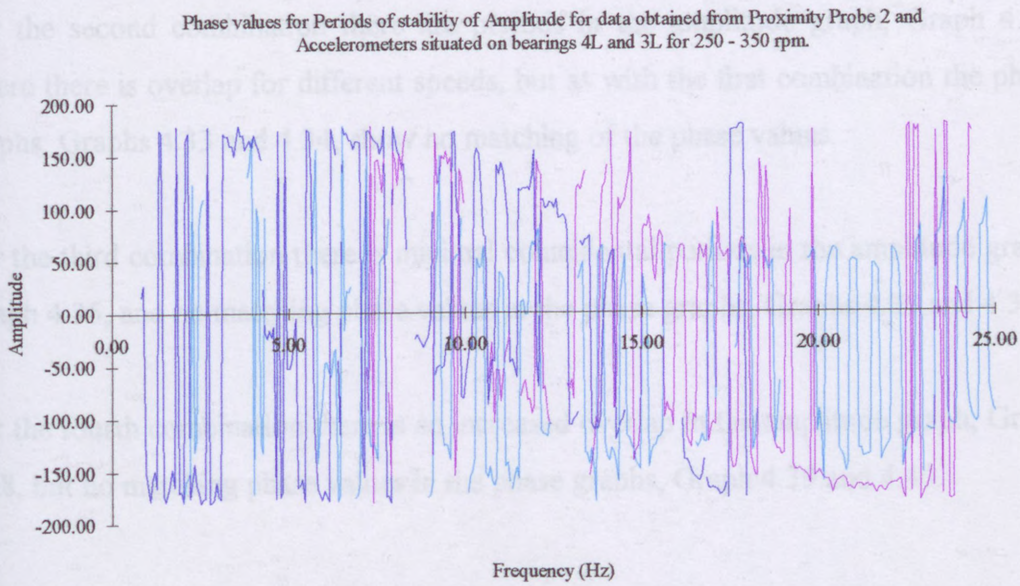

Graph 4.40: A graph of phase values corresponding to periods of stability for the amplitude, for speeds 250 - 350 rpm.

4.8. Analysis Of The Periods Of Stability.

It can be clearly seen from the amplitude graph for the first combination, as described in Chapter 4.6., of instrumentation Graph 4.29, that there are certain periods of stability that coincide for different speeds. These primarily being from 5 - 6 Hz for speeds 100 and 150 rpm, 11.5 - 12 Hz for 150 and 350 rpm and 21 - 23 Hz for 150 and 300 rpm. There are other periods where the frequency ranges overlap but the amplitudes are to dissimilar to be able to say that they coincide. When these periods of stability are further examined by looking at the graphs of the phase values, Graphs 4.30 and 4.31, for the periods of amplitude stability clearly show that there is no matching of phase values. It can be concluded from this that for the first combination there is no periods over the frequency range under investigation where the α_{11} values are constant for the different camshaft speeds looked at.

For the second combination there are periods in the amplitude graph, Graph 4.32, where there is overlap for different speeds, but as with the first combination the phase graphs, Graphs 4.33 and 4.34, show no matching of the phase values.

For the third combination there is minimal coincidental periods in the amplitude graph, Graph 4.35, and no matching phase values in the phase graphs, Graphs 4.36 and 4.37.

For the fourth combination there is an increased overlap in the amplitude graph, Graph 4.38, but no matching phase values in the phase graphs, Graph 4.39 and 4.40.

4.9 Conclusion.

The ideal case for the values of the influence coefficients would provide both constant amplitude and phase values, thus providing a straight forward relationship between the two sets of vibration. The graphs examining one combination of transducer signals, Graphs 4.17 to 4.28, show that the values calculated were very uneven. It was decided to more closely examine these graphs to determine whether there were any frequency periods within the frequency range under investigation where the values were constant, Graphs 4.28 to 4.40. This was again found not to be the case, with the calculated values appearing to have no particular pattern to them.

This is because the engine is a complex mechanism with many different components moving at many different speeds and directions which provides many opportunities for different levels of vibration at different parts of the engine. All these vibrations will be transmitted to other parts of the engine, including up through the camshaft bearings. The design of the actual test rig may have unwittingly also caused unwanted vibrations that were also transmitted through the engine.

It is these unwanted vibrations, in addition to the camshaft vibration, that are transmitted through the bearings and are measured by the accelerometers. Thus invalidating the initial assumption of trying to directly relate the vibration measured at the camshaft to the vibration transmitted through the bearings. This can clearly be seen in the graphs of amplitude and phase for α_{11} where the values are nowhere like the expected constant values.

Another possible cause for concern is the initial assumption of making α_{12} a unity vector could still be called into doubt, even though it was found to have a minimal effect on the calculations.

CHAPTER 5

DISCUSSION

5.1. Introduction.

This chapter will basically be an extended discussion chapter. It will describe some of the main problems associated with the construction of the test rig and what actions were undertaken to overcome them. It will also discuss in more detail the outcome of all the experimental work done during this project. It will also reiterate the findings from the influence coefficient calculations. Some of the point will have already been touched upon in the appropriate parts of Chapter 3.

5.2. The Test Rig.

One of the main problems with this research project was with the construction of the test rig.

The initial manufacture of the individual components took far longer than was expected, with some parts taking up to three and a half months to complete. This was mainly due to the fact that the departmental laboratories were undergoing reconstruction at the time and the manpower was not available to swiftly make the parts that was required.

Another delaying factor was the selection of the D.C. motor. The initial problem, and one which continued throughout the construction of the test rig, was the fact that most of the people that had to be consulted were in a different department, the School of Electrical and Electronic Engineering (S.E.E.E), at the University. This meant that there was sometimes a significant time delay between arranging a meeting and the meeting actually taking place. Another problem was the misjudgment of the torque requirements of the engine and the torque capabilities of the available motors. Some of the available motors, within the S.E.E.E. department, were old (20 - 30 years old in some cases) and the documentation for them had been mislaid, so it basically came down to an educated guess to the capabilities of the motor and a 'try it and see if it works' method. It was decided that, with the availability of motors within the University, this method would be quicker than the purchase of a new motor and have to wait up to three months for delivery. The first motor tried in this way did not have the required torque needed to turn the engine. So a second, larger motor had to be tried. This involved altering the test rig to accommodate the difference in motor sizes. This motor had the required torque but even after altering the windings slightly it could only turn the engine up to approximately 700 r.p.m.

The relatively low speeds that the engine was run at also led to an unforeseen problem with the oil pump. The oil pump required an initial burst of speed to get the suction of the lubrication oil started. This frequently did not happen, especially if the engine had been unused for a period of time, so the lubrication system for the engine did not work. This problem was overcome by persistence, i.e. the engine would be repeatedly stopped and then started again until it did work.

Once the final motor was placed in the test rig a new belt tensioner had to be designed and manufactured. This was designed in two parts, one of which was bought, the other part was made within the department. Again this process took time, delaying the final construction of the test rig by a few weeks.

Again once the motor was in place it was found that the test rig would have to be stiffened to help reduce vibrations, caused by the rotating parts of the engine. The brackets were removed and small supporting webs were made and welded into place on the brackets.

It was originally decided to try and keep the engine to the bare minimum of parts needed to run it. This was to try and keep the engine as simple as possible so that the camshaft subsystem would not be effected by outside influences. It was soon discovered that a number of parts, such as the pistons, had to be reintroduced into the engine to help the overall balance.

5.3. The Proximity Probes.

When the calibration tests for the proximity probes were completed it was discovered that there were slight discrepancies between the experimentally determined sensitivities and the manufacturers stated values. In this case the sensitivity for proximity probe 1 was found to be 204.9 mV/mil, giving a difference of 2.4% and for probe 2 the sensitivity was 178.9 mV/mil, giving a difference of 10.6%, where both values have a experimental error of ± 0.1 mV/mil.

Another point that was noted during the experiment was the fact that when both probes had the same airgap distance they gave slightly different voltage readings, which was unexpected. The graph of Airgap Distance against Voltage (as seen in Chapter 3.2.4) show that both proximity probes peak (in a negative sense) at about 75 - 80 mil, though probe 2 peaks slightly earlier and at a smaller voltage.

These two points could indicate a problem with misalignment of the probes, especially with probe 2. The impedance variation principle used in eddy current transducers measures the amount of disruption in an electromagnetic field caused by the generation of the eddy currents in a target, as shown in Figure 5.1.

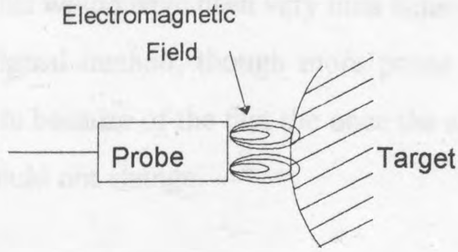

Figure 5.1: The electromagnetic field.

To utilize most of the electromagnetic field the probe has to be perpendicular to the target, to ensure that the most eddy currents possible are created and thus voltage output from the probe. If the probe is slightly misaligned then the full electromagnetic field would not be in contact with the target, thus not as many eddy currents would be induced. This is shown in Figure 5.2 in an exaggerated manner.

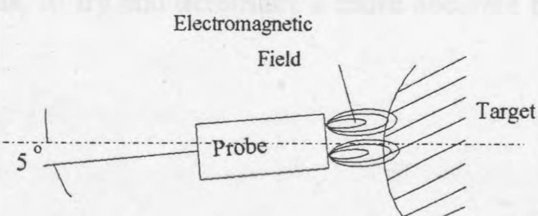

Figure 5.2: An exaggerated example of misalignment of the proximity probe at 5°

misalignment.

This slight misalignment could be attributed to the manufacture of the positioner for the proximity probes. The 'V' shape part of the positioner, where the probes are attached to the positioner, is meant to be at an exact angle of 90°. This would ensure that the probes are at an angle of 45° perpendicular to the camshaft. This is the ideal case, but it was not possible to get this part of the positioner to such a precise angle. Another point during the manufacture of the positioner where possible distortion to this angle may have occurred would be when the two flat plates were welded to the 'V' section. The heat generated during the welding process may have caused slight distortion to the overall positioner. The only sure way to ensure an accurate angle would have been to make the positioner from one piece of metal. This would have been very time consuming and very wasteful, so it was decided that the original method, though more prone to misalignment, was still good enough for the purpose because of the fact the once the sensitivity had been set, just before the experiment, it would not change.

The material that the camshaft is made from may also have affected the probe. For the probe to work properly the material has to be fully conductive, to allow the eddy currents to be generated. Any impurities in the material, or minute internal defects may impede the generation of eddy currents, reduce the sensitivity slightly.

The least squares method used to determine the best fit straight line was taken between 10 - 35 mils, whereas the working range for the probe was 10 - 30 mils. It may have been better to take the working range of the probe to be either slightly bigger, 5 - 35 mils, or slightly less, 15 - 25 mils, to try and determine a more accurate best fit line to match the voltage readings.

5.4. The Accelerometers.

The calibration tests for the accelerometers showed that of the four accelerometers used in the test rig, serial numbers 22222 to 22225, two of them were within 2.5 % of the manufacturers sensitivity values and the other two accelerometers, serial numbers 22222 and 22224, had a 26.2 % and 15.1% difference respectively.

The first possible fault that may have occurred during the calibration test is due to the calibration exciter itself. There was no method available to determine whether the exciter was itself calibrated properly. The calibration certificate for the exciter had been lost so it was not possible to know when the last calibration check was carried out on it. It was known however that it had not been checked in the last eight years and has been in laboratory use in all that time and may have been affected by regular use.

The peak values determined by the accelerometers were at a frequency of 159 Hz and not 159.2 Hz as it was supposed to be. This is however only a 0.1% difference from the expected value, and indicates that there is a slight alteration from its original setting but that this 'drift' should remain constant during the calibration tests. The excitation level produced by the exciter may also have changed from 10 m/s^2 . The only sure way of checking this would be to return the exciter back to its manufacturer for re-calibration.

The threaded bar used to connect the accelerometer and the exciter was too long to obtain a snug fit between the exciter and the accelerometer. Even though the threaded stud bar provides the best transmission there may have been some loss if the vibration produced by the exciter caused the accelerometer to loosen slightly.

The FFT Analyser used a flat top window on the vibration signal. This type of window was chosen because it provided the best amplitude accuracy but can to affected by leakage, i.e. where some of the energy of the peak spills out into the adjacent frequencies making the peak appear wider and shorter. The RMS value was measured over the frequency range of 150.5 - 168.0 Hz (± 8.8 Hz) to try and take leakage into account, but there may have been a small amount of the signal lost at the bottom of the peak. The frequency range taken during this test seemed to provided a wide enough range. This can be seen in Figure 5.3.

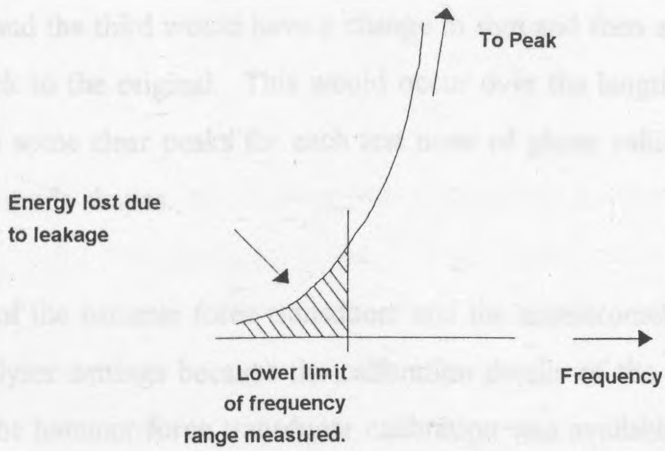

Figure 5.3: Energy loss due to leakage.

The two accelerometers that gave values of sensitivities that were different from the manufacturers values were re-tested to try and experimentally determine their sensitivities. This was done by experimentally altering the sensitivities on the FFT analyser settings until the experimental RMS value was within 1% of the expected value. These gave new values of the sensitivities to be 12.2 mV/g for accelerometer 22222 and 8.4 mV/g for accelerometer 22224. As these values are approximately ± 2 mV/g than what the manufacturer had intended, indicates that the accelerometers had been damaged in the time between the two tests. It may be a possibility that the accelerometers are continually getting worse so the calibration tests were undertaken just before the main experimental work was carried out.

5.5. The Hammer Impact Tests

The graphs for the Hammer Impact Tests, Graphs 3.8. to 3.17. do not provide any clear indication of the natural frequencies for the transducer platforms. The first natural frequency would have a mode shape similar to that of a bow, and would be shown on the graphs as a change in magnitude but similar sign of the phase value (i.e. positive or negative) et the different positions tested. The second would have a change in the sign of the phase value, and the third would have a change in sign and then another change in the phase sign to back to the original. This would occur over the length of the test subject. Though there are some clear peaks for each test none of phase values give the expected indications of the mode shapes.

The sensitivities of the hammer force transducer and the accelerometer were not entered into the FFT analyser settings because the calibration details of the accelerometer could not be found. The hammer force transducer calibration was available but was left at the set value on the charge amplifier. The accelerometer sensitivity could have been determined using the same method as the Monitran accelerometers, as described in Chapter 3.3. but it was decided to leave the values to a set value. This is because the Hammer Impact Test provides a ratio between the force of the impact and the vibration measured by the accelerometer and as long as the charge amplifier conversion values were not changed during the experiment then the frequency response values obtained would therefore be relative to each other. This ratio would stay the same throughout each test and thus even though the test results did not give the exact values, each set of results would be relative to each other.

The accelerometer was attached to the test subjects using beeswax, which was the best available method for temporary experimental set up for an small accelerometer. The beeswax was prone to detaching the accelerometer from the positioner if the shock of the impact was too great. So care had to be taken when using the hammer, especially at position 2 on the proximity probe positioner which was only 18 mm away from the accelerometer. This led to both the hammer signal and the accelerometer signal amplitudes to be small, so care had to be taken when setting up the FFT analyser input settings.

The size of the accelerometer platform was only big enough to allow for two impact positions. This would only obtain minimal experimental information on the mode shape of the subject under investigation. It was not possible to include the main accelerometer, even though it was considered as a part of the test system, in the impact range in case it got damaged during the tests.

The calibration details of the small accelerometer was unknown, thus there was no way of checking whether it had been damaged during it previous uses. The frequency response graphs seemed to give reasonable values at the lower frequency range but as the working frequency range of the accelerometer was also not known it was not possible to tell whether these values were valid.

These set of tests were undertaken within a very limited period of time. There was not an opportunity to redo the tests to check the validity of the original tests, and to determine whether the fact that the results were unclear was caused by the experimental technique used.

5.6. Spectral Analysis.

The spectral analysis of the transducers at all speeds clearly show visible running speed lines. For the accelerometers the most prominent running speed is the four times running speed and for the proximity probes the most prominent running speed is the one times running speed. On closer inspection of the accelerometer traces other running speeds lines can be seen, though these are very small in comparison to the four times running speed lines. These other lines can only be seen on two of the accelerometers spectral analysis traces. Other running speed lines are clear on the proximity probe traces, but again are not as significant.

As mentioned in Chapter 3.5. these traces are not proper waterfall plots. The reason for doing this was because the motor speed controller could not be accurately set to provide a specific ramp up rate, i.e. the rate at which the motor would accelerate over a period of time. So it was decided to take the individual readings and merge them into one single graph. This may not provide a true waterfall picture, but would provide a reasonable enough display to provide similar information on the running speeds.

The proximity probes show the one times running speed as the most prominent value. This could be due to the fact that they read the vibrations directly form the camshaft, and the most prominent measurement would be from the running speed, unless the camshaft was perfectly smooth and had a perfect orbit, which it does not.

The accelerometers show the four time running speed line as the most prominent values, with all the other running speed lines only showing minimal values. This may be attributable to another rotating part of the engine, that is rotating at four times the speed of the camshaft. One possible way to check whether this is true would be to measure the vibrations caused by as many of the rotating parts of the engine as possible by using an accelerometer located on the engine close to these parts and determining which vibration signature, in terms of the frequency of the vibration, closely matched the four times running speed.

There are possible resonance values showing on the spectrum test graphs, but the amount of traces on each graph does not allow for a clear indication whether they are resonance values or not. One method to check this would be to take spectral readings over a larger speed range. This however, was not possible because of the problems with the construction of the test rig, mainly the limited speed range obtained by the motor, that have already been mentioned this chapter. Another way to check the peaks would be to redo the tests while decreasing the speed increment between each test, from 50 r.p.m. increments to 10 or 20 r.p.m. increments, within the speed range available. This would provide a more accurate picture of the magnitudes increasing to a maximum value. This would be very time consuming to undertake and due to the time constraints on the project was not able to be done.

5.7. The Influence Coefficients.

The idea behind the development of the equation was to determine whether the proposed influence coefficients directly connected the vibration measured at the camshaft and the vibration transmitted through the bearings. The influence coefficients, when calculated, should have perfectly constant amplitude and phase value on their appropriate graphs. Even when taking into consideration the possibility a small amount of experimental error, which would be represented on the graphs by small fluctuations in the graphs, they graphs are nowhere near constant. The focus then moved to consider whether there was any periods within the frequency range that were constant over the speed range. The magnitude graphs showed that for some speeds there were certain frequencies that showed relatively constant magnitude values over a frequency range. When the phase graphs were taken into consideration they showed that over those frequency ranges their values still remain essentially random in appearance. This lead to the conclusion that the vibration measured at the camshaft bearings had to be influenced by more than just the vibration on the camshaft itself. The engine has many rotating parts all of which could cause vibrations that could be transmitted to the bearings which could affect the measured vibration.

Doubt could be cast over the validity of using the influence coefficient hypothesis. The influence coefficient theory assumes that the two loads applied to a static beam are independent of each other, but both have an effect on the deflection of the beam. In the case under study, the vibration measured at each bearing would be slightly affected by the vibration transmitted from other vibrations sources. Thus each measured vibration would not be truly independent of each other.

Chapter 6

Future Work.

The main reason that the equations were not valid was the fact that the accelerometers were measuring vibration transmitted from throughout the engine. This problem can be tackled in either one of two ways.

Firstly, by altering the equations. The new equations would have to incorporate more terms to include all the other moving components such as the crankshaft, oil pump, pistons e.t.c. This would vastly increase the complexity of the problem.

The second method would be to try to measure the vibrations of the other moving parts at the positions as close to them as possible. This way the most prominent vibration measured, (which should be the largest peak on the spectral analysis), would be due to that moving part. If the frequency that was found was fundamentally different from the camshaft running speed, or one of its harmonics then it could be eliminated / ignored from the accelerometer signal, if it was not different then it could be tried to be removed form the vibration signal measured by the accelerometer. This would have to involve a look at the transmissibility of vibration through the engine, which would be a major undertaking in itself.

The most obvious way to improve the test rig would be to try and to run the engine in its full working speed range, from 0 to 3000 r.p.m. (camshaft speed). One way to try and achieve this would be to increase the rigidity of the test rig, thus reducing the vibrations caused by running the engine at high speeds. A larger motor capable of much greater running speeds (0 - 6000 r.p.m.) under load would be needed.

Another way to alter the test rig would be to introduce valvetrain springs with a lower stiffness. This would, hopefully induce some sort of instability in the cam follower, most likely the jump phenomenon, and would lead into the investigation of the valve vibration.

Conclusion

The aim of this research project was to determine whether there was a direct relationship between the vibration measure from the camshaft and the vibration transmitted through the camshaft bearings. The main problem with trying to achieve this aim was the construction of the test rig. The test rig continually evolved from its simple original design throughout the first two years of this project. These changes stemmed mainly from the unforeseen problems that appeared once one part of the test rig was completed. This in fact caused the start of the experimental work to be delayed until the final year of the project. During this time work was undertaken on the literature review and also experimentation to familiarise the use of the FFT equipment.

Once the test rig was constructed to a standard suitable for experimental tests, all the tests were carried out. These included the calibration of the transducers, resonance tests (in the form of Hammer Impact tests) on the transducer positioners, spectral analysis using all transducers and frequency response tests which related all the transducers to the key phasor pulse at all speeds under investigation. All these required a reasonable degree of working knowledge of various signal processing equipment. These tests were generally successfully completed. Though two accelerometer sensitivities were found to be significantly different from the manufacturers values and because of time constraints, the results from the hammer impact tests could not be fully analysed and must be treated as a guideline only.

The working relationship between the two sets of vibration was based upon influence coefficients used for a static linear system. For the ideal case then the amplitude and phase values for the calculated influence coefficients should remain constant. Once the experimental values obtained from the frequency response tests were used in these equations it was found that the calculated values for the influence coefficients were far removed from the ideal values. This is due to the fact that the initial assumption was to determine if there was a relationship between the two sets of vibration. This would assume that the accelerometers on the camshaft bearings only measured vibration transmitted through them by the camshaft. The engine has many moving parts at many different speeds, thus producing varying amounts of vibration that is transmitted throughout the engine. It is these vibrations that were measured by the accelerometers, thus invalidating the initial assumption, that there was a simple relationship between both sets of vibration. The transmission of vibrations from throughout the engine could also call into doubt the validity of using the influence coefficient method for static loads in this particular case of dynamic motion in the valvetrain.

References

1. Wilcox, J.B.; 1967; Dynamic Balancing Of Rotating Machinery; Sir Isaac Pitman and Sons Inc.; 24 - 43

2. Esposito, A. and Thrower, J.R.; 1991; Machine Design Second Edition; Delmar Publishers Inc.; 109 - 134

3. Phelan, R.M.; 1967; Dynamics Of Machinery; McGraw-Hill Book Company; 43 - 44, 117 - 121

4. Prentis, J.M. ;1986; Dynamics Of Mechanical Systems Second Edition; John Wiley and Sons; 117 - 124, 388

5 Morrison, J.L.M. and Crossland, B. ; 1970; Mechanics Of Machines Second Edition; Longman Scientific And Technical; 343 - 348

6. Jehle, F. and Spiller, W.R.; 1929; Idiosyncrasies of valve mechanisms and their causes; SAE Journal; 24; pp 133 - 143

7. Donkin, W.T. and Clark, H.H.; 1929; Electric telemeter and valve-spring surge; SAE Journal; 24; pp 315 - 326

8. Dudley, W.M.; 1948; New methods in valve cam design ;SAE Quarterly Transactions; 2; pp 19 - 33

9. Thoren, T.R., Engemann, H.H. and Stoddart, D.A.; 1952; Cam design as related to valve train dynamics ;SAE Quarterly Transactions; 6; pp 1 - 14

10. Hrones, J.A.; 1948; An analysis of dynamic forces in a cam-driven system ; Transactions of ASME; 70; pp 473 - 482

11. Mitchell, D.B.; 1950; Tests on dynamic response of cam-follower systems; Mechanical Engineering; 72; pp 467 - 471

12. Neklutin, C.N.; 1954; Vibration analysis of cams ; Machine Design; 26; pp 190 - 198

13. Kwakernakk, H. and Smit, J.; 1968; Minimum vibration cam profiles; Journal of Mechanical Engineering Science; 10; pp 219 - 227

14. Chen, F.Y.; 1973; Analysis an design of cam driven mechanisms with nonlinearities; Journal of Engineering for Industry; August; pp 685 - 694

15. Akiba, K., Shimizu, A. and Sakai, H.; 1981; A comprehensive simulation of high speed driven valve trains ; SAE Technical Paper Number 810865

16. Chan, C. and Pisano, A.P.; 1987; Dynamic model of a fluctuating rocker-arm ratio cam system; Journal of Mechanisms Transmissions and Automation in Design; 109; pp 356 - 365

17. Phlips, P.J., Schamel, A.R. and Meyer, J.; 1989; An efficient model for valvetrain and spring dynamics; SAE Technical Paper Number 890619

Bibliography

For Chapter 2.2.2. : D.C. Motor.

1. Liwschitz-Garik, M. and Weil, R.T.; 1952; DC and AC Machines, Based on Fundamental Laws; D. Van Nostrand Company, INC.; 61 -91
2. Edwards, J.D.; 1991; Electrical Machines and Drives; Macmillan Education Ltd.; 67 - 70
3. Hughes, A.; 1990; Electric Motors and Drives: Fundamentals, Type and Applications; Heinemann Newnes; 95 - 105
4. Sen, P.C.; 1989; Principles of Electric Machines and Power Electronics; John Wiley and Sons, Inc.; 181 - 195
5. Orthwein, W.; 1990; Machine Component Design; West Publishing Company; 907 - 913

For Chapter 2.3.1. : Proximity Probes.

1. Jackson,C; 1979 ; The Practical Vibration Primer; Gulf Publishing Company Book Division.
2. Wowk,V; 1991; Machinery Vibration ; McGraw-Hill Inc.
3. Kaufman,AB ; 1976 ; Vibration - a warning signal that shouldn't be ignored ; Instruments and Control Systems ; 49(7) ; 23 - 25.
4. Hitchen,IR ; 1980 ; Vibration Monitoring for Rotating Machinery ; Measurement and Control ; 13(March) ; 97 - 102.
5. Bently,DE ; 1982 ; Shaft Vibration Measurement and Analysis Techniques ; 52nd Symposium on Shock and Vibration Part 1 ; Defence Nuclear Agency ; 81 - 93.
6. Scunthorpe,BR and Johnson,KM ; 1987 ; Vibration Monitoring Techniques on Reactor Coolant Pumps ; Sound and Vibration ; 21(9) ; 18 - 21.

7. Lifshits,A, Simmons,HR and Smalley,AJ ; 1986 ; More Comprehensive Vibration Limits for Rotating Machinery ; 31st International Gas Turbine Conference ; ASME ; Dusseldorf ; 1 - 8.

8. Seippel,RG ; 1983 ; Transducers, Sensors and Detectors ; Reston Publishing Company.

For Chapter 2.3.2. : Acceloerometers.

1. Parr,E.A.; 1987; Industrial Control Handbook Volume 2 : Technique; B.S.P. Professional Books

2. Sinclair,I.R.; 1988; Sensors and Transducers, A Guide for Technicians; B.S.P. Professional Books.

3. Seippel,R.G.; 1983; Transducers, Sensors and Detectors: Reston Publishing Company

4. Jackson,C.; 1979; The Practical Vibration Primer; Gulf Publishing Company Book Division.

5 Serridge,M. And Torben,R.L.; 1987; Piezoelectric Accelerometer and Vibration Preamplifier Handbook; Bruel and Kjaer.

6 Bently,D.E.; 1982; Shaft Vibration Measurement and Analysis Techniques; 52nd Symposium on Shock and Vibration (Part 1); Defence Nuclear Agency; 81 - 95.

7 Hitchen,I.R.; 1980; Vibration Monitoring for Rotating Machinery; Measurement and Control; 13 (March); 91-102.

For Chapter 2.3.3. : FFT Analyser.

1. Brook, D. and Wynne, R.J.; 1988; Signal Processing: Principles and Applications: Edward Arnold; 79, 90 - 92, 134 - 139, 263

For Chapter 2.4.2. : Valvetrain Components

1. Stone, R.; 1992; Introduction to Internal Combustion Engines: 2nd Edition; The Macmillan Press Ltd; 231 - 257
2. Lichty, L.C.; 1967; Combustion Engine Processes; McGraw-Hill Book Company;; 371 - 403.
3. McKellar, M.R.; 1966; Overhead Camshaft Stirs New Tempest; Society of Automotive Engineers Journal; 77 (11); 69 - 73
4. Bakonyi, S.M.; 1968; The Advantages of Overhead Camshafts - What Are They?; Society of Automotive Engineers Technical Paper Number 680028
5. Bevan, T.; 1960; The Theory of Machines: 3rd Edition; Longmans, Green and Co. Ltd; 282 - 300
6. Lent, D.; 1970; Analysis and Design of Mechanisms: 2nd Edition; Prentice-Hall, Inc.; 351 - 368
7. Cowie, A.; 1961; Kinematics and Design of Mecanisms; International Textbook Company.
8. Norton, R.L.; 1992; Design of Machinery; Mcgraw-Hill International Editions Inc
9. Phlips, P and Schamel, A.; 1991; The Dynamics of Valvetrains with Hydraulic Lash Adjusters and the Interaction With The Gas Exchange Process; Society of Automotive Engineers Technical Paper Number 910071
10. Cowie, A.; 1961; Kinematics and Design of Mechanisms; International textbook Company; pp 330 - 335, 353 - 358, 361 - 365
11. Rothbart, H.A.; 1956; Cams; John Wiley and Sons, Inc.
12. Norton, R.L.; 1992; Design of Machinery; McGraw-Hill International Editions, Inc.; pp 295 - 339

For Chapter 3.2. : Calibration Of The Proximity Transducer Systems.

1. Stroud, K.A.; 1987; Engineering Mathematics: Third Edition; Macmillan Education Ltd; 378 - 387

For Chapter 3.3. : Calibration Of The Accelerometers.

1. Stroud K.A.; 1987; Engineering Mathematics, 3rd Edition; Macmillan Education Ltd.

2. Brook, D. and Wynne, R.J.; 1988; Signal Processing: Principles and Applications; Edward Arnold.

3. Gere, J.M. and Timoshenko, S.P.; 1987; Mechanics of Materials, Second SI Edition; Van Nostrand Reinhold (UK) Co. Ltd

For Chapter 3.4. : Hammer Impact Tests

1. ISO / DIS 7626-5; 1991; Vibration and Shock - Experimental determination of mechanical mobility - Part 5: Measurements using impact excitation with an exciter which is not attached to the structure.

2. BS 6897: Part 2: 1990; Methods for the experimental Determination of mechanical Mobility - Part 2: Measurements Using Single-Point translation Excitation with an Attached Vibration Exciter.

3. Peterson, E.L. and Klosterman, A.L. ; 1978; Obtaining Good Results from an Experimental Modal Survey; Journal of the Society of Environmental Engineers; 17 (1) ; 3 - 10.

4. Brown, D, Carbon, G and Ramsey, K. ; 1977; Survey of Excitation Techniques Applicable t to the Testing of Automotive Structures; Society of Automotive Engineers Technical Paper Number 770029.

5. Halvosen, W.G. and Brown, D.L.; 1977; Impulse Technique for Structural Frequency Response Testing; Sound and Vibration; November 1977; 8 - 21.

6. Ewins, D.J.; 1984; Modal Testing: Theory and Practice; Research Studies Press Limited.

7. Brook, D. and Wynne, R.J.; 1988; Signal Processing: Principles and Applications: Edward Arnold.

For Chapter 3.5. : Spectral Analysis.

1. Turner, J.D.; 1988; Instrumentation For Engineers; Macmillan Education Ltd.; 167 - 168
2. Ewins, D.J.; 1984; Modal Testing: Theory and Practice; Research Studies Press; 89, 112 - 115, 261 - 264
3. Brook, D and Wynne, R.J.; 1988; Signal Processing: Principles and Applications; Edward Arnold; 79, 177 - 181
4. Lynn, P.A.; 1989; An Introduction to the Analysis and Processing of Signals; Macmillan Education Ltd.; 10, 51, 62, 185
5. Smith, J.D. ; 1989; Vibration Measurement and Analysis; Butterworth and Co. (Publishers) Ltd.; 75 - 77

For Chapter 4.2.: Theory.

1. Tse, F.S., Morse,I.E. and Hinkle, R.T. ; 1963; Mechanical Vibrations; Prentice-Hall International; 131 - 138.
2. MacDuff, J.N. and Curreri, J.R.; 1958; Vibration Control; McGraw-Hill Book Company, Inc. ; 250 - 253
3. Meirovitch, L.; 1975; Elements of Vibration Analysis; International Students Edition; 150 - 155

For Chapter 5.2: The Proximity Probes

1. Smith, J.D.; 1989; Vibration Measurement and Analysis; Butterworth and Co (Publishers) Ltd; 22 - 23

For Chapter 5.4: The Accelerometers

1. Turner, J.D.; 1988; Instrumentation For Engineers; Macmillan Education Ltd.; 190 - 199

2. Ewins, D.J.; 1984; Modal Testing: Theory and Practice; Research Studies Press; 120 - 122

3. Brook, D and Wynne, R.J.; 1988; Signal Processing: Principles and Applications; Edward Arnold; 170 - 178

4. Serridge, M and Licht, T.R.; 1987; Piezoelectric Accelerometer and Vibration Preamplifier Handbook; Brüel and Kjær ; 88 - 102

5. Haddard, R.A. and Parsons, T.W.; 1991; Digital Signal Processing: Theory, Applications and Hardware; Computer Science Press; 566 - 580

Appendix 1

Engineering Drawings

1. Plinth.
2. Motor Base Plate.
3. Engine Bracket ; Right Side
4. Engine Bracket ; Left Side Front
5. Engine Bracket ; Left Side Back.
6. Crankshaft Attachment.
7. Belt Tensioner Plate.
8. Proximity Probe Positioner.
9. Pulse Proximity Probe Positioner.
10. Accelerometer Platform.

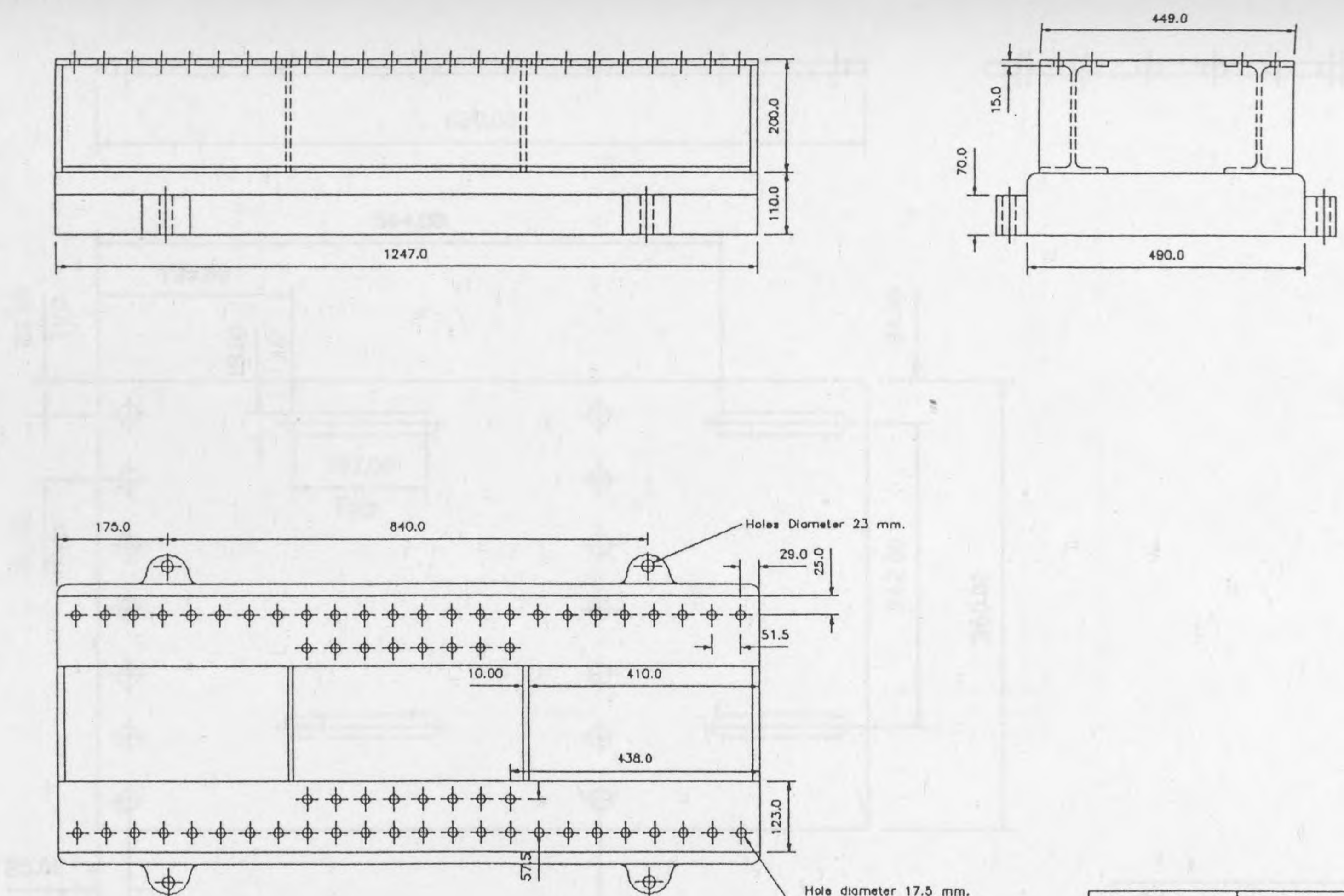

Tolerance + 0.5 − 0.5 Unless Otherwise Stated	*All Dimensions in mm.*	
	Title: Base Plinth	
	Projection	*Quantity:* 1
Material Mild Steel		*Drawn by:* S. Anderson
		Date: 25.07.93
Drawing No. 001	*Original Scale* 1.1	The ROBERT GORDON UNIVERSITY School of Mech.& Offshore Eng.

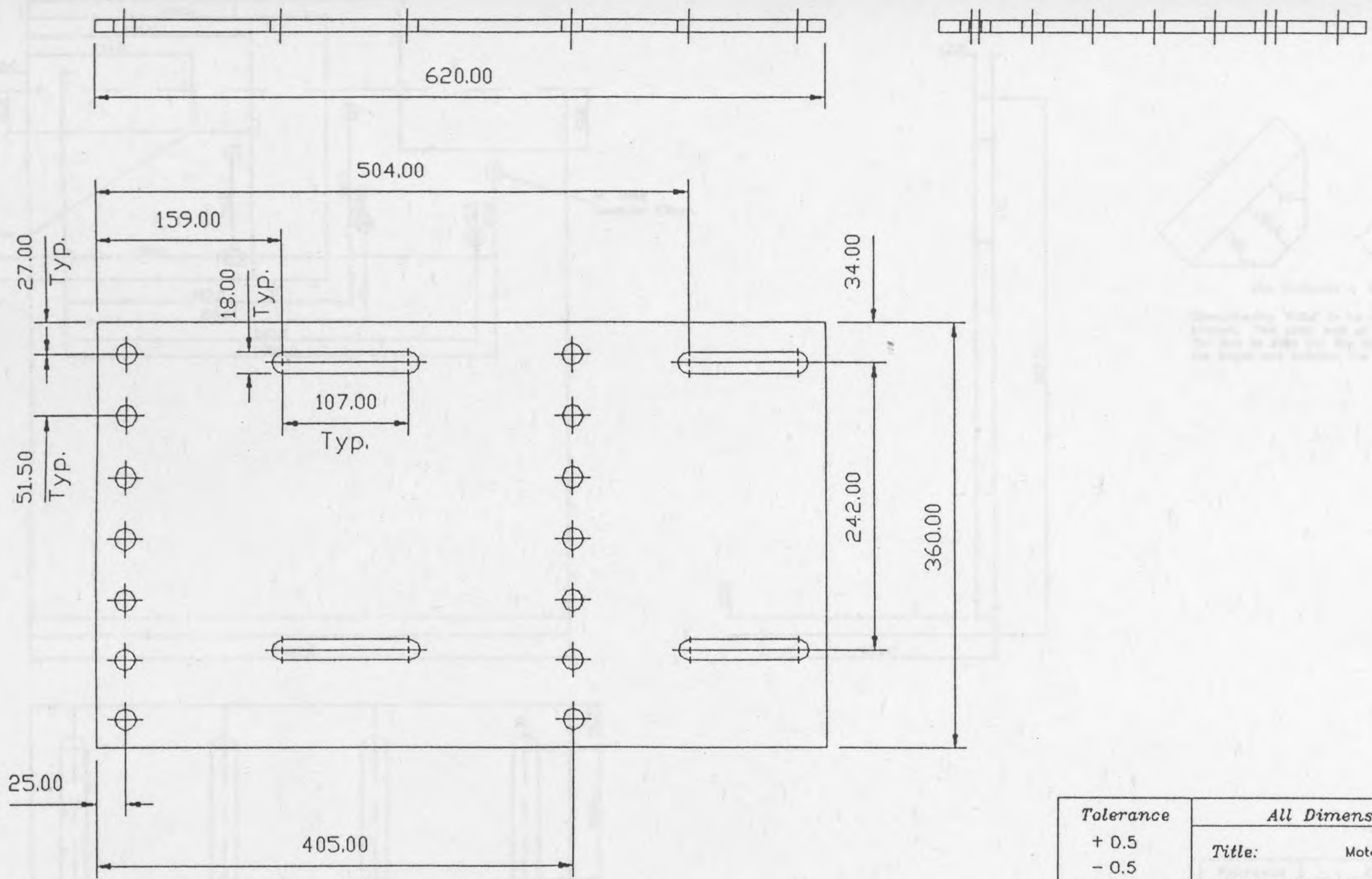

Tolerance + 0.5 − 0.5 Unless Otherwise Stated	*All Dimensions in mm.*		
	Title: Motor Base Plate		
Material Mild Steel	*Projection*	*Quantity:* 1	
		Drawn by: S. Anderson	
		Date: 03.08.93	
Drawing No. 002	*Original Scale* 1:1	The ROBERT GORDON UNIVERSITY School of Mech.& Offshore Eng.	

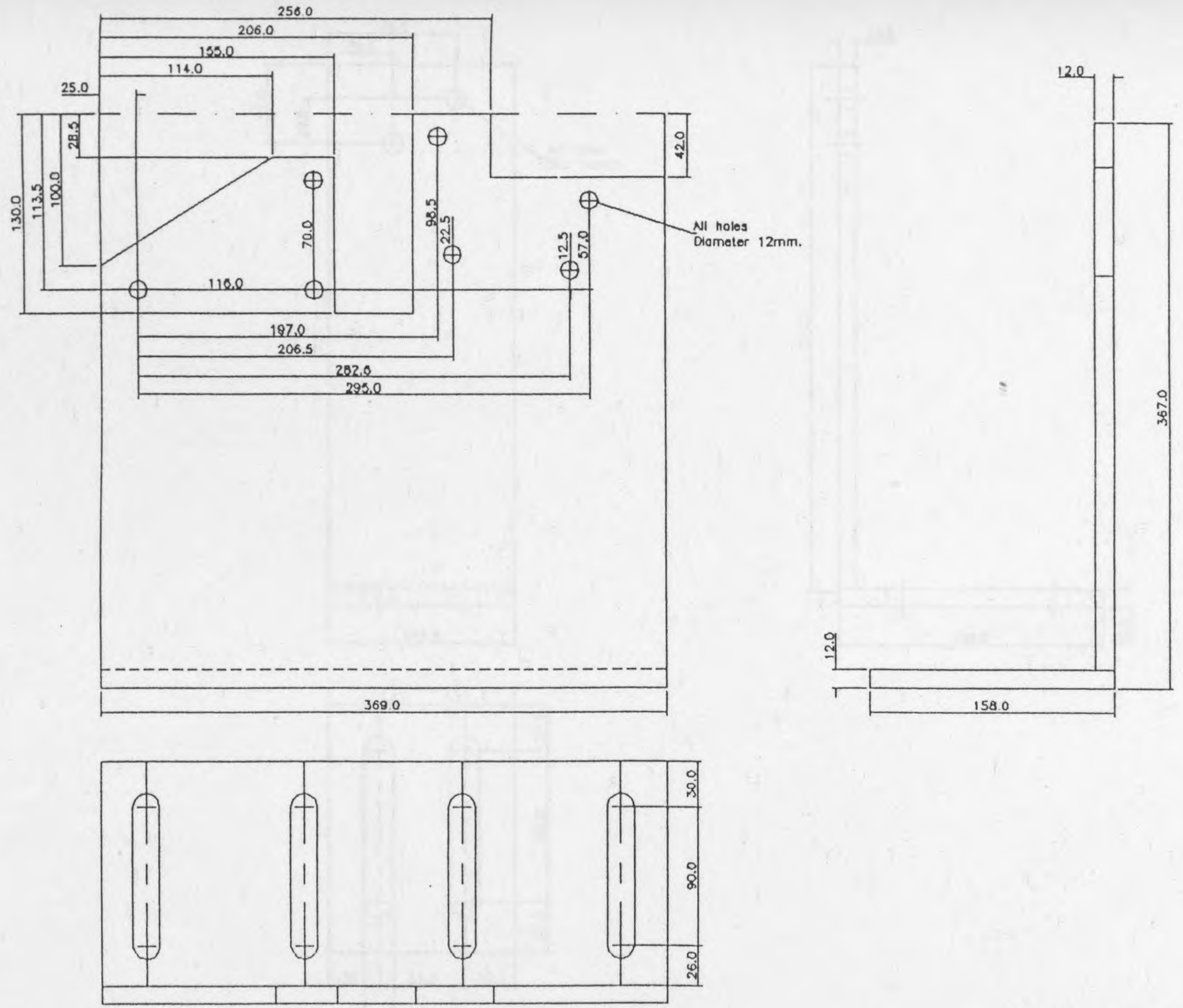

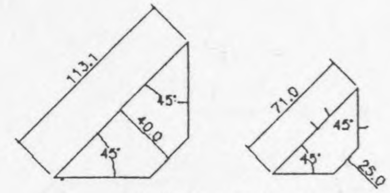

Web Thickness = 12 mm

Strengthening 'Webs' to be welded onto the bracket. The small web at midpoint between the first to slots (on the left hand side) and the larger web between the last two slots.

Additional Tolerance Specification:
Hole Positions: $\pm$ 0.25

All hidden detail has been ommitted.

Tolerance +0.5 −0.5 Unless Otherwise Stated	All Dimensions in mm.	
	Title: Engine Bracket (Right Side)	
	Projection	Quantity: 1
Material Mild Steel		Drawn by: S. Anderson
		Date: 27.08.93
Drawing No. 003	Original Scale 1:1	The ROBERT GORDON UNIVERSITY School of Mech.& Offshore Eng.

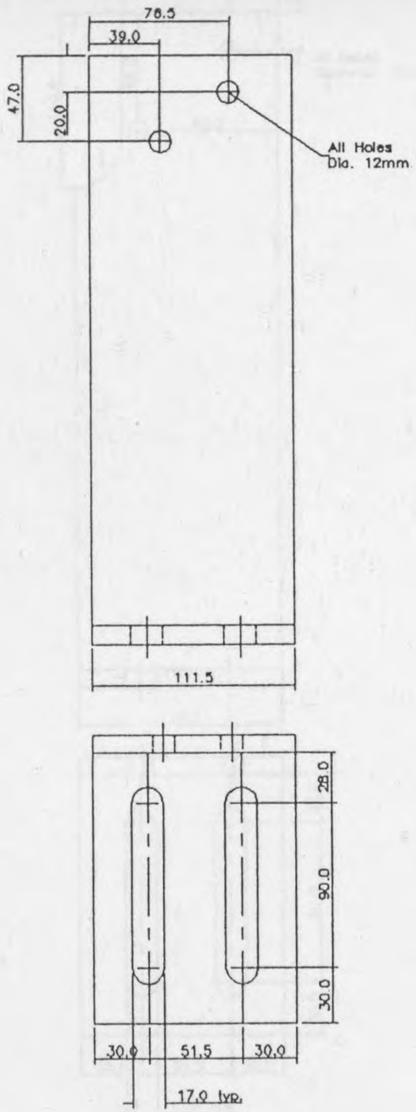

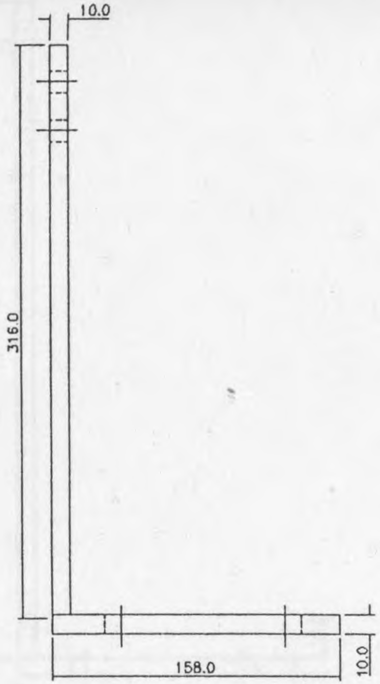

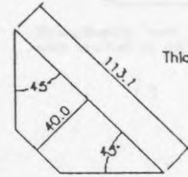

Thickness = 12 mm.

Strengthening 'web' to be welded onto bracket midway between slots.

Additional Tolerance Specification:

Hole Positions: $^{+\,0.25}_{-\,0.25}$

Tolerance + 0.5 − 0.5 Unless Otherwise Stated	*All Dimensions in mm.*	
	Title: Engine Bracket (Left Side Front)	
Material Mild Steel	*Projection*	*Quantity:* 1
		Drawn by: S. Anderson
		Date: 27.08.93
Drawing No. 004	*Original Scale* 1:1	The ROBERT GORDON UNIVERSITY School of Mech.& Offshore Eng.

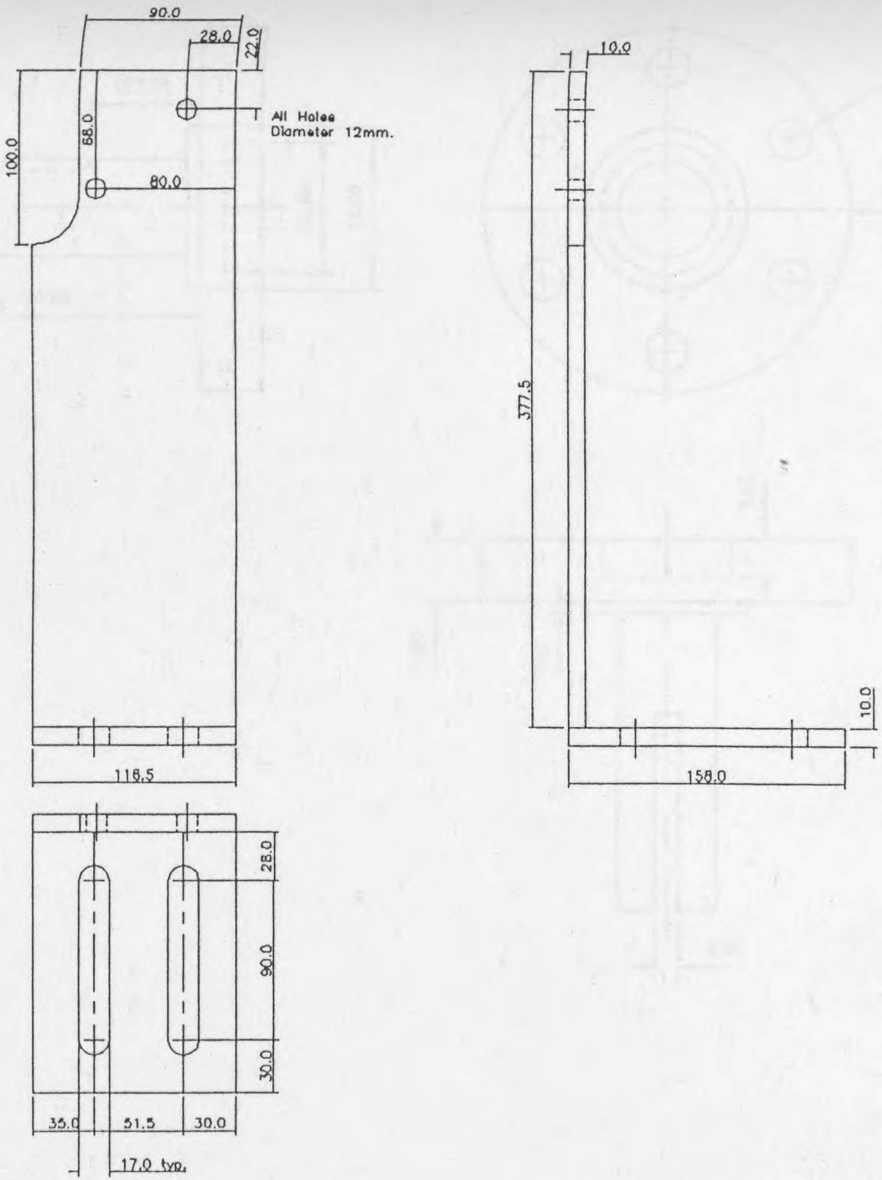

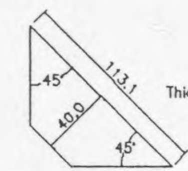

Thickness = 12 mm.

Strengthening 'web' to be welded onto bracket at midpoint between slots.

Additional Tolerance Specification:
Hole Positions: $\pm$ 0.25

Tolerance	All Dimensions in mm.	
+ 0.5 − 0.5 Unless Otherwise Stated	Title: Engine Bracket (Left Side Back)	
Material Mild Steel	Projection	Quantity: 1 Drawn by: S. Anderson Date: 27.08.93
Drawing No. D05	Original Scale 1:1	The ROBERT GORDON UNIVERSITY School of Mech & Offshore Eng.

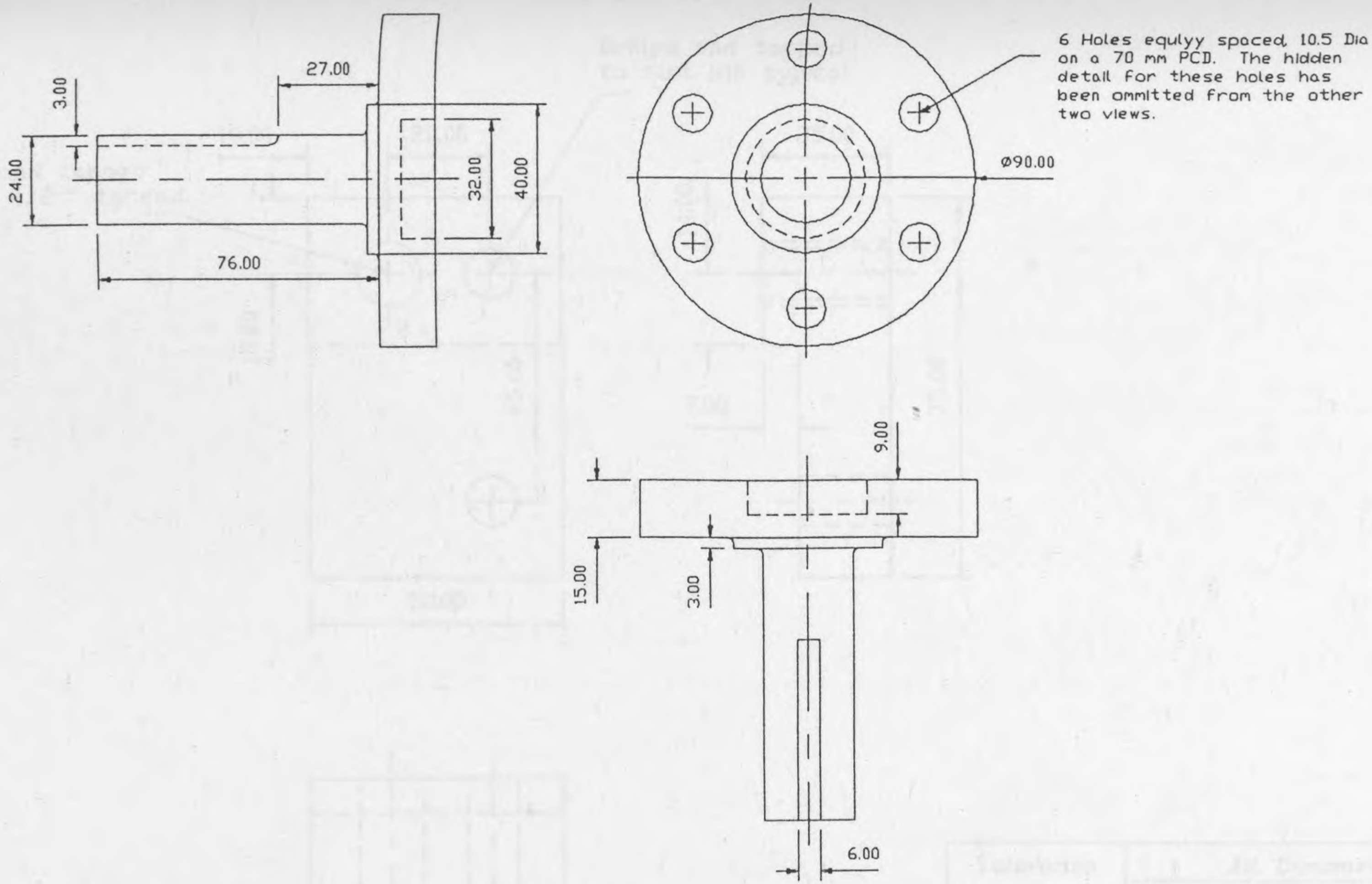

Tolerance	All Dimensions in mm.	
+ 0.5 − 0.5 Unless Otherwise Stated	Title:	Crankshaft Attachment
Material Mild Steel	Projection	Quantity: 1 Drawn by: S. Anderson Date: 31.01.94
Drawing No. 006	Original Scale 1:1	The ROBERT GORDON UNIVERSITY School of Mech.& Offshore Eng.

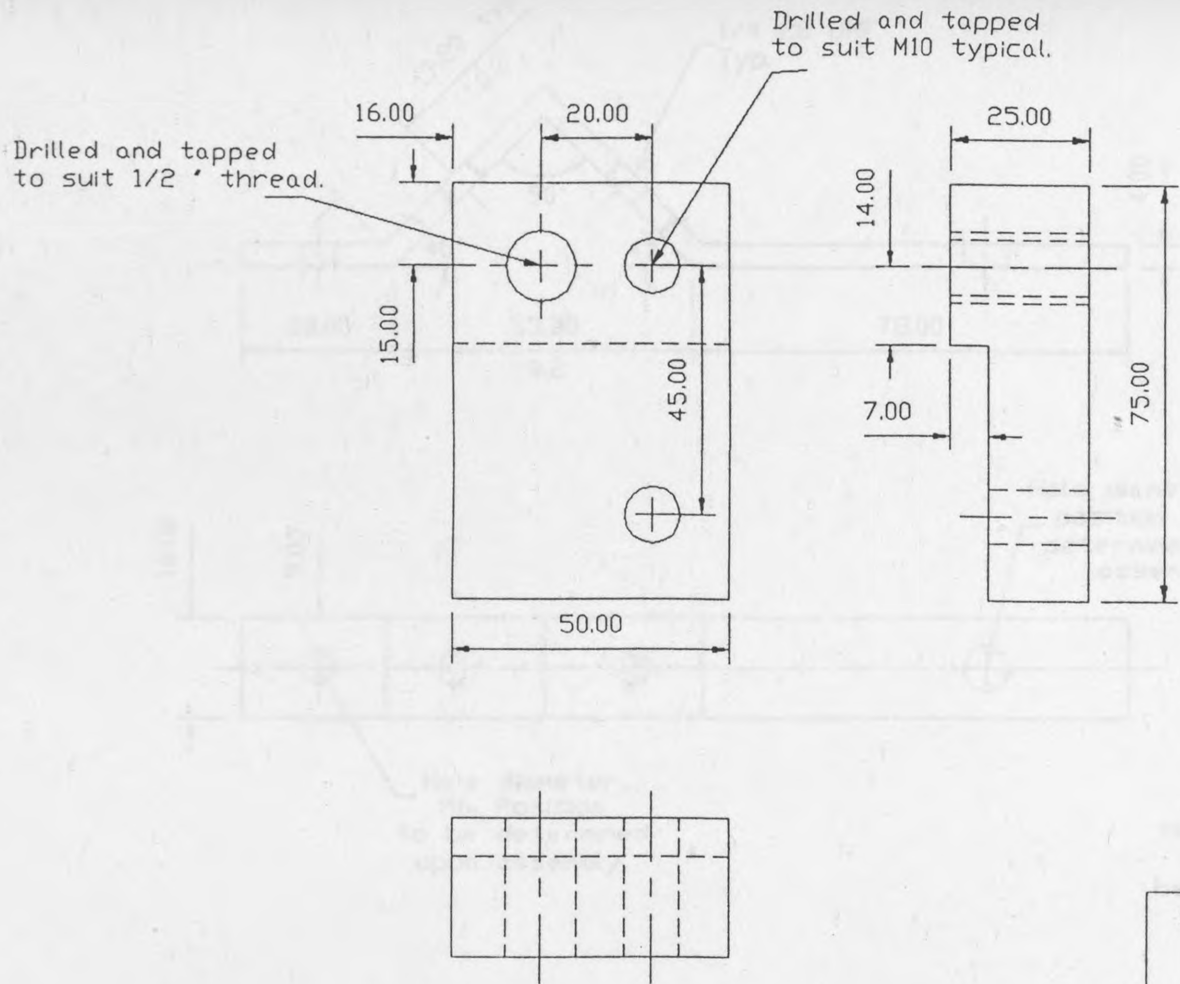

Tolerance + 0.5 − 0.5 Unless Otherwise Stated	*All Dimensions in mm.*	
	Title:	Belt Tensioner Plate
Material Mild Steel	*Projection*	*Quantity:* 1
		Drawn by: S. Anderson
		Date: 05.01.95
Drawing No. 013	*Original Scale* 1:1	The ROBERT GORDON UNIVERSITY School of Mech.& Offshore Eng.

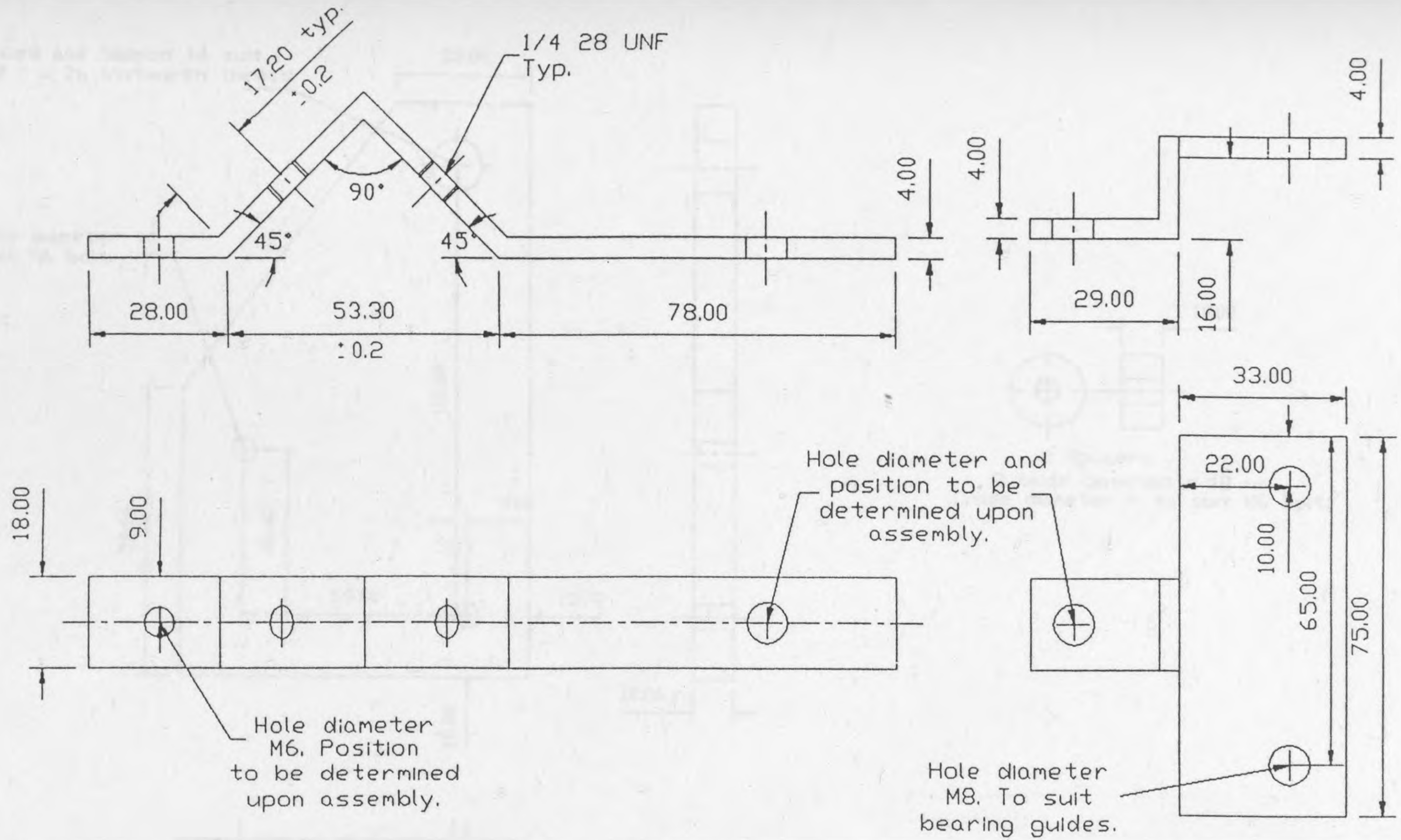

Angle Tolerances
±0.5°

All hidden detail in plan
has been ommitted.

Tolerance +0.5 −0.5 Unless Otherwise Stated	*All Dimensions in mm.*	
	Title: Proximity Probe Positioner	
Material As appropriate	*Projection*	*Quantity:* 1
		Drawn by: S. Anderson
		Date. 16.06.94
Drawing No. 012	*Original Scale* 1:1	The ROBERT GORDON UNIVERSITY School of Mech & Offshore Eng.

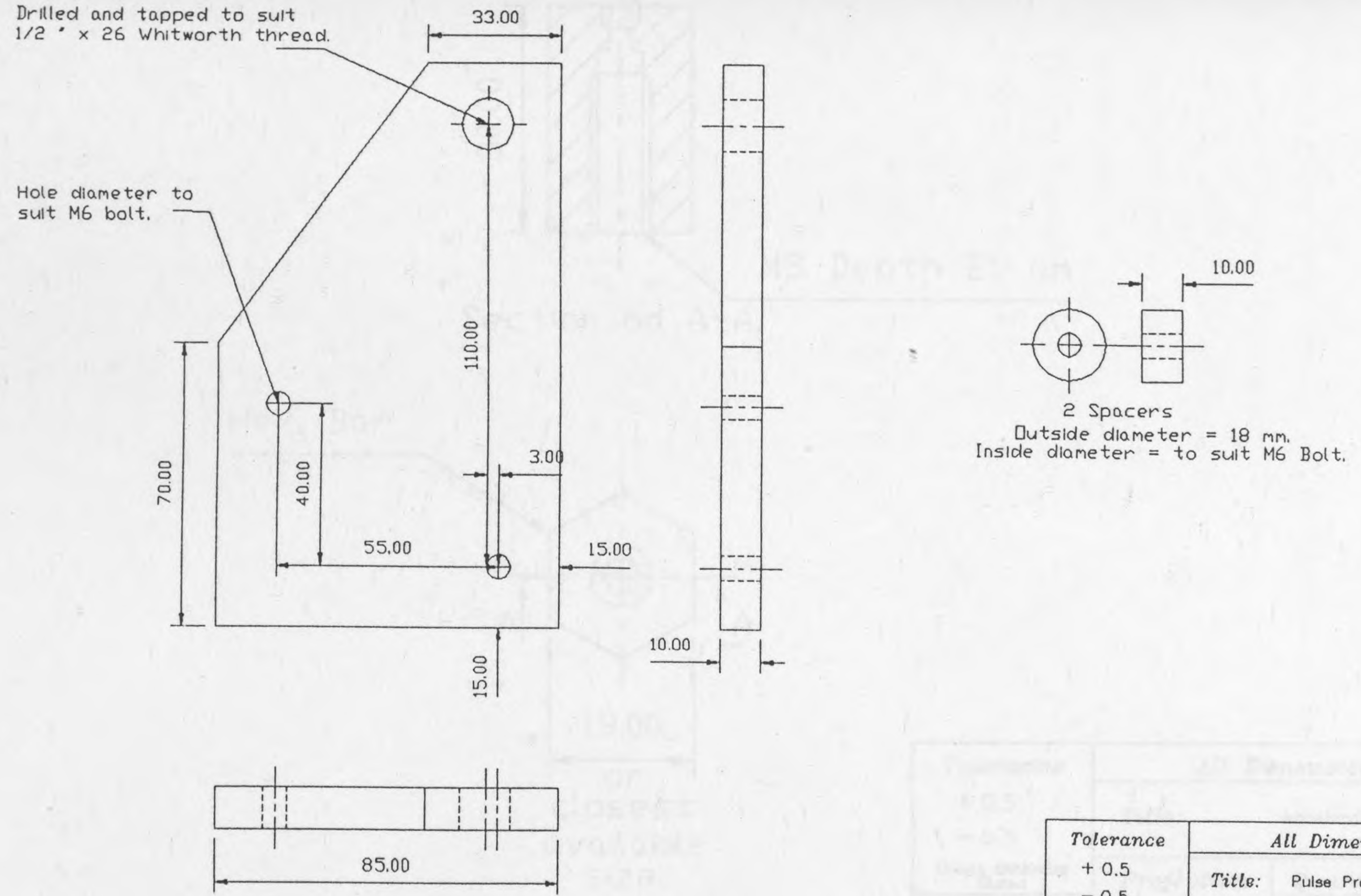

Tolerance + 0.5 − 0.5 Unless Otherwise Stated	*All Dimensions in mm.*	
	Title: Pulse Proximily Probe Positioner	
Material Mild Steel	*Projection*	*Quantity:* 1
		Drawn by: S. Anderson
		Date: 11.01.95
Drawing No. 012	*Original Scale* 1:1	The ROBERT GORDON UNIVERSITY School of Mech.& Offshore Eng.

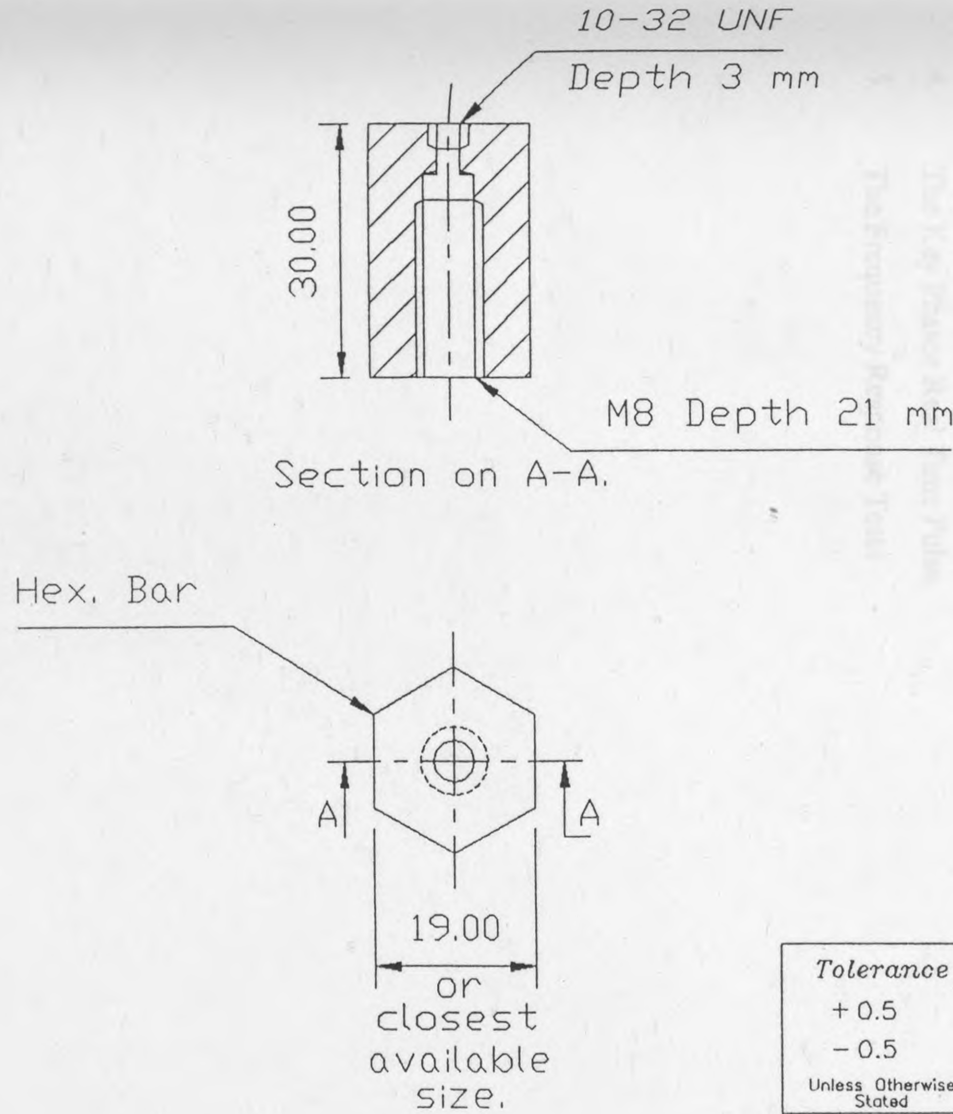

Tolerance +0.5 −0.5 Unless Otherwise Stated	*All Dimensions in mm.*	
	Title: Accelerator Platforms	
	Projection	*Quantity:* 4
Material Mild Steel		*Drawn by:* S. Anderson
		Date: 11.05.94
Drawing No. 011	*Original Scale* 1:1	The ROBERT GORDON UNIVERSITY School of Mech.& Offshore Eng.

Appendix 2

FFT Analyser Settings

The following settings were the actual FFT analyser settings used in the experimental work that required the use of the analyser. They were;

1. The Calibration Of The Accelerometers
2. The Hammer Impact Tests.
3 Spectral Analysis.
4. The Key Phasor Real Time Pulse.
5. The Frequency Response Tests

A.2.1. FFT Analyser Settings Used For Calibration Of The Accelerometers.

The FFT analyser menus, on each screen, had specific settings to ensure that the calibration tests were undertaken correctly. Any menu missed out in the following list was not in use during the tests.

<u>INPUT SCREEN:</u>

INPUT 1:		FSR
COUP 1:		ACCEL
INTEGR 1:		OFF

<u>TRIGGER SCREEN:</u>

MODE:		1 SHOT
LEVEL:	LEVEL:	10
	SLOPE:	+ SLOPE
SOURCE:	CH1:	CH 1
DELAY:	CH1:	0
	CH2:	0

<u>FREQUENCY SCREEN:</u>

BANDWIDTH:		200 kHz
SAMP / LINE:		1024 / 400
ZOOM:		OFF
X-AXIS:		LINEAR
CLOCK:		INTERNAL
A/ALIAS:		OFF
FILTER:		OFF
ACQ TIME:		2.000 SECS

<u>PROCESS SCREEN:</u>

DATA A:		SPEC CH1
Y-AXIS:		LINMAG
WINDOW:		FLATTOP
AVERAGE:	TIME AV:	1
	PROC AV:	5
	AV TYPE:	RMS
PROC OPTS:	TURBO:	OFF
	FAST AVG:	ON

	PREVIEW:	OFF	

MEMORY SCREEN.

DIRECTORY:		SAPPNSE	
FILENAME:		C5172	(For accelerometer s/n 5172)
		C22223	(For accelerometer s/n 22223)
		C22222	(For accelerometer s/n 22222)
		C22225	(For accelerometer s/n 22225)
		C22224	(For accelerometer s/n 22224)

DISPLAY SCREEN.

FORMAT:		A ONLY	
SCALE CH1:	AUTO:	53	(For accelerometer s/n 5172)
		9.3	(For accelerometer s/n 22223)
		9.7	(For accelerometer s/n 22222)
		9.2	(For accelerometer s/n 22225)
		9.9	(For accelerometer s/n 22224)
TYPE:	CH1:	ACCEL	
DETECT:	CH1:	RMS	
FSR:	CH1:	2 G	

Notes on FFT Analyser Settings.

Input Screen: There is only one input setting necessary as the accelerometer does not require a triggering pulse. F.S.R. means Full Scale Range. this function is used in conjunction with the AUTOEU setting on the display screen. It allows a method of defining the range to be displayed that will be maintained if sensitivity and scaling factors have been changed. This function is especially good for comparing sets of data.

Frequency Screen: The bandwidth was set at 200 Hz because the exciter provides an excitation frequency of 159.2 Hz.

Process Screen: A flat top window was used to give best amplitude accuracy, with tolerable leakage over the frequency range inspected of 150.5 - 168.0 Hz.

Display Screen: The AUTOEU function was set for the sensitivity of each accelerometer tested. FSR; Ch1 was set at 2 G because the theoretical level was calculated to be 1.019 G, so a display range of 2 G would provide a clear indication of the peak.

There is a method for determining the power under the peak. this is in the form of the PWR key. This is a soft key option, (i.e. not on a menu), and it allows the power to be measured between two definable limits. This is used in conjunction with the DETECT; CH1: RMS option on the display screen and gives the value in RMS. The limits set in this case being 159.2 ± 8.8 Hz.

A.2.2. FFT Analyser Settings For All The Transducers For The Hammer Impact Tests.

The following settings were the ones used for the hammer impact tests as described in Chapter 3.4. Any menu not listed was not used during the tests.

INPUT SCREEN:

INPUT 1:		10mV
COUP 1:		AC
INTEGR 1:		OFF
INPUT 2:		10mV
COUP 2:		AC
INTEGR 2:		OFF
A-WEIGHT:		OFF

TRIGGER SCREEN:

MODE:		1 SHOT
LEVEL:	LEVEL:	4
	SLOPE:	+ SLOPE
SOURCE:		CH1
DELAY:	CH1:	0
	CH2:	0

FREQUENCY SCREEN:

BANDWIDTH:	25 Hz
SAMP / LINE:	256/100
ZOOM:	OFF

X-AXIS:		LINEAR	
CLOCK:		INTERNAL	
A/ALIAS:		OFF	
FILTER:		OFF	
ACQ TIME:		4.000 SECS	

<u>PROCESS SCREEN:</u>

DATA A:		FREQ RESP	
Y-AXIS A:		LINMAG	
DATA B:		FREQ RESP	
Y-AXIS B:		PHASE	
WINDOW:		FORCE/EXP	
FORCE/EXP	FORCE%L:	10	
	EXP TC:	4	
AVERAGE:	TIME AV:	1	
	PROC AV:	10	
	AV TYPE:	RMS	
PROC OPTS:	TURBO:	OFF	
	FAST AVG:	OFF	
	PREVIEW:	ON	

<u>MEMORY SCREEN.</u>

DIRECTORY:		STEFAN	
FILENAME:		ACC1	(for accelerometer platform at position 1)
		ACC2	(for accelerometer platform at position 2)
		PROX1	(for prox probe positioner at position 1)
		PROX2	(for prox probe positioner at position 2)
		PROX3	(for prox probe positioner at position 3)
ACTIVE MEM:		INTERNAL	

<u>DISPLAY SCREEN.</u>

FORMAT:		A ABOVE B	
SCALE CH1:		VOLTS	
SCALE CH2:		VOLTS	

A.2.3. FFT Analyser Settings For All The Transducers For The Spectral Analysis Tests.

The following settings were the ones used for the spectrum tests as described in Chapter 3.5. The tests were conducted on 7th June 1995. Any menu not listed was not used during the tests.

A.2.3.1. FFT Analyser Settings for Proximity Probes 1 and 2.

Where input 1 signifies proximity probe 1 and input 2 signifies proximity probe 2.

INPUT SCREEN:

INPUT 1:		FSR
COUP 1:		AC
INTEGR 1:		OFF
INPUT 2:		FSR
COUP 2:		AC
INTEGR 2:		OFF
A-WEIGHT:		OFF

TRIGGER SCREEN:

MODE:		1 SHOT
LEVEL:	LEVEL:	10
	SLOPE:	+ SLOPE
SOURCE:		FREERUN
DELAY:	CH1:	0
	CH2:	0

FREQUENCY SCREEN:

BANDWIDTH:		25 Hz
SAMP / LINE:		1024/400
ZOOM:		OFF
X-AXIS:		LINEAR
CLOCK:		INTERNAL
A/ALIAS:		OFF
FILTER:		OFF
ACQ TIME:		16.000 SECS

PROCESS SCREEN:

DATA A:		SPEC CH1
Y-AXIS A:		LINMAG
DATA B:		SPEC CH2
Y-AXIS B:		LINMAG
WINDOW:		FORCE/EXP
FORCE/EXP	FORCE%L:	10
	EXP TC:	4
AVERAGE:	TIME AV:	3
	PROC AV:	3
	AV TYPE:	RMS
PROC OPTS:	TURBO:	OFF
	FAST AVG:	ON
	PREVIEW:	OFF

MEMORY SCREEN.

DIRECTORY:	100SPEC	(for tests at 100 rpm)
	150SPEC	(for tests at 150 rpm)
	200SPEC	(for tests at 200 rpm)
	250SPEC	(for tests at 250 rpm)
	300SPEC	(for tests at 300 rpm)
	350SPEC	(for tests at 350 rpm)
FILENAME:	100P1P2	(for tests at 100 rpm)
	150P1P2	(for tests at 150 rpm)
	200P1P2	(for tests at 200 rpm)
	250P1P2	(for tests at 250 rpm)
	300P1P2	(for tests at 300 rpm)
	350P1P2	(for tests at 350 rpm)
ACTIVE MEM:	INTERNAL	

DISPLAY SCREEN.

FORMAT:		A ABOVE B
SCALE CH1:	AUTO EU:	8.067
TYPE:	CH1:	DISP
DETECT:	CH1:	RMS
FSR:	CH1:	5μm
SCALE CH2:	AUTO EU:	7.043
TYPE:	CH2:	DISP
DETECT:	CH2:	RMS
FSR:	CH2:	5μm

A.2.3.2. FFT Analyser Settings for Accelerometers 22223 and 22222.

Where input 1 is accelerometer 22223, on bearing 2L and input 2 is for accelerometer 22222, on bearing 3L. The FFT analyser settings are the same as that for the Proximity Probes, unless otherwise stated.

INPUT SCREEN:

COUP 1:		ACCEL
COUP 2:		ACCEL

MEMORY SCREEN.

FILENAME:	1002L3L	(for tests at 100 rpm)
	1502L3L	(for tests at 150 rpm)
	2002L3L	(for tests at 200 rpm)
	2502L3L	(for tests at 250 rpm)
	3002L3L	(for tests at 300 rpm)
	3502L3L	(for tests at 350 rpm)

DISPLAY SCREEN.

SCALE CH1:	AUTO EU:	9.3
TYPE:	CH1:	ACCEL
FSR:	CH1:	1 G
SCALE CH2:	AUTO EU:	12.2
TYPE:	CH2:	ACCEL
FSR:	CH2:	1 G

A.2.3.3. FFT Analyser Settings for Accelerometers 22225 and 22224.

Where input 1 is accelerometer 22225, on bearing 4L and input 2 is for accelerometer 22224, on bearing 5L. The FFT analyser settings are the same as that for the Proximity Probes, unless otherwise stated.

INPUT SCREEN:

COUP 1:		ACCEL
COUP 2:		ACCEL

MEMORY SCREEN.

FILENAME:	1004L5L	(for tests at 100 rpm)
	1504L5L	(for tests at 150 rpm)
	2004L5L	(for tests at 200 rpm)
	2504L5L	(for tests at 250 rpm)
	3004L5L	(for tests at 300 rpm)
	3504L5L	(for tests at 350 rpm)

DISPLAY SCREEN.

SCALE CH1:	AUTO EU:	9.2
TYPE:	CH1:	ACCEL
FSR:	CH1:	1 G
SCALE CH2:	AUTO EU:	8.4
TYPE:	CH2:	ACCEL
FSR:	CH2:	1 G

A.2.4. FFT Analyser Settings For All The Key Phasor Pulse.

The following settings were the ones used to capture the key phasor pulse as described in Chapter 4.3.3. Any menu not listed was not used during the tests.

INPUT SCREEN:

INPUT 1:		100mV
COUP 1:		ACCEL
INTEGR 1:		OFF
A-WEIGHT:		OFF

TRIGGER SCREEN:

MODE:		1 SHOT
LEVEL:	LEVEL:	0
	SLOPE:	+ SLOPE
SOURCE:		FREERUN
DELAY:	CH1:	0
	CH2:	0

FREQUENCY SCREEN:

BANDWIDTH:		200 Hz
SAMP / LINE:		512/200
ZOOM:		OFF
X-AXIS:		LINEAR
CLOCK:		INTERNAL
A/ALIAS:		OFF
FILTER:		OFF
ACQ TIME:		1 SEC

PROCESS SCREEN:

DATA A:		TIME CH1
Y-AXIS A:		REAL
WINDOW:		HANN
AVERAGE:	TIME AV:	1
	PROC AV:	3
	AV TYPE:	RMS
PROC OPTS:	TURBO:	OFF
	FAST AVG:	OFF
	PREVIEW:	ON

MEMORY SCREEN.

DIRECTORY:	SAPPNSE	
FILENAME:	PUL100	(for pulse at 100 rpm)
	PUL200	(for pulse at 150 rpm)
ACTIVE MEM:	INTERNAL	

DISPLAY SCREEN.

FORMAT:	A ONLY
SCALE CH1:	VOLTS

A.2.5. FFT Analyser Settings For Frequency Response Tests.

The following settings for the FFT analyser were for the frequency response tests undertaken on the 5th June 1995. These were between the appropriate transducer and the key phasor. The results of which can be seen in Chapter 4.3. Any menu not mentioned in the following lists was not used during the individual tests.

A.2.5.1. FFT analyser settings for proximity probe 1 at speeds 100 - 200 r.p.m.

INPUT SCREEN:

INPUT 1:		100mV
COUP 1:		ACCEL
INTEGR 1:		OFF
INPUT 2:		1V
COUP 2:		AC
INTEGR 2:		OFF
A-WEIGHT:		OFF

TRIGGER SCREEN:

MODE:		1 SHOT
LEVEL:	LEVEL:	10
	SLOPE:	+ SLOPE
SOURCE:		CH 1
DELAY:	CH1:	0
	CH2:	0

FREQUENCY SCREEN:

BANDWIDTH:		25 Hz
SAMP / LINE:		1024/400
ZOOM:		OFF
X-AXIS:		LINEAR
CLOCK:		INTERNAL
A/ALIAS:		OFF
FILTER:		OFF
ACQ TIME:		16.000 SECS

PROCESS SCREEN:

DATA A:		FREQ RESP
Y-AXIS A:		LINMAG
DATA B:		FREQ RESP
Y-AXIS B:		PHASE
WINDOW:		FORCE/EXP
FORCE/EXP:	FORCE%L:	10

	EXP TC:	4	
AVERAGE:	TIME AV:	3	
	PROC AV:	3	
	AV TYPE:	RMS	
PROC OPTS:	TURBO:	ON	
	FAST AVG:	ON	
	PREVIEW:	OFF	

MEMORY SCREEN.

DIRECTORY:	SA100C	(for camshaft speed 100 r.p.m.)
	SA150C	(for camshaft speed 150 r.p.m.)
	SA200C	(for camshaft speed 200 r.p.m.)
FILENAME:	100P1	(for camshaft speed 100 r.p.m.)
	150P1	(for camshaft speed 150 r.p.m.)
	200P1	(for camshaft speed 200 r.p.m.)
ACTIVE MEM:	INTERNAL	

DISPLAY SCREEN.

FORMAT:		A ABOVE B
SCALE CH1:		VOLTS
SCALE CH2:	AUTO EU:	8.067
TYPE:	CH2:	DISP
DETECT:	CH2:	RMS
FSR:	CH2:	OFF

A.2.5.2. FFT analyser settings for proximity probe 1 at speeds 250 - 350 r.p.m.

The FFT Analyser settings are the same as before except for:

INPUT SCREEN:

INPUT 1:	200mV

MEMORY SCREEN.

DIRECTORY:	SA250C	(for camshaft speed 250 r.p.m.)
	SA300C	(for camshaft speed 300 r.p.m.)
	SA350C	(for camshaft speed 350 r.p.m.)
FILENAME:	250P1	(for camshaft speed 250 r.p.m.)

	300P1	(for camshaft speed 300 r.p.m.)
	350P1	(for camshaft speed 350 r.p.m.)

A.2.5.3. FFT analyser settings for proximity probe 2 at speeds 100 - 200 r.p.m.

These settings are the same as for Proximity probe 1 at speeds 100 - 200 r.p.m. except for the following:

MEMORY SCREEN.

DIRECTORY:	SA100C	(for camshaft speed 100 r.p.m.)
	SA150C	(for camshaft speed 150 r.p.m.)
	SA200C	(for camshaft speed 200 r.p.m.)
FILENAME:	100P2	(for camshaft speed 100 r.p.m.)
	150P2	(for camshaft speed 150 r.p.m.)
	200P2	(for camshaft speed 200 r.p.m.)

DISPLAY SCREEN.

SCALE CH2: AUTO EU: 7.043

A.2.5.4. FFT analyser settings for proximity probe 2 at speeds 250 - 350 r.p.m.

These settings are the same as for Proximity probe 1 at speeds 100 - 200 r.p.m. except for the following:

INPUT SCREEN:

INPUT 1: 200mV

MEMORY SCREEN.

DIRECTORY:	SA250C	(for camshaft speed 250 r.p.m.)
	SA300C	(for camshaft speed 300 r.p.m.)
	SA350C	(for camshaft speed 350 r.p.m.)
FILENAME:	250P2	(for camshaft speed 250 r.p.m.)

	300P2	(for camshaft speed 300 r.p.m.)
	350P2	(for camshaft speed 350 r.p.m.)

DISPLAY SCREEN.

SCALE CH2: AUTO EU:	7.043	

A.2.5.5. FFT analyser settings for accelerometer 22223 at speeds 100 - 200 r.p.m.

These settings are the same as for Proximity probe 1 at speeds 100 - 200 r.p.m. except for the following:

INPUT SCREEN:

INPUT 2:		FSR
COUP 2:		ACCEL

MEMORY SCREEN.

DIRECTORY:	SA100C	(for camshaft speed 100 r.p.m.)
	SA150C	(for camshaft speed 150 r.p.m.)
	SA200C	(for camshaft speed 200 r.p.m.)
FILENAME:	1002L	(for camshaft speed 100 r.p.m.)
	1502L	(for camshaft speed 150 r.p.m.)
	2002L	(for camshaft speed 200 r.p.m.)

DISPLAY SCREEN.

SCALE CH2:	AUTO EU:	9.3
TYPE:	CH2:	ACCEL
FSR:	CH2:	1G

A.2.5.6. FFT analyser settings for accelerometer 22223 at speeds 250 - 350 r.p.m.

These settings are the same as for Proximity probe 1 at speeds 100 - 200 r.p.m. except for the following:

INPUT SCREEN:

INPUT 1:	200mV
INPUT 2:	FSR
COUP 2:	ACCEL

MEMORY SCREEN.

DIRECTORY:	SA250C	(for camshaft speed 250 r.p.m.)
	SA300C	(for camshaft speed 300 r.p.m.)
	SA350C	(for camshaft speed 350 r.p.m.)
FILENAME:	2502L	(for camshaft speed 250 r.p.m.)
	3002L	(for camshaft speed 300 r.p.m.)
	3502L	(for camshaft speed 350 r.p.m.)

DISPLAY SCREEN.

SCALE CH2:	AUTO EU:	9.3
TYPE:	CH2:	ACCEL
FSR:	CH2:	1G

A.2.5.7. FFT analyser settings for accelerometer 22222 at speeds 100 - 200 r.p.m.

These settings are the same as for Proximity probe 1 at speeds 100 - 200 r.p.m. except for the following:

INPUT SCREEN:

INPUT 2:	FSR
COUP 2:	ACCEL

MEMORY SCREEN.

DIRECTORY:	SA100C	(for camshaft speed 100 r.p.m.)
	SA150C	(for camshaft speed 150 r.p.m.)
	SA200C	(for camshaft speed 200 r.p.m.)
FILENAME:	1003L	(for camshaft speed 100 r.p.m.)
	1503L	(for camshaft speed 150 r.p.m.)
	2003L	(for camshaft speed 200 r.p.m.)

SCALE CH2:	AUTO EU:	12.2
TYPE:	CH2:	ACCEL
FSR:	CH2:	1G

A.2.5.8. FFT analyser settings for accelerometer 22222 at speeds 250 - 350 r.p.m.

These settings are the same as for Proximity probe 1 at speeds 100 - 200 r.p.m. except for the following:

INPUT SCREEN:

INPUT 1:	200mV
INPUT 2:	FSR
COUP 2:	ACCEL

MEMORY SCREEN.

DIRECTORY:	SA250C	(for camshaft speed 250 r.p.m.)
	SA300C	(for camshaft speed 300 r.p.m.)
	SA350C	(for camshaft speed 350 r.p.m.)
FILENAME:	2503L	(for camshaft speed 250 r.p.m.)
	3003L	(for camshaft speed 300 r.p.m.)
	3503L	(for camshaft speed 350 r.p.m.)

DISPLAY SCREEN.

SCALE CH2:	AUTO EU:	12.2
TYPE:	CH2:	ACCEL
FSR:	CH2:	1G

A.2.5.9. FFT analyser settings for accelerometer 22225 at speeds 100 - 200 r.p.m.

These settings are the same as for Proximity probe 1 at speeds 100 - 200 r.p.m. except for the following:

INPUT SCREEN:

INPUT 2:	FSR

COUP 2:		ACCEL	

MEMORY SCREEN.

DIRECTORY:	SA100C	(for camshaft speed 100 r.p.m.)
	SA150C	(for camshaft speed 150 r.p.m.)
	SA200C	(for camshaft speed 200 r.p.m.)
FILENAME:	1004L	(for camshaft speed 100 r.p.m.)
	1504L	(for camshaft speed 150 r.p.m.)
	2004L	(for camshaft speed 200 r.p.m.)

DISPLAY SCREEN.

SCALE CH2:	AUTO EU:	9.2
TYPE:	CH2:	ACCEL
FSR:	CH2:	1G

A.2.5.10. FFT analyser settings for accelerometer 22225 at speeds 250 - 350 r.p.m.

These settings are the same as for Proximity probe 1 at speeds 100 - 200 r.p.m. except for the following:

INPUT SCREEN:

INPUT 1:	200mV
INPUT 2:	FSR
COUP 2:	ACCEL

MEMORY SCREEN.

DIRECTORY:	SA250C	(for camshaft speed 250 r.p.m.)
	SA300C	(for camshaft speed 300 r.p.m.)
	SA350C	(for camshaft speed 350 r.p.m.)
FILENAME:	2504L	(for camshaft speed 250 r.p.m.)
	3004L	(for camshaft speed 300 r.p.m.)
	3504L	(for camshaft speed 350 r.p.m.)

DISPLAY SCREEN.

SCALE CH2:	AUTO EU:	9.2
TYPE:	CH2:	ACCEL

FSR:	CH2:	1G

A.2.5.11. FFT analyser settings for accelerometer 22224 at speeds 100 - 200 r.p.m.

These settings are the same as for Proximity probe 1 at speeds 100 - 200 r.p.m. except for the following:

INPUT SCREEN:

INPUT 2:	FSR
COUP 2:	ACCEL

MEMORY SCREEN.

DIRECTORY:	SA100C	(for camshaft speed 100 r.p.m.)
	SA150C	(for camshaft speed 150 r.p.m.)
	SA200C	(for camshaft speed 200 r.p.m.)
FILENAME:	1005L	(for camshaft speed 100 r.p.m.)
	1505L	(for camshaft speed 150 r.p.m.)
	2005L	(for camshaft speed 200 r.p.m.)

DISPLAY SCREEN.

SCALE CH2:	AUTO EU:	8.4
TYPE:	CH2:	ACCEL
FSR:	CH2:	1G

A.2.5.12. FFT analyser settings for accelerometer 22224 at speeds 250 - 350 r.p.m.

These settings are the same as for Proximity probe 1 at speeds 100 - 200 r.p.m. except for the following:.

INPUT SCREEN:

INPUT 1:	200mV
INPUT 2:	FSR

COUP 2:		ACCEL	

<u>MEMORY SCREEN.</u>

DIRECTORY:	SA250C	(for camshaft speed 250 r.p.m.)
	SA300C	(for camshaft speed 300 r.p.m.)
	SA350C	(for camshaft speed 350 r.p.m.)
FILENAME:	2505L	(for camshaft speed 250 r.p.m.)
	3005L	(for camshaft speed 300 r.p.m.)
	3505L	(for camshaft speed 350 r.p.m.)

<u>DISPLAY SCREEN.</u>

SCALE CH2:	AUTO EU:	8.4
TYPE:	CH2:	ACCEL
FSR:	CH2:	1G

Appendix 3

Frequency Response Test Results

The frequency response tests are outline, in detail, in Chapter 4.3. The tests were taken between the key phasor pulse and all the transducers for all the speeds under consideration. These provided information on the amplitude and phase values over the 0 - 25 Hz frequency range. The speeds under investigation were:

1. 100 r.p.m.
2. 150 r.p.m.
3. 200 r.p.m.
4 250 r.p.m.
5. 300 r.p.m.
6. 350 r.p.m.

The graphs for the speed at 150 r.p.m. have been shown as an example for the tests. The other graphs, though having different quantities are similar, with the main information extracted and used throughout Chapter 4.

Frequency response tests for all transducers at a speed of 150 rpm.

The following graphs are between all transducers and the key phasor at 150 r.p.m

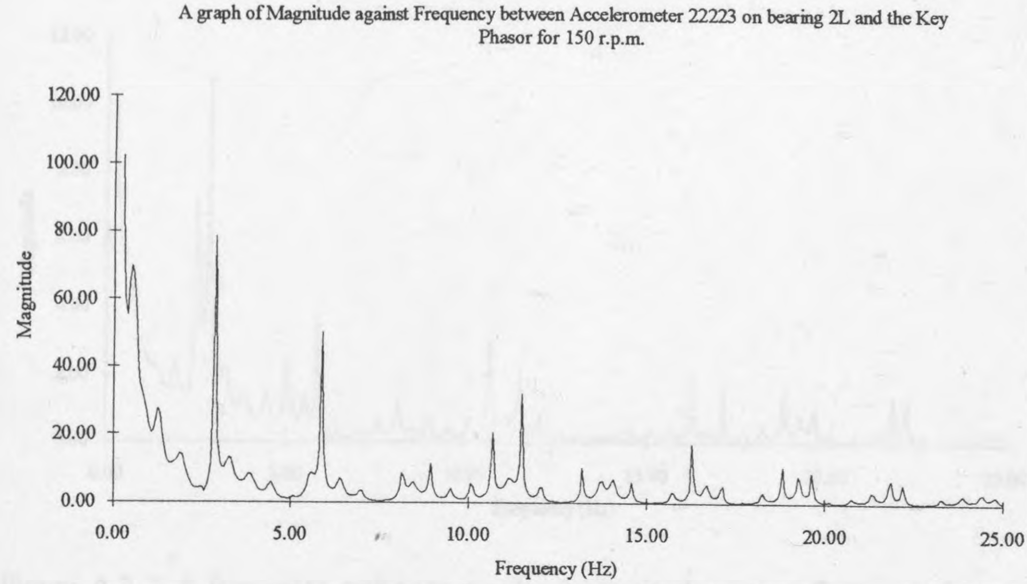

Figure A.3.1: A frequency response graph of magnitude against frequency between accelerometer 22223, situated on bearing 2L and the key phasor.

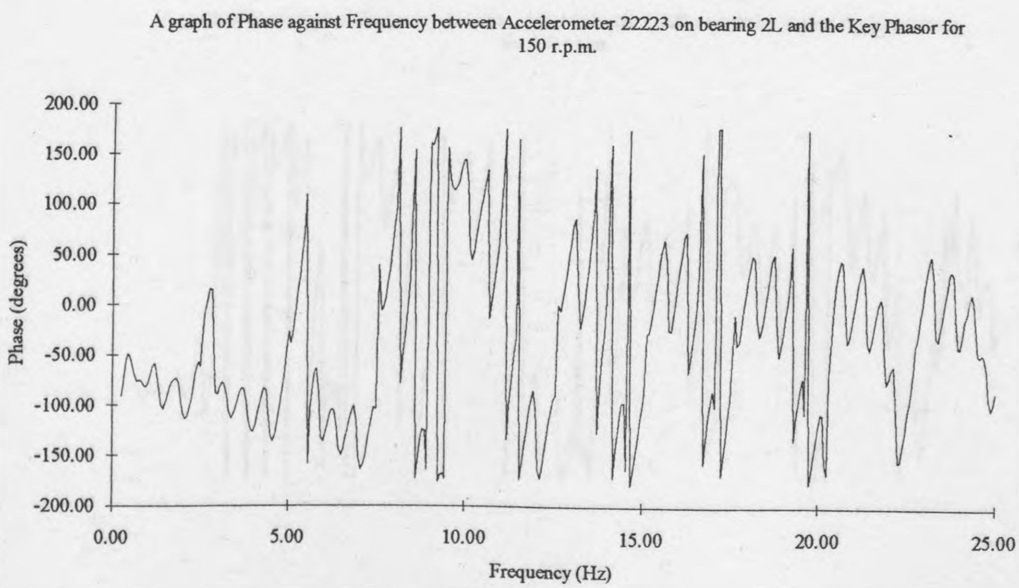

Figure A.3.2: A frequency response graph of phase against frequency between accelerometer 22223, situated on bearing 2L and the key phasor.

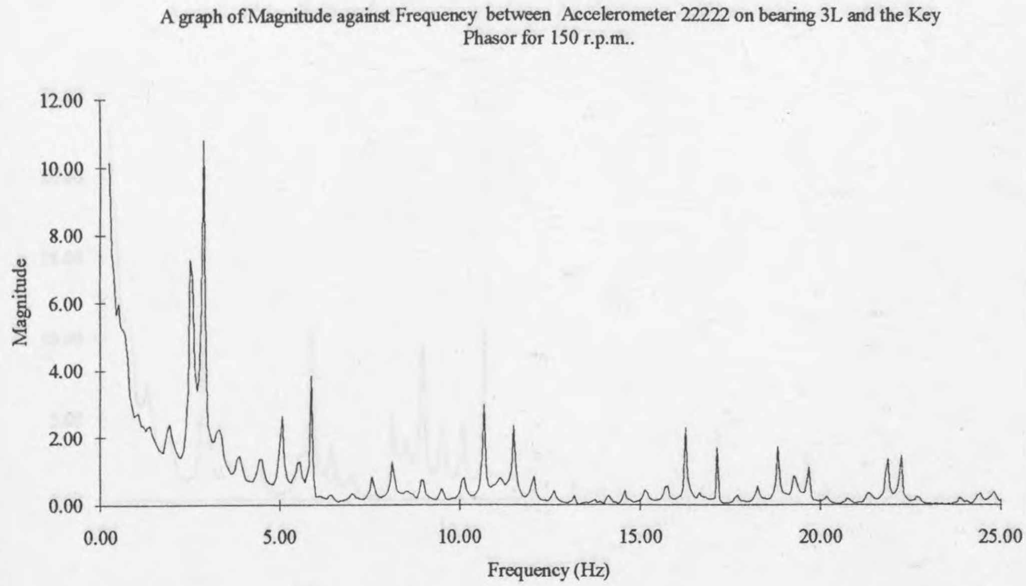

Figure A.3.3: A frequency response graph of magnitude against frequency between accelerometer 22222, situated on bearing 3L and the key phasor.

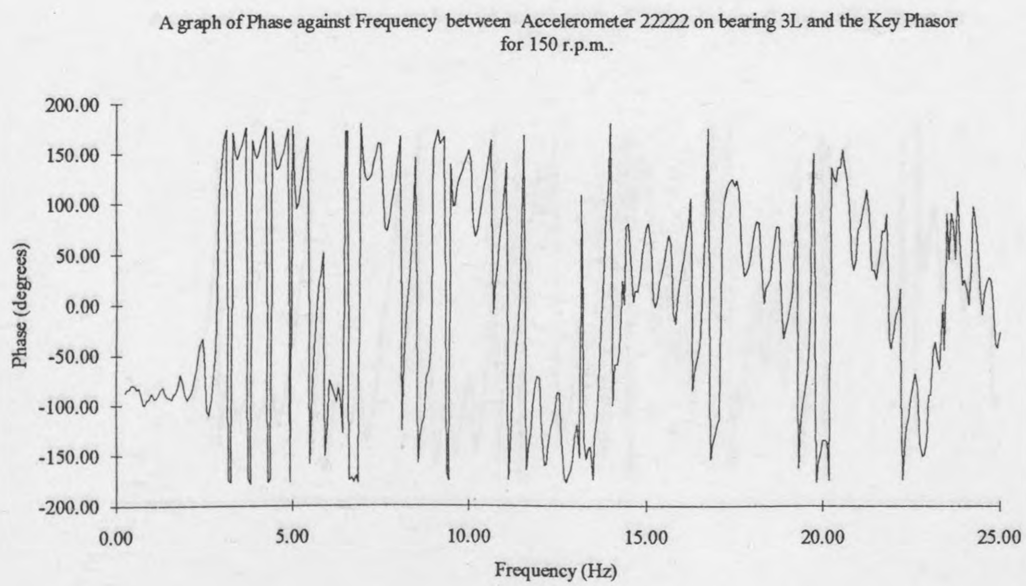

Figure A.3.4: A frequency response graph of phase against frequency between accelerometer 22222, situated on bearing 3L and the key phasor.

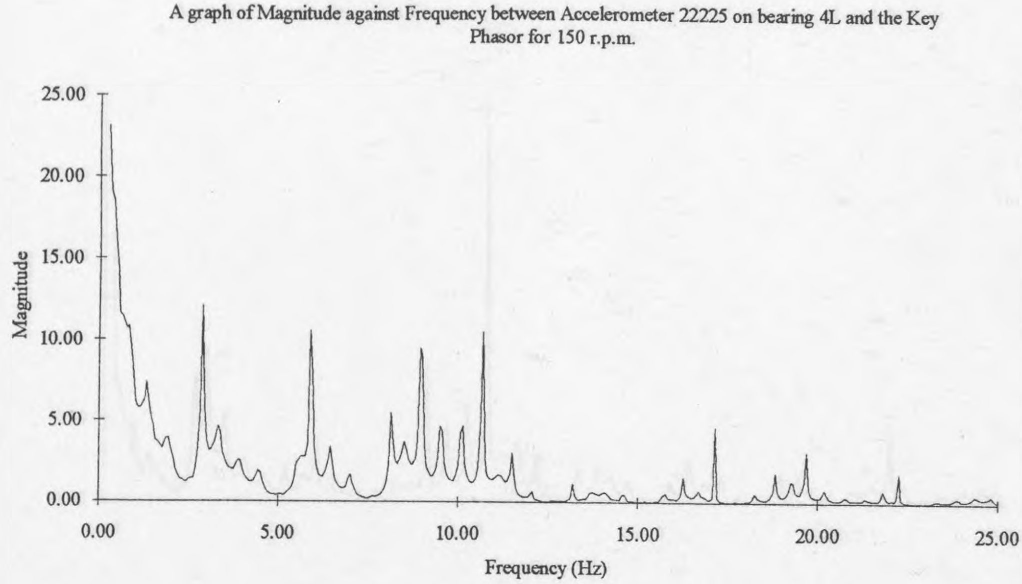

Figure A.3.5: A frequency response graph of magnitude against frequency between accelerometer 22225, situated on bearing 4L and the key phasor.

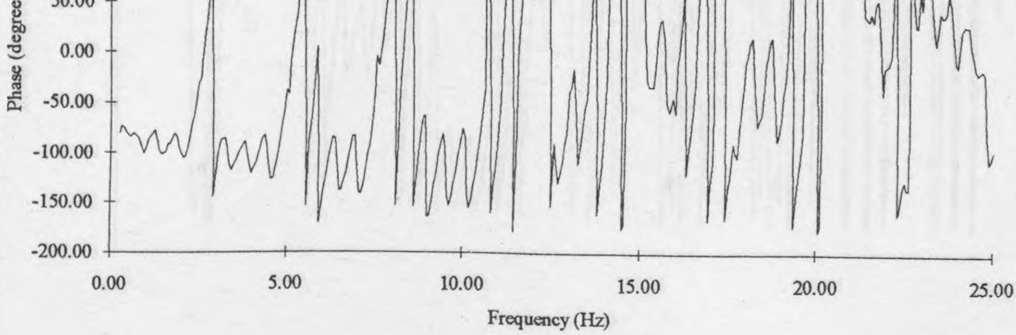

Figure A.3.6: A frequency response graph of phase against frequency between accelerometer 22225, situated on bearing 4L and the key phasor.

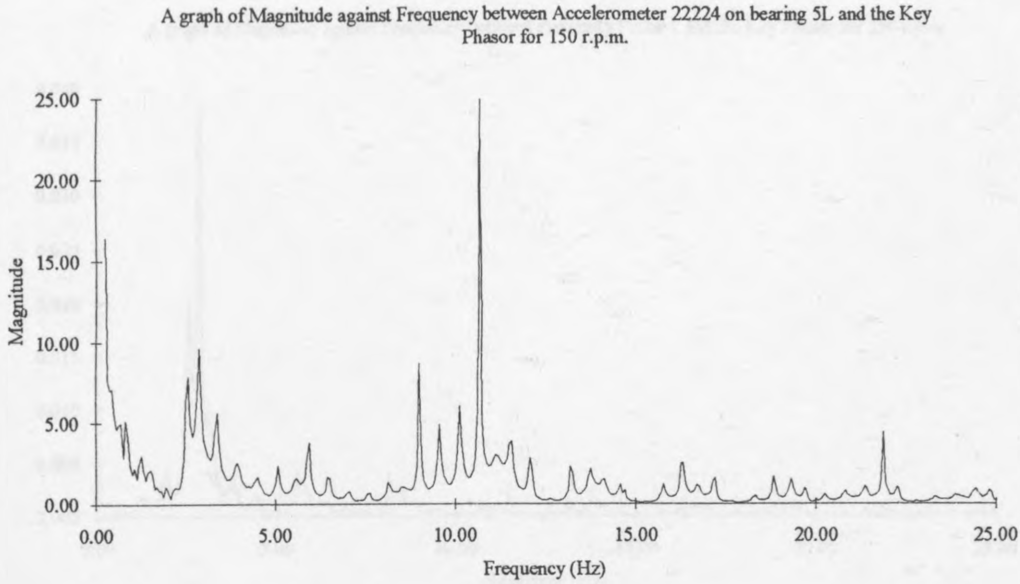

Figure A.3.7: A frequency response graph of magnitude against frequency between accelerometer 22224, situated on bearing 5L and the key phasor.

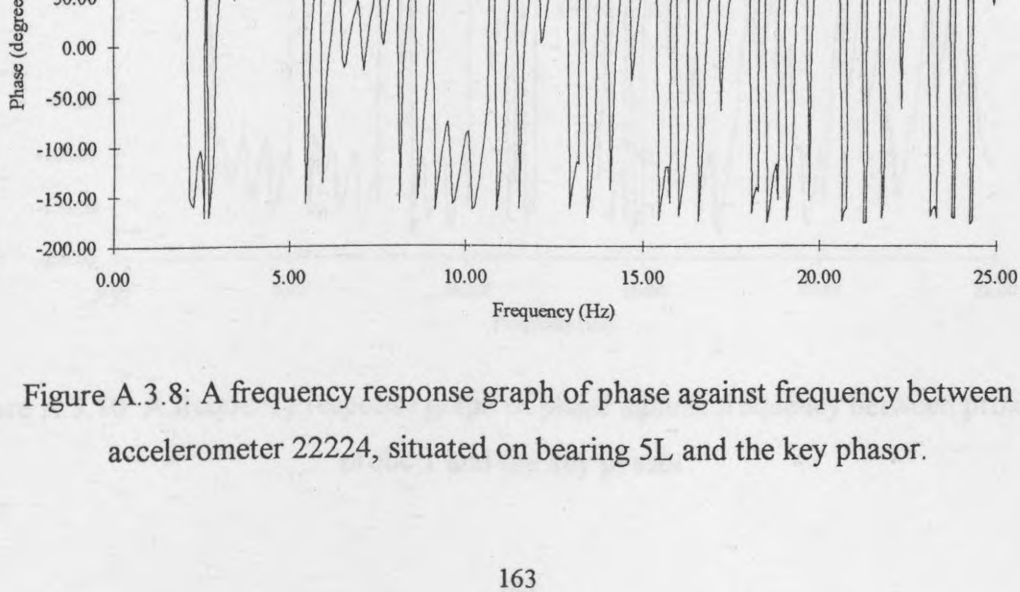

Figure A.3.8: A frequency response graph of phase against frequency between accelerometer 22224, situated on bearing 5L and the key phasor.

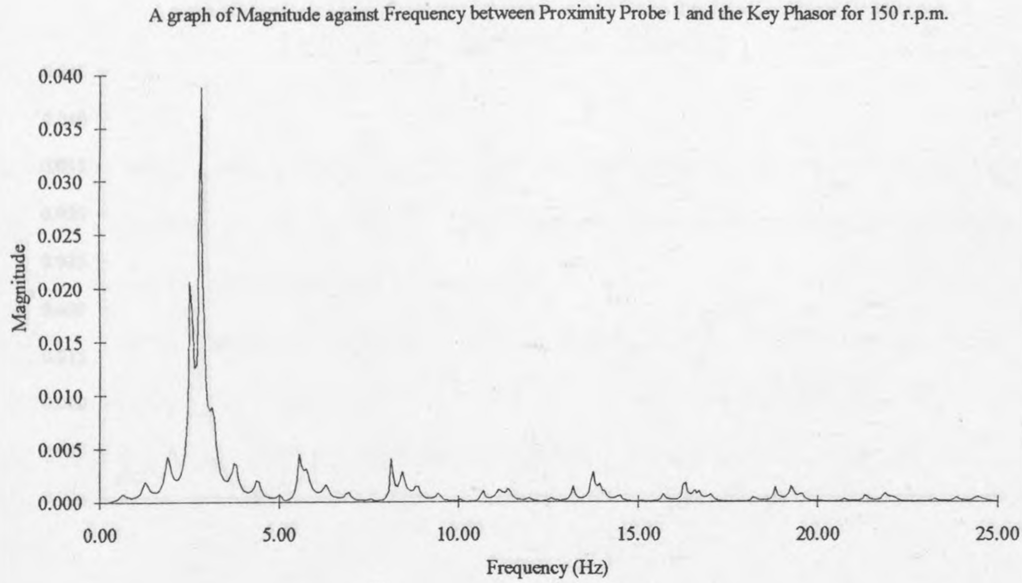

Figure A.3.9: A frequency response graph of magnitude against frequency between proximity probe 1 and the key phasor.

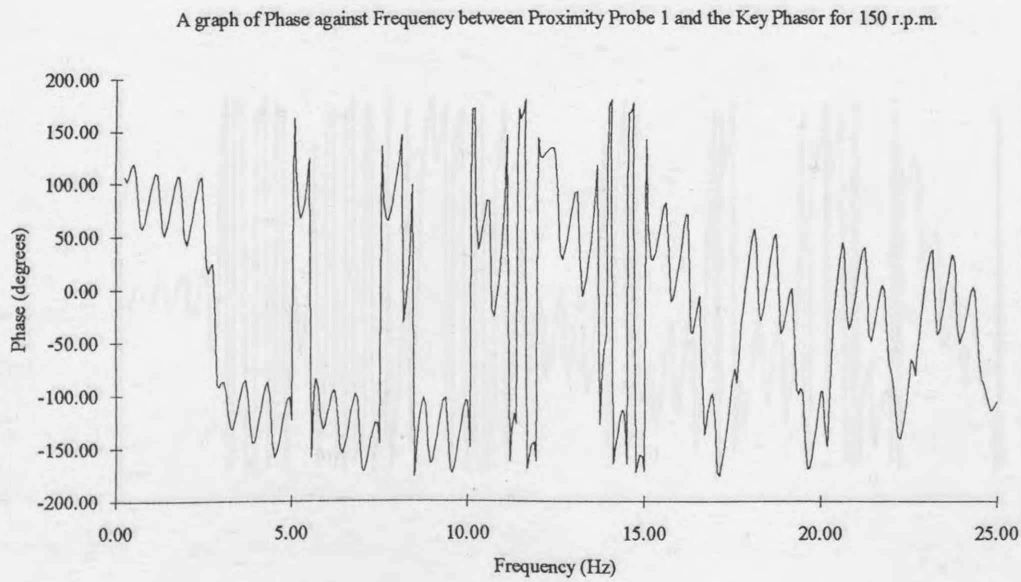

Figure A.3.10: A frequency response graph of phase against frequency between proximity probe 1 and the key phasor.

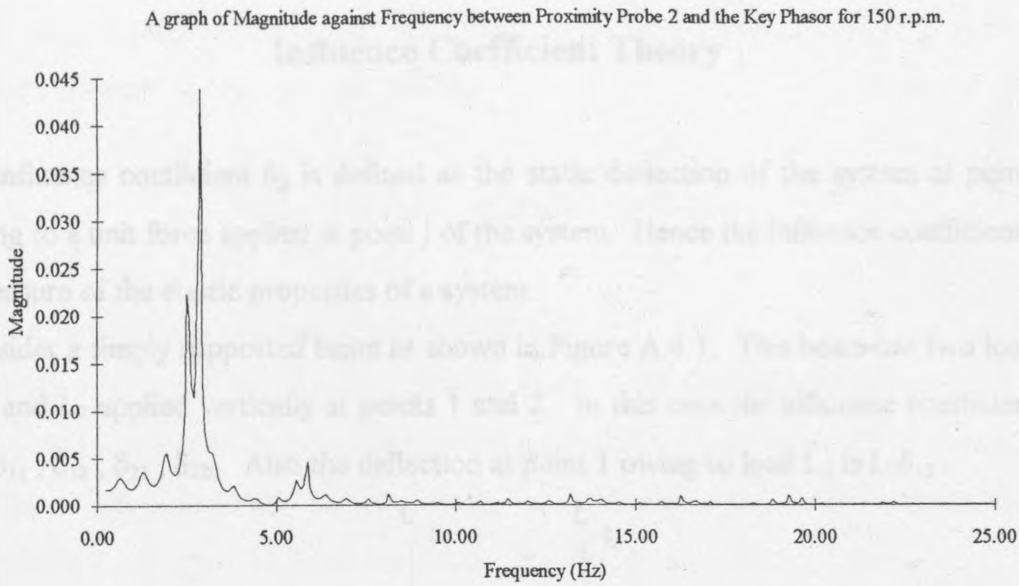

Figure A.3.11: A frequency response graph of magnitude against frequency between proximity probe 2 and the key phasor.

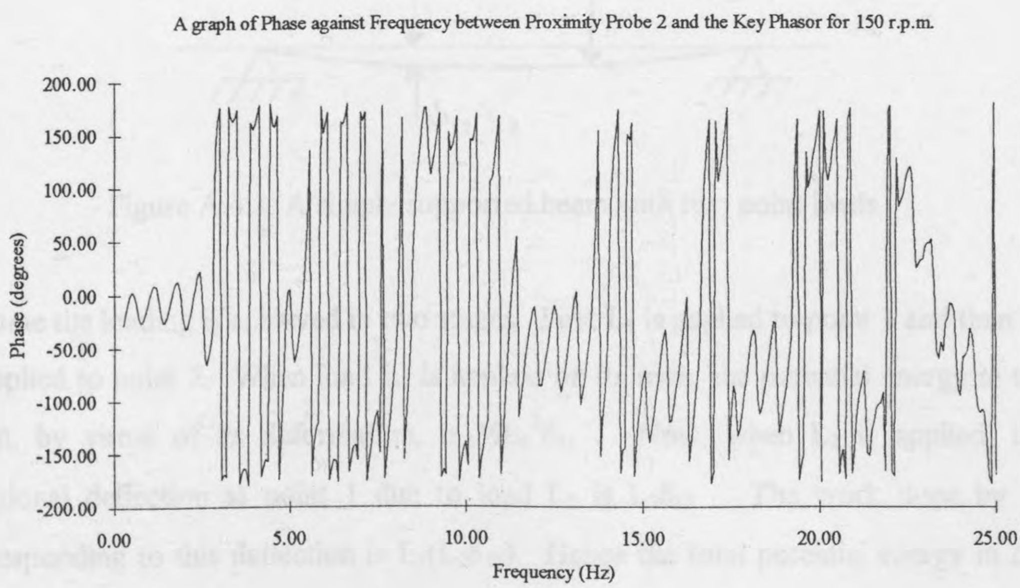

Figure A.3.12: A frequency response graph of phase against frequency between proximity probe 2 and the key phasor.

Appendix 4

Influence Coefficient Theory

An influence coefficient δ_{ij} is defined as the static deflection of the system at point i owing to a unit force applied at point j of the system. Hence the influence coefficient is a measure of the elastic properties of a system.

Consider a simply supported beam as shown in Figure A.4.1. This beam has two loads , L_1 and L_2 applied vertically at points 1 and 2. In this case the influence coefficients are δ_{11} , δ_{12} , δ_{21} , δ_{22} . Also the deflection at point 1 owing to load L_2 is $L_2\delta_{12}$.

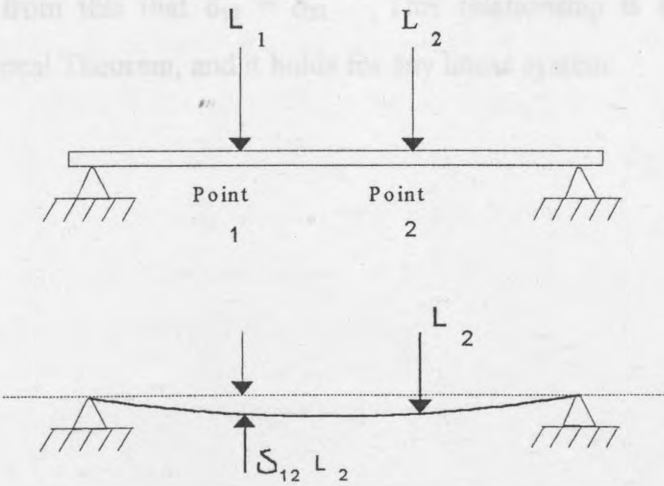

Figure A.4.1: A simply supported beam with two point loads.

Assume the loading is achieved in two stages. First L_1 is applied to point 1 and then L_2 is applied to point 2. When load L_1 is applied on its own, the potential energy in the beam, by virtue of its deformation, is $\frac{1}{2}L_1^2\delta_{11}$. Now, when L_2 is applied, the additional deflection at point 1 due to load L_2 is $L_2\delta_{12}$. The work done by L_1 corresponding to this deflection is $L_1(L_2\delta_{12})$. Hence the total potential energy in the system is:

$$U = 0.5L_1^2\delta_{11} + L_1(L_2\delta_{12}) + 0.5L_2^2\delta_{22}$$

The last two terms represent the additional potential energy which is due to the application of L_2 .

If the loading process is reversed with L_2 applied to point 2 and L_1 applied to point 1, then the potential energy equation will be:

$$U = 0.5L_2^2\delta_{22} + L_2(L_1\delta_{21}) + 0.5L_1^2\delta_{11}$$

The last two terms in this equation are due to L_1 .

Since the final states are identical for both methods of loading, the conservation of energy will apply, and the potential energies expressed by both cases are the same. It can be deduced from this that $\delta_{12} = \delta_{21}$. This relationship is sometimes called Maxwell's Reciprocal Theorem, and it holds for any linear system.

Appendix 5

Sample Calculations For α_{11}

In Chapter 4.4 a sample calculation was undertaken for determining a value of α_{11} at 10 Hz and a rotational speed of 100 rpm. The instrumentation was set up such that d_1 uses the values obtained from the proximity probe P1 and the key phasor, a_1 uses the values obtained between the accelerometer on bearing 2L and the key phasor and a_2 uses the values obtained between the accelerometer on bearing 5L and the key phasor. This calculation was redone for the same conditions of instrumentation set up and frequency, but for different speeds. These values would, once again, aide in the construction of a spreadsheet package simplifying all further calculations of this type. All the values are obtained from the appropriate frequency response graphs obtained in Chapter 4.3. the graphs for when the engine was at 150 r.p.m. is shown in Appendix 3. The calculations were done for the following speeds.

1. 150 r.p.m.
2. 200 r.p.m.
3. 250 r.p.m.
4. 300 r.p.m.
5. 350 r.p.m.

A.5.1. Sample Calculation For α_{11} for a speed of 150 rpm at 10 Hz frequency.

The values used for these calculations are:

	Magnitude	Phase
P1	0.0001724	-105.8901
2L	2.5343	145.1247
5L	1.9311	-87.9300

Magnitude $M_{a2\alpha12}$ and phase $\theta_{a2\alpha12}$ can be determined thus:

$$M_{a2\alpha 12} = M_{a2} * M_{\alpha 12} = 1.9311 * 1 = 1.9311$$
$$\theta_{a2\alpha 12} = \theta_{a2} + \theta_{\alpha 12} = -87.9300 + 0 = -87.9300$$

changing into its real and imaginary parts

$$r_{a2\alpha 12} = M_{a2\alpha 12} * \cos(\theta_{a2\alpha 12}) = 1.9311 * \cos(-87.9300) = 0.06975$$
$$i_{a2\alpha 12} = M_{a2\alpha 12} * \sin(\theta_{a2\alpha 12}) = 1.9311 * \sin(-87.9300) = -1.9299$$

changing d_1 into its real and imaginary parts

$$r_{d2} = M_{d1} * \cos(\theta_{d1}) = 0.0001724 * \cos(-105.8901) = -0.0000472$$
$$i_{d2} = M_{d2} * \sin(\theta_{d1}) = 0.0001724 * \sin(-105.8901) = -0.0001658$$

$$\Rightarrow d_1 - a_2\alpha_{12} = (r_{d1} + i_{d1}) - (r_{a2\alpha 12} + i_{a2\alpha 12}) = (r_{d1} - r_{a2\alpha 12}) + j(i_{d1} - i_{a2\alpha 12})$$
$$= (-0.0000472 + -.06975) + j(-.00001658 + 1.9299)$$
$$= -0.06980 + j1.92970$$

Now changing back into vector notation for magnitude and phase

$$M_{d1-a2\alpha 12} = \sqrt{\left(r_{d1} - r_{a2\alpha 12}\right)^2 + \left(i_{d1} - i_{a2\alpha 12}\right)^2} = \sqrt{(-0.069801)^2 + (1.92970)^2} = 1.9310$$
$$\theta_{d1-a2\alpha 12} = \tan^{-1}\left(\frac{i_{d1} - i_{a2\alpha 12}}{r_{d1} - r_{a2\alpha 12}}\right) = \tan^{-1}\left(\frac{1.92970}{-0.069801}\right) = -87.9284$$

Now from the initial equation

$$\alpha_{11} = \frac{d_1 - a_2\alpha_{12}}{a_1}$$

Therefore

$$M_{\alpha 11} = \frac{M_{d1 - a2\alpha 12}}{M_{a1}} = \frac{1.9310}{2.5343} = 0.7619$$

$$\theta_{\alpha 11} = \theta_{d1 - a2\alpha 12} - \theta_{a1} = -87.9284 - 145.1247 = -233.0531$$

A.5.2. Sample Calculation For α_{11} for a speed of 200 rpm at 10 Hz frequency.

The values used for these calculations are:

	Magnitude	Phase
P1	0.0002368	170.5858
2L	0.12818	-124.9920
5L	0.47934	50.9061

Magnitude $M_{a2\alpha 12}$ and phase $\theta_{a2\alpha 12}$ can be determined thus:

$$M_{a2\alpha 12} = M_{a2} * M_{\alpha 12} = 0.47934 * 1 = 0.47934$$
$$\theta_{a2\alpha 12} = \theta_{a2} + \theta_{\alpha 12} = 50.9061 + 0 = 50.9061$$

changing into its real and imaginary parts

$$r_{a2\alpha 12} = M_{a2\alpha 12} * \cos(\theta_{a2\alpha 12}) = 0.47934 * \cos(50.9061) = 0.3023$$
$$i_{a2\alpha 12} = M_{a2\alpha 12} * \sin(\theta_{a2\alpha 12}) = 0.47934 * \sin(50.9061) = 0.3720$$

changing d_1 into its real and imaginary parts

$$r_{d2} = M_{d1} * \cos(\theta_{d1}) = 0.0002368 * \cos(170.5858) = -0.0002336$$
$$i_{d2} = M_{d2} * \sin(\theta_{d1}) = 0.0002368 * \sin(170.5858) = 0.0000387$$

$$\Rightarrow d_1 - a_2\alpha_{12} = (r_{d1} + i_{d1}) - (r_{a2\alpha12} + i_{a2\alpha12}) = (r_{d1} - r_{a2\alpha12}) + j(i_{d1} - i_{a2\alpha12})$$
$$= (-0.0002336 - 0.3023) + j(0.0000387 - 0.3720)$$
$$= -0.3025 - j0.3720$$

Now changing back into vector notation for magnitude and phase

$$M_{d1-a2\alpha12} = \sqrt{\left(r_{d1} - r_{a2\alpha12}\right)^2 + \left(i_{d1} - i_{a2\alpha12}\right)^2} = \sqrt{(-0.3025)^2 + (-0.3720)^2} = 0.4795$$

$$\theta_{d1-a2\alpha12} = \tan^{-1}\left(\frac{i_{d1} - i_{a2\alpha12}}{r_{d1} - r_{a2\alpha12}}\right) = \tan^{-1}\left(\frac{-0.3720}{-0.3025}\right) = 50.8816$$

Now from the initial equation

$$\alpha_{11} = \frac{d_1 - a_2\alpha_{12}}{a_1}$$

Therefore

$$M_{\alpha11} = \frac{M_{d1-a2\alpha12}}{M_{a1}} = \frac{0.4795}{0.1282} = 3.7406$$

$$\theta_{\alpha11} = \theta_{d1-a2\alpha12} - \theta_{a1} = 50.8816 + 124.9920 = 175.8736$$

A.5.3. Sample Calculation For α_{11} for speed of 250 rpm at 10 Hz frequency.

The values used for these calculations are:

	Magnitude	Phase
P1	0.0008795	28.0817
2L	1.4448	-55.2127
5L	1.0363	133.1817

Magnitude $M_{a2\alpha12}$ and phase $\theta_{a2\alpha12}$ can be determined thus:

$$M_{a2\alpha 12} = M_{a2} * M_{\alpha 12} = 1.0363 * 1 = 1.0363$$
$$\theta_{a2\alpha 12} = \theta_{a2} + \theta_{\alpha 12} = 133.1817 + 0 = 133.1817$$

changing into its real and imaginary parts

$$r_{a2\alpha 12} = M_{a2\alpha 12} * \cos(\theta_{a2\alpha 12}) = 1.0363 * \cos(133.1817) = -0.7091$$
$$i_{a2\alpha 12} = M_{a2\alpha 12} * \sin(\theta_{a2\alpha 12}) = 1.0363 * \sin(133.1817) = 0.7556$$

changing d_1 into its real and imaginary parts

$$r_{d2} = M_{d1} * \cos(\theta_{d1}) = 0.0008795 * \cos(28.0817) = 0.0007760$$
$$i_{d2} = M_{d2} * \sin(\theta_{d1}) = 0.008795 * \sin(28.0817) = 0.0004140$$

$$\Rightarrow d_1 - a_2\alpha_{12} = (r_{d1} + i_{d1}) - (r_{a2\alpha 12} + i_{a2\alpha 12}) = (r_{d1} - r_{a2\alpha 12}) + j(i_{d1} - i_{a2\alpha 12})$$
$$= (0.0007760 + 0.7091) + j(0.0004140 - 0.7556)$$
$$= 0.7099 - j0.7552$$

Now changing back into vector notation for magnitude and phase

$$M_{d1-a2\alpha 12} = \sqrt{\left(r_{d1} - r_{a2\alpha 12}\right)^2 + \left(i_{d1} - i_{a2\alpha 12}\right)^2} = \sqrt{(0.7099)^2 + (-0.7552)^2} = 1.0365$$

$$\theta_{d1-a2\alpha 12} = \tan^{-1}\left(\frac{i_{d1} - i_{a2\alpha 12}}{r_{d1} - r_{a2\alpha 12}}\right) = \tan^{-1}\left(\frac{-0.7552}{0.7099}\right) = -46.7714$$

Now from the initial equation

$$\alpha_{11} = \frac{d_1 - a_2\alpha_{12}}{a_1}$$

Therefore

$$M_{\alpha 11} = \frac{M_{d1 - a2\alpha 12}}{M_{a1}} = \frac{1.0365}{1.4448} = 0.7174$$

$$\theta_{\alpha 11} = \theta_{d1 - a2\alpha 12} - \theta_{a1} = -46.7714 + 55.2127 = 8.4413$$

A.5.4. Sample Calculation For α_{11} for speeds of 300 rpm at 10 Hz frequency.

The values used for these calculations are:

	Magnitude	Phase
P1	0.0002648	-117.2095
2L	0.5213	-22.8906
5L	0.4741	-136.5251

Magnitude $M_{a2\alpha12}$ and phase $\theta_{a2\alpha12}$ can be determined thus:

$$M_{a2\alpha 12} = M_{a2} * M_{\alpha 12} = 0.4741 * 1 = 0.4741$$
$$\theta_{a2\alpha 12} = \theta_{a2} + \theta_{\alpha 12} = -136.5251 + 0 = -136.5251$$

changing into its real and imaginary parts

$$r_{a2\alpha 12} = M_{a2\alpha 12} * \cos(\theta_{a2\alpha 12}) = 0.4741 * \cos(-136.5251) = -0.3441$$
$$i_{a2\alpha 12} = M_{a2\alpha 12} * \sin(\theta_{a2\alpha 12}) = 0.4741 * \sin(-136.5251) = -0.3262$$

changing d_1 into its real and imaginary parts

$$r_{d2} = M_{d1} * \cos(\theta_{d1}) = 0.0002648 * \cos(-117.2095) = -0.0001211$$
$$i_{d2} = M_{d2} * \sin(\theta_{d1}) = 0.0002648 * \sin(-117.2095) = -0.0002355$$

$$\begin{aligned}\Rightarrow d_1 - a_2\alpha_{12} &= (r_{d1} + i_{d1}) - (r_{a2\alpha 12} + i_{a2\alpha 12}) = (r_{d1} - r_{a2\alpha 12}) + j(i_{d1} - i_{a2\alpha 12}) \\ &= (-0.0001211 + 0.3441) + j(-0.0002355 + 0.3262) \\ &= 0.3439 + j0.3260\end{aligned}$$

Now changing back into vector notation for magnitude and phase

$$M_{d1 - a2\alpha 12} = \sqrt{\left(r_{d1} - r_{a2\alpha 12}\right)^2 + \left(i_{d1} - i_{a2\alpha 12}\right)^2} = \sqrt{(0.3439)^2 + (0.3260)^2} = 0.4739$$

$$\theta_{d1 - a2\alpha 12} = \tan^{-1}\left(\frac{i_{d1} - i_{a2\alpha 12}}{r_{d1} - r_{a2\alpha 12}}\right) = \tan^{-1}\left(\frac{0.3260}{0.3439}\right) = 43.4643$$

Now from the initial equation

$$\alpha_{11} = \frac{d_1 - a_2\alpha_{12}}{a_1}$$

Therefore

$$M_{\alpha 11} = \frac{M_{d1 - a2\alpha 12}}{M_{a1}} = \frac{0.4739}{0.5130} = 0.9239$$

$$\theta_{\alpha 11} = \theta_{d1 - a2\alpha 12} - \theta_{a1} = 43.4643 + 22.8906 = 66.3549$$

A.5.5. Sample Calculation For α_{11} for speed of 350 rpm at 10 Hz frequency.

The values used for these calculations are:

	Magnitude	Phase
P1	0.0001235	134.1662
2L	0.6585	74.7449
5L	2.9704	-49.9217

Magnitude $M_{a2\alpha12}$ and phase $\theta_{a2\alpha12}$ can be determined thus:

$$M_{a2\alpha12} = M_{a2} * M_{\alpha12} = 2.9704 * 1 = 2.9704$$
$$\theta_{a2\alpha12} = \theta_{a2} + \theta_{\alpha12} = -49.9217 + 0 = -49.9217$$

changing into its real and imaginary parts

$$r_{a2\alpha12} = M_{a2\alpha12} * \cos(\theta_{a2\alpha12}) = 2.9704 * \cos(-49.92171) = 1.9124$$
$$i_{a2\alpha12} = M_{a2\alpha12} * \sin(\theta_{a2\alpha12}) = 2.9704 * \sin(-49.9217) = -2.2728$$

changing d_1 into its real and imaginary parts

$$r_{d2} = M_{d1} * \cos(\theta_{d1}) = 0.0001235 * \cos(134.1662) = -0.0008607$$
$$i_{d2} = M_{d2} * \sin(\theta_{d1}) = 0.0001235 * \sin(134.1662) = 0.0008861$$

$$\begin{aligned}\Rightarrow d_1 - a_2\alpha_{12} &= (r_{d1} + i_{d1}) - (r_{a2\alpha12} + i_{a2\alpha12}) = (r_{d1} - r_{a2\alpha12}) + j(i_{d1} - i_{a2\alpha12}) \\ &= (0.0008861 - 1.9124) + j(0.0008861 + 2.2728) \\ &= -1.9133 + j2.2737\end{aligned}$$

Now changing back into vector notation for magnitude and phase

$$M_{d1-a2\alpha12} = \sqrt{(r_{d1} - r_{a2\alpha12})^2 + (i_{d1} - i_{a2\alpha12})^2} = \sqrt{(-1.9133)^2 + (2.2737)^2} = 2.9716$$
$$\theta_{d1-a2\alpha12} = \tan^{-1}\left(\frac{i_{d1} - i_{a2\alpha12}}{r_{d1} - r_{a2\alpha12}}\right) = \tan^{-1}\left(\frac{2.2737}{-1.9133}\right) = -49.9200$$

Now from the initial equation

$$\alpha_{11} = \frac{d_1 - a_2\alpha_{12}}{a_1}$$

Therefore

$$M_{\alpha 11} = \frac{M_{d1-a2\alpha 12}}{M_{a1}} = \frac{2.9716}{0.6585} = 4.5127$$

$$\theta_{\alpha 11} = \theta_{d1-a2\alpha 12} - \theta_{a1} = -49.9200 - 74.7449 = -124.6649$$